

UCLA

UCLA Electronic Theses and Dissertations

Title

Memory and spatial representations in the human medial temporal lobe: insights from intracranial electrophysiology during virtual reality and real-world ambulation

Permalink

<https://escholarship.org/uc/item/1p07t84d>

Author

Maoz, Sabrina Leah Levy

Publication Date

2023

Supplemental Material

<https://escholarship.org/uc/item/1p07t84d#supplemental>

Peer reviewed|Thesis/dissertation

UNIVERSITY OF CALIFORNIA  
Los Angeles

Memory and spatial representations in the human medial temporal lobe: insights from  
intracranial electrophysiology during virtual reality and real-world ambulation

A dissertation submitted in partial satisfaction of the  
requirements for the degree Doctor of Philosophy  
in Bioengineering

by

Sabrina Leah Levy Maoz

2023

© Copyright  
Sabrina Leah Levy Maoz  
2023

# ABSTRACT OF THE DISSERTATION

Memory and spatial representations in the human medial temporal lobe: insights from intracranial electrophysiology during virtual reality and real-world ambulation

by

Sabrina Leah Levy Maoz  
Doctor of Philosophy in Bioengineering  
University of California, Los Angeles, 2023  
Professor Nanthia A. Suthana, Co-Chair  
Professor Wentai Liu, Co-Chair

Our ability to recall memories of personal experiences is an essential part of daily life. These episodic memories often involve movement through space and thus require continuous encoding of one's position relative to the surrounding environment. Formation of successful episodic memories (of personal events) requires the integration of contextual information within a spatial environment. Memory decline accompanies numerous neurological and psychiatric diseases. To inform the development of effective therapies, understanding how complex memories are encoded in the medial temporal lobe (MTL) is critical.

To examine how MTL neural representations flexibly encode spatial memories, rare recordings in humans were collected from two complementary cohorts: (1) freely moving participants with chronic intracranial electroencephalographic (iEEG) electrodes and (2) stationary participants with single neuron recording electrodes. All participants completed an ecologically meaningful 3D immersive virtual reality (VR) spatial memory task.

Our results highlight the utility of an immersive VR behavioral paradigm to interrogate multi-scale neurophysiology of episodic memory and spatial navigation in humans. We found that MTL theta oscillations dynamically represent memory and spatial variables to support momentary cognitive task demands. Theta oscillations were modulated by (i) memory performance during memory retrieval immediately before conscious recall, (ii) proximity to spatial boundaries or (ii) latently accessed memory representations of previously learned positions. We found that the immersive VR spatial memory paradigm elicited hexadirectional modulation of theta bandpower and also grid cell-like population activity. Interestingly, these hexadirectional modulation spatial representations exhibited putative grid axes reorientation during changing environmental contexts, and preliminary findings suggest that grid cells also may exhibit similar reorientation, suggesting that spatial codes may be context-specific.

Altogether, these results demonstrate how human MTL oscillations and single neurons can represent both memory and space in a temporally flexible manner during interactive spatial navigation and memory retrieval. These findings advance our understanding of medial temporal lobe representations of spatial navigation, memory, and the effect of contextual changes that will together serve as a scientific foundation for development of neurological therapies for disorders of memory.

The dissertation of Sabrina Leah Levy Maoz is approved.

Barbara Knowlton

Andrew M. Wikenheiser

Nanthia A. Suthana, Committee Co-Chair

Wentai Liu, Committee Co-Chair

University of California, Los Angeles

2023

## DEDICATION

To my grandmother *Riesha*, an academic at heart and feminist ahead of her time, whose drive, support, and belief in me allowed me to dream of and pursue limitless aspirations,

*and*

to my daughter *Adi*, for whom I too wish a world of vast dreams to one day be realized.

*“Memory is the scribe of the soul.”*

*– Aristotle*

# TABLE OF CONTENTS

Abstract .....	ii
List of Figures.....	ix
List of Tables.....	x
Supplemental Materials .....	xi
Glossary .....	xii
Introduction .....	1
Background.....	5
2.1 The medial temporal lobe as the seed of episodic memory .....	5
2.2 Neuronal populations that encode space and memory .....	6
2.2.1 Spatial codes.....	7
2.2.2 Memory codes.....	8
2.2.3 Remapping .....	9
2.3 Oscillations .....	10
2.3.1 Theta oscillations support spatial and memory processes.....	10
2.4 Overview.....	13
Intracranial neural recordings in humans .....	14
3.1 Introduction.....	14
3.2 Mobile iEEG recordings.....	15
3.2.1 Chronically implanted neural sensing devices.....	18
3.2.2 Limited sampling of brain regions.....	20
3.3 Stationary single-unit recordings.....	21
3.3.1 Spike sorting.....	23
3.3.2 Advantages and limitations.....	25
3.4 Virtual Reality.....	26
3.5 Current findings.....	28
3.5.1 Findings from mobile iEEG recordings .....	28
3.5.2 Findings from single-unit electrophysiology .....	31



3.6 Technical challenges .....	33
3.7 Clinical confounds.....	38
3.8 Ethical considerations.....	39
3.9 Promises and future opportunities.....	40
Dynamic neural representations of memory and space in freely moving humans .....	43
4.1 Introduction.....	43
4.2 Methods .....	44
4.2.1 Participants .....	44
4.2.2 Spatial memory task in immersive virtual reality .....	45
4.2.3 iEEG data acquisition .....	46
4.2.4 Electrode localization .....	47
4.2.5 Detection of epileptic events .....	48
4.2.6 Behavioral analyses .....	49
4.2.7 iEEG data analysis.....	50
4.2.8 Statistical comparisons & data subsampling.....	52
4.3 Results .....	54
4.3.1 Measuring spatial memory using ambulatory VR and motion tracking .....	55
4.3.2 Successful memory retrieval is associated with increased MTL theta bandpower.....	60
4.3.3 MTL theta bandpower is modulated by spatial position .....	63
4.3.4 Theta bandpower fluctuations are robustly driven by memory accuracy or proximity to boundaries and not by movement variables .....	67
4.3.5 Coupling between theta and gamma oscillations during retrieval and directed search .....	74
4.4 Discussion .....	75
Contextually-changing spatial representations .....	80
5.1 Introduction.....	80
5.2 Methods .....	82
5.2.1 Participants .....	82

5.2.2 Spatial memory task in immersive VR in stationary and ambulatory movement formats .....	83
5.2.3 Single-unit or iEEG data acquisition .....	85
5.2.4 Behavioral analysis.....	86
5.2.5 Single-unit data analysis .....	86
5.2.6 iEEG data analysis.....	88
5.3 Results .....	89
5.3.1 Measuring spatial memory using VR during human single-unit and mobile iEEG recordings .....	89
5.3.2 Spatial codes in the human MTL.....	94
5.3.3 Spatial representations are context-specific.....	100
5.3.4 The relationship between context-specific spatial representations and memory .....	104
5.4 Discussion .....	107
References .....	111

## LIST OF FIGURES

[Figure 2-1. Medial Temporal Lobe Anatomy](#)

[Figure 2-2. Spatially Periodic MTL Cells](#)

[Figure 2-3 MTL theta oscillations.](#)

[Figure 3-1. Ambulatory Intracranial Recording Set Up](#)

[Figure 3-2. Electrodes used to record human single neurons](#)

[Figure 3-3. Example Findings From Mobile iEEG Studies](#)

[Figure 4-1. Experimental setup and ambulatory spatial memory task](#)

[Figure 4-2. Memory performance during the ambulatory spatial navigation task](#)

[Figure 4-3. MTL theta bandpower increased during correct compared to incorrect retrieval, visible halo, or arrow trials](#)

[Figure 4-4. Movement speed during different task conditions](#)

[Figure 4-5. Oscillatory prevalence across task conditions](#)

[Figure 4-6. MTL theta bandpower increased at non-target halo positions](#)

[Figure 4-7. MTL theta bandpower is modulated by position relative to environmental boundaries](#)

[Figure 4-8. Robustness of memory and spatial modulation of theta power](#)

[Figure 4-9. Memory accuracy and proximity to boundaries drive theta bandpower fluctuations](#)

[Figure 4-10: Theta-gamma phase-amplitude-coupling is increased during correct retrieval trials](#)

[Figure 5-1. Experimental and neurophysiology recording set up in ambulatory and stationary task formats](#)

[Figure 5-2. VR spatial memory task](#)

[Figure 5-3. Memory performance during the stationary spatial navigation task](#)

[Figure 5-4. MTL channels exhibit hexadirectional modulation](#)

[Figure 5-5. Spatially-modulated single neurons](#)

[Figure 5-6. Context-specific hexadirectional modulation](#)

[Figure 5-7. Grid cell axis reorientation](#)

[Figure 5-8. Relationship between memory performance and spatial coding metrics](#)

[Figure 5-9. Stripe cells increase their firing rate in relation to successful memory retrieval](#)

## LIST OF TABLES

[Table 3-1. Overview of Implantable Neurostimulator Devices](#)

[Table 3-2. Wearable Sensors and Accessories](#)

[Table 4-1. Participant demographics, experimental task info, and localizations of electrodes](#)

## SUPPLEMENTARY MATERIALS

Supplemental video 1. Ambulatory spatial navigation task (encoding).

Supplemental video 2. Ambulatory spatial navigation task (retrieval).

Supplemental video 3. Increased MTL theta bandpower prior to successful recall.

## GLOSSARY

<i>Bipolar channel</i>	A recording channel that records neural activity by subtracting the difference in voltage across two (often adjacent) electrode contacts, where one is treated as the positive contact and the other is the negative contact.
<i>Closed-loop system</i>	A system in which calculations are computed in real-time during ongoing continuous neural recordings. Typically, a real-time calculation is used to detect a neural biomarker or feature. Detection of this event of interest will then initiate some program that may involve a particular stimulation pattern or some other change of variables.
<i>CT, MRI, fMRI</i>	Computed tomography (CT), magnetic resonance imaging (MRI), and functional magnetic resonance imaging (fMRI). CT and MRI brain scans provide anatomical information while fMRI illustrates changes in brain region activity, measured according to rapid changes in a particular brain region's hemodynamic response.
<i>Deep brain stimulator</i>	A medical device that has stimulation capabilities at one or more electrodes that are intracranially implanted in deep brain structures (i.e., below the cortex).
<i>Ecological validity</i>	A measure of the extent to which the findings of a research study predict or can be generalized to natural behavior in real-world settings.
<i>Encoding</i>	The process of transferring information into the neural systems (e.g., forming a neural representation of spatial information, or storing a memory).
<i>Episodic memory</i>	A memory of a personal experience (combining information about time, location, associated emotions, and other contextual information).
<i>Electrode lead</i>	A probe inserted intracranially that can contain one or more contacts for recording and/or stimulation. Depending on the diameter, an electrode may be described as a micro-electrode or a macro-electrode. Micro-electrodes can record single neuron and local field potential (LFP) activity and are currently only available in acute post-surgical hospital settings, while macro-electrodes record intracranial EEG and are currently used with chronic sensing and stimulation devices.
<i>Electrode contact</i>	A metal contact on an electrode that is typically constructed from silicon, platinum, tungsten, or other metallic substances. There may be one or more contacts on an electrode.
<i>Hexadirectional modulation</i>	A specific pattern of brain activation, where neural population-level signals recorded using fMRI or

	iEEG are modulated by the direction of one's movement within an environment, thought to reflect the coordinated activity of grid cell populations (also called grid-cell-like representations).
<i>Interictal epileptiform discharge (IED)</i>	A typical neural activity pattern that commonly occurs in the SOZ of epilepsy patients. These are not clinical-level seizures.
<i>Intracranial electroencephalography (iEEG)</i>	The measurement and recording of electrical brain activity via macro-electrodes (~1.5 mm in diameter) that are surgically implanted into the brain.
<i>Latency</i>	Temporal delays introduced when multiple devices send electronic messages serially. A good practice is to characterize the temporal latencies of a system to ensure that they remain lower than the temporal resolution of the neural signals of interest.
<i>Local field potential (LFP)</i>	Electric potential recorded extracellularly from a population of synchronous neurons, typically using small diameter (40 $\mu\text{m}$ ) micro-wire electrodes.
<i>Medial temporal lobe (MTL)</i>	A region of the brain involved in encoding episodic memories and spatial navigation and comprised of subregions including the hippocampus, entorhinal cortex and surrounding cortical areas.
<i>Neural representation</i>	A pattern of neural activity that is related to a specific stimulus (e.g., an environmental feature), behavior, or mental content.
<i>Retrieval</i>	The process of accessing information that has been previously encoded in neural systems.
<i>Seizure onset zone (SOZ)</i>	A region of the brain where clinical seizures originate from. Electrode placements are selected to target hypothesized seizure onset zones, in the case of epilepsy.
<i>Single-unit recordings</i>	Putative neuron firing activity recorded extracellularly, typically using small diameter (40 $\mu\text{m}$ ) micro-wire electrodes.
<i>Synchronization</i>	A strategy used to align the timestamps across multiple continuous and simultaneous data streams. One example strategy may involve a signal sent from one device simultaneously to all data streams to define an absolute timepoint that can be used to align timestamps across different data streams.
<i>Theta oscillations</i>	Rhythmic brain activity in the form of a neural oscillation with a frequency between 3-12 Hz, typically recorded with electrophysiological recording methods.
<i>Responsive neurostimulator</i>	A closed-loop device that continuously records neural activity and delivers a pulse of current stimulation when an imminent seizure or IED event is predicted, in order to prevent the manifestation of a clinical seizure.

# Acknowledgements

Completing my PhD reflects reaching a dream I set out for myself many years ago in two ways: first by arriving at a milestone that once felt beyond reach and second by ascertaining principles of human neural cognition that were once only conceivable as theoretical hypotheses and have now become testable through the advent of paradigm-shift advances in engineering. First and foremost, I would like to thank my outstanding adviser and thesis committee co-chair, Dr. Nanthia Suthana for her unparalleled mentorship, support, training, and friendship. Dr. Suthana has taught me a breadth of scientific principles (in and beyond the field of cognition), experimental approaches, how to implement the scientific method with integrity and ethics, effective scientific communication, and how to be an exceptional scientist, leader, and community member. Her mentorship is one that I will forever cherish and her indelible impact on me is long-lasting. I am truly grateful for her unwavering support and guidance. I would like to thank Dr. Wentai Liu, my thesis committee co-chair, for his continued support of my career and for providing me with an excellent foundation in the fundamentals of neuroengineering. I would like to thank Dr. Barbara Knowlton and Dr. Andrew Wikenheiser along with the rest of my thesis committee for their support, guidance, thought-provoking questions, and insight that helped me refine my research.

This research exemplifies collaboration in its purest form and could not have been possible without the team effort of the entire Suthana Lab and collaborations with others. I would like to thank Dr. Zahra Aghajan, Dr. Matthias Stangl, and Dr. Martin Seeber for countless impactful discussions that helped refine my research interests, analytical approaches, and general edification over the many years. I am so fortunate to have been part of the team with Sonja Hiller, an incredible lab manager who was the glue to the lab who kept everything running effortlessly, monitored every detail, and always provided a positive outlook and warm comfort that helped me get through the toughest and longest



days recording with patients after facing obstacle after obstacle. I am grateful to her for her unending kindness, composure, and dedication. I would like to thank Dr. Uros Topalovic for his ingenuity, selflessness, and technical mastery which he used frequently to help quickly solve all kinds of never-before seen problems that regularly occurred on patient recording days. I would like to thank Daniel Batista for his invaluable support and contributions implementing the virtual reality task and collaborating on creating the optimal participant experience.

I am so fortunate to have had the opportunity to work with and learn from so many selfless, resilient, kind, and wise epilepsy patients that trusted myself alongside our team to use cutting-edge approaches to listen to the music and symphonies of their very own neurons. These patients inspire me, and our interactions served as anchoring moments through an arduous graduate school process, reminding me of the importance and potential future impact of my work. To the many neurosurgeons, Dr. Itzhak Fried, Dr. Aria Fallah, Dr. Jean-Philippe Langevin, Dr. Ausaf Bari and neurologists, Dr. Dawn Eliashiv, Dr. John Stern, I am grateful for the mentorship on how to embark on this rare and beautiful line of research and for the privilege to work with their patients. I would also like to thank our collaborations with Neuropace and Blackrock for helping provide the tools and collaboration to collect this rare and precious data.

\* \* \*

**Chapter 3** is modified primarily from: *Maoz SL, Stangl MS, Suthana N. The future of iEEG: What are the promises and challenges of mobile iEEG recordings? In: Intracranial EEG: A Guide for Cognitive Neuroscientists. Editor: Axmacher N. Springer, 2023. ISBN: 978-3-031-20909-3*; with small excerpts from: *Stangl MS, Maoz SL, Suthana N. Invasive electrophysiological recordings from humans during navigation. In: Encyclopedia of the Human Brain, 2nd edition. Editor: Ekstrom E. Elsevier, in press*; and from: *Stangl MS, Maoz SL, Suthana N. Mobile cognition: Studying the human brain in*

*the 'real world'. Nature Reviews Neuroscience. 2023. 24: 347-362. doi.org/10.1038/s41583-023-00692-y.*

**Chapter 4** is modified from: *Maoz SL, Stangl M, Batista D, Topalovic U, Hiller S, Aghajan S, Knowlton B, Stern J, Langevin JP, Fried I, Eliashiv D, Suthana N. Dynamic neural representations of memory and space in freely-moving humans, in revision.*

\* \* \*

My graduate training was supported by the National Institute of Mental Health NRSA F30 Training Fellowship (F30-MH125534), the UCLA Training in Neurotechnology Program (T32NS115753-01), and the UCLA Medical Scientist Training Program (T32-GM008042).

I would like to thank Dr. Jay Gill, Dr. Whitney Griggs, and the rest of my MSTP cohort for countless scientific discussions, camaraderie, and support on this journey. I would also like to thank Amy Schauer for first inspiring me to study cognitive neuroscience and providing me with the pivotal early experiences that cemented my passion.

Finally, I would like to thank my family. I am grateful to my parents Rosy and Andrew Levy for their unwavering support, love, and selflessness. I would like to thank my brother Avi Levy for intellectual discussions and collaboration on mathematical approaches, as well as setting an excellent example for me and his enthusiastic support. To my greatest champion, my husband Nir Maoz, who inspires me, motivates me, and has believed in me through every trough and peak along this journey, your love and support means everything to me.

# VITA

2014 BS in Bioengineering, University of California, Berkeley, Berkeley, California

## SELECTED PUBLICATIONS

Stangl MS, Maoz SL, Suthana N. Invasive electrophysiological recordings from humans during navigation. In: Encyclopedia of the Human Brain, 2nd edition. Elsevier, In press.

Maoz SL, Stangl MS, Suthana N. The future of iEEG: What are the promises and challenges of mobile iEEG recordings? In: Intracranial EEG: A Guide for Cognitive Neuroscientists. Springer, In press.

Stangl MS, Maoz SL, Suthana N. Mobile cognition: Studying the human brain in the ‘real world’. (2023). Nature Reviews Neuroscience.

Topalovic U, Barclay S, Ling C, Alzuhair A, Yu W, Hokhikyan V, Chandrakumar H, Rozgic D, Jiang W, Basir-Kazeruni S, Maoz SL, Inman C, Bari A, Fallah A, Eliashiv D, Fried I, Suthana N, Markovic D. (2023) A wearable platform for closed-loop stimulation and recording of single-neuron and local field potential activity in freely moving humans. Nat Neurosci 2023 8:1–11.

Maoz SL, Canalis, RF. From Galen to Eustachio: Discovering the Anatomy of the Facial Nerve. Otology & Neurotology 42(9):1434-1441.

Pendharkar A, Smerin D, Gonzalez, L, Wang E, Levy S, Wang, S, Ishizaka S, Ito, M, Cheng, M, Steinberg GK. (2020) Optogenetic stimulation reduces neuronal nitric oxide synthase expression after stroke. Translational Stroke Research.

Ito M, Aswendt M, Lee AG, Ishizaka S, Cao Z, Wang EH, Levy SL, Smerin DL, McNab J, Leuze CUW, Goubran M, Cheng MY, Steinberg GK. (2018) RNA sequencing analysis revealed a distinct motor cortex transcriptome in spontaneously-recovered mice after stroke. Stroke 49(9):2191-2199.

Pellionisz PA, Levy SL, Liang J, Namiri N, Cheng H, Hu Y, Taylor Z, Grundfest W, St. John MA, Messadi D. (2018). Emerging Technology for Screening of Oral Cancer. In: Translational Research: Recent Progress and Future Directions. ISBN: 978-1-53614-598-4.

Newman ZL, Hoagland A, Aghi K, Worden KL, Levy SL, Son JH, Lee LP, Isacoff EY. (2017) Input-specific plasticity and homeostasis at the Drosophila larval neuromuscular junction. Neuron. 93(6):1245-7.

Shah AM, Ishizaka S, Cheng MY, Wang EH, Bautista AR, Levy SL, Smerin D, Sun G, Steinberg GK. (2017) Optogenetic neuronal stimulation of the lateral cerebellar nucleus promotes persistent functional recovery after stroke. *Scientific Reports*. 7, 46612.

Levy SL, White JJ, Lackey EP, Schwartz L, Sillitoe RV. (2017) WGA-Alexa conjugates for axonal tracing. *Current Protocols in Neuroscience*. 79;1.28.1-1.28.24.

Pendharkar A\*, Levy SL\*, Ho A, Sussman E, Cheng M, Steinberg G. (2016) Optogenetic Modulation in Stroke Recovery. *Journal of Neurosurgery*. 40(5):E6.

Levy SL, White JJ, Sillitoe RV. (2015) Wheat Germ Agglutinin (WGA) Tracing: A Classic Approach for Unraveling Neural Circuitry. In: *Neural Tracing Methods*. (51-66). Springer New York.

#### SELECTED PRESENTATIONS & POSTERS:

Maoz SL, et al. Spatially-periodic stripe single neurons identified in the human MTL and beyond during immersive virtual reality. Human Single Neuron Meeting. November 11, 2022.

Maoz SL, et al. Successful retrieval is preceded by higher MTL theta power in freely moving humans performing a virtual reality memory task. Park City Winter Conference on the Neurobiology of Learning and Memory. January 6, 2022.

Maoz SL, Suthana N. An Ecologically Valid Platform for Recording Single Neuron and Oscillatory Activity in Naturally Behaving Humans. Data Blitz Presentation, UCLA Symposium on Neurotechnology. May 2021.

Maoz SL, et al. Virtual reality as a tool to study spatial navigation with deep brain recordings in ambulatory and stationary participants. Society for Neuroscience Meeting. November 14, 2022.

Maoz SL, et al. Neural dynamics of memory retrieval in the medial temporal lobe of freely-moving humans. UCLA Medical Scientist Training Program Annual Research Conference. September 23, 2022.

Maoz SL, et al. Successful memory retrieval modulates spatial maps in the MTL of freely ambulating humans. Interdisciplinary Navigation Symposium (iNAV). June 14, 2022.

Maoz, SL, Suthana N. Single-unit and Oscillatory Encoding of Spatial Navigation in Naturally Behavior Humans. UCLA Medical Scientist Training Program Seminar Presentation. November 8, 2021.

Maoz SL, et al. Whole brain activation dynamics after stroke. Society for Neuroscience, November 2016.

# CHAPTER 1:

## Introduction

*“As long as we can love each other, and remember the feeling of love we had, we can die without ever really going away. All the love you created is still there. All the memories are still there.”*

*– Mitch Albom, Tuesdays with Morrie*

A fundamental aspect of our human identities is embedded in our sequential experiences, encoded in the fabric of our being through episodic memories that shape and are updated through each subsequent instance that we retrieve them. Although classic studies of learning and memory began with the study of simple reflexive circuits in invertebrate models such as *Aplysia californica*, how humans experience, learn, and retrieve life events and importantly transfer learned knowledge from one experience to the next can be simplified into a question of what information is transmitted from one context to another. Applying principles learned to unfamiliar contexts is foundational to the human experience. From creating and interpreting new sentences from grammar and language principles learned previously, to inferring and adapting to customs and social environments when travelling to foreign countries, to problem-solving creatively by drawing on principles from past solutions to solve new problems, the transmission of contextual information is vital to the human experience.

Understanding the neural machinery that supports episodic memories is a complicated and long-standing endeavor. Studies in rodents, nonhuman primates, and humans have identified that the machinery supporting episodic memories is intrinsically

intertwined and oftentimes the same as that which supports spatial cognition. These fundamental neural substrates that conjunctively encode spatial and memory variables, are often tied to geographically to the medial temporal lobe (MTL) of the brain, and include single neurons that are tuned to spatial, environmental, goal/object-oriented, and memory features and local field potential oscillations that rhythmically support memory encoding/retrieval, spatial navigation, and movement variables.

Determining how single cells and network assemblies encode episodic memories is crucial towards understanding memory decline and treating related neurological diseases. How the human brain encodes and retrieves memories remains to be answered, and importantly, how these processes are affected in neurological diseases including Alzheimer's disease, dementia, epilepsy, Parkinson's disease, traumatic brain injury, among many others, remains to be understood in terms of functional mechanisms. Notably, spatial representations in the MTL have been observed to be reduced in strength in young adults are APOE- $\epsilon$ 4 carriers, a gene inked with an increased risk for developing Alzheimer's disease later in life (Kunz et al., 2015; Bierbrauer et al., 2020). Thus, these spatial MTL representations are an important area of investigation to advance our understanding of spatial cognition, memory encoding, and neural processing deficits in memory dysfunction in the setting of neurological disease.

Critical gaps that remain unanswered include (1) how the MTL neural substrates dynamically represent spatial and memory processes during real-world experiences, navigation and exploration, (2) how human MTL single neurons support space and memory during 3D navigation in ecologically valid behavioral paradigms, and (3) how the single-unit and oscillatory representations interact to support ecologically-valid spatial memory processes. Bridging these gaps using human neurophysiology is challenging, given the rarity of access to single neuron and deep intracranial electroencephalographic (iEEG) recordings in humans, especially in the setting of ecologically-valid behaviors.

Importantly, due to the unwieldy and complex recording equipment required, traditional neuroimaging approaches are typically constrained to studying humans in immobile set-ups, and often utilize 2-dimensional (2D) view-based virtual environments (e.g. on a laptop or screen). Evidence from rodents suggests that 2D environments may impair the development of spatial selectivity of neurons, based on findings in rodents comparing 2D and 3D VR (Aghajian et al., 2015). Given advancement in VR technology, graphics, and interfaces, we address these critical open questions using immersive 3D VR, both in ambulatory and stationary approaches, to construct more ecologically-valid behaviors that elicit robust spatial and memory processing.

Investigating spatial representations during real-world ambulation in humans is a critical step forward. Notably, studies in freely moving humans have identified that oscillations (specifically theta band) occur in non-continuous bursts of activity (“theta bouts”) that are modulated by movement speed and differ from theta oscillations present in rodents and non-human primates (Aghajian et al., 2017, 2019; Bohbot et al., 2017). These findings suggest that movement cues contribute to spatial navigation in the real world and emphasize the importance of interrogating spatial and memory processing in humans during real-world interactive navigation.

In Chapter 2, we present an overview of key literature and findings from both the rodent and human brain in spatial and memory processing.

In Chapter 3, we describe recent technological advances that have enabled access to precious mobile iEEG and single neuron recordings in humans during ecologically-valid behavior paradigms by incorporating head-mounted immersive virtual reality.

In Chapter 4, we present findings from mobile iEEG recordings during immersive VR that demonstrate MTL theta oscillations dynamically represent spatial and memory variables in relation to momentary cognitive task demands.

In Chapter 5, we demonstrate the utility of an immersive VR as a platform to probe single neuron and mobile iEEG mechanisms in humans. We further highlight complimentary spatial coding mechanisms (e.g. grid cells and hexadirectional modulation of theta oscillatory power) and that these grid cell representations exhibit orientation changes across changing environmental contexts.

A decline in memory, unfortunately, is all too common in neurological and psychiatric diseases and is routinely regarded as an expected progression of disease and aging, despite the devastating impact it can have on individuals and their loved ones. We must determine the neurophysiology of human episodic memories in real-world settings and with ecologically meaningful behavioral paradigms in order to lay the foundation for the development of novel interventions that target focused memory symptoms.

*“In a way, geographical distance did not exist for us, because we could always talk about our hometowns and childhood memories, and thereby create a common space.”*

*– Viktor Frankl, Man’s Search for Meaning*



# CHAPTER 2:

## Background

### 2.1 The medial temporal lobe as the seed of episodic memory

The hippocampus, a slender and curved region nestled in the medial temporal lobe, is thought to support the formation and subsequent recall of episodic memories (Tulving, 1983). Early evidence tracing episodic memories to the hippocampus came from neurologic patients that suffered from focal amnesia and deficits in spatial orientation associated with highly localized damage to medial temporal lobe (MTL) regions. The most widely known case was that of the patient H.M. who underwent bilateral hippocampal resection for the treatment of severe epilepsy and suffered from subsequent retrograde amnesia (Scoville and Milner, 1957). This case study, along with others, provided novel insights into the neuroanatomical underpinnings of memory, leading to a new era of memory and spatial cognition research that spanned organisms from humans to rodents.

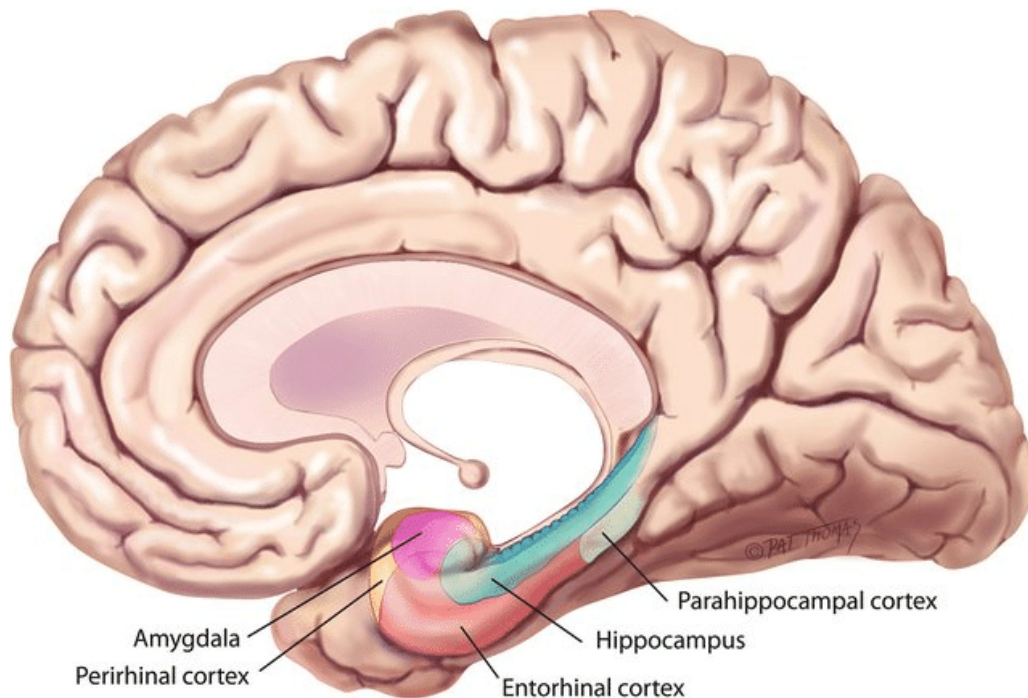


**Figure 2-1. Medial Temporal Lobe Anatomy.** Illustration of the human medial temporal lobe anatomy including the perirhinal cortex, entorhinal cortex, hippocampus, and parahippocampal cortex.

### 2.1.2 Medial temporal lobe anatomy

The MTL is comprised of a diversity of functional and anatomical subregions including the hippocampus and nearby perirhinal, entorhinal cortex, parahippocampal cortices (Ulmer and Jansen, 2013), see Fig 1-1. The hippocampus receives inputs from the entorhinal cortex and is comprised of subregions: the dentate gyrus which projects to the cornua ammonis (CA) 1-3, that projects to the subiculum (Squire et al., 2004).

## 2.2 Neuronal populations that encode space and memory

Extracellular electrophysiological recordings in animals have enabled neuroscientists to draw conclusions about the firing properties of single neurons (or single neurons as they are commonly referred to) in relation to an animal's behavior or reaction to some presented stimuli. This electrophysiological approach has yielded immense insight into the MTL circuitry and how neurons process incoming information. Classically, the electrophysiological approach has been utilized in animal models, where recording from large numbers of single neurons is feasible, either simultaneously or through numerous consecutive experiments. In recent decades, rare human MTL electrophysiology experiments have become feasible by leveraging neurosurgical procedures for the clinical treatment of epilepsy that transiently place electrodes, with the capability of recording single-unit activity, throughout many brain regions while patients are under observation in a hospital setting (Fried et al., 2014). These experiments have allowed neuroscientists to begin to investigate the MTL single-unit neural representations in humans.

These approaches have introduced the important question of how the neurophysiology of the MTL in humans is similar or different in relation to studies from rodents and non-human primates. While concrete behavioral variables, such as navigational movement patterns or speed are readily available to study in animals, understanding how these variables interact with internal cognitive processes, such as

retrieving episodic memories, can be more readily assessed in humans without the need for overtraining the subject in order to master a memory task. More importantly, critical open questions include whether the neurophysiology of spatial and memory variables differ between animals and humans and how neural representations of spatial and memory variables in humans are encoded during ecologically-valid experiences.

### 2.2.1 Spatial codes

Seminal work in rodents identified MTL neuronal populations that support neural representations of space, supporting an early and prominent theory of a “cognitive map” initially proposed by Tolman (Tolman, 1948). Place cells, or hippocampal single neurons that fire selectively in a particular location in an environment, were first identified in rodents freely moving through an open field environment (O’Keefe and Dostrovsky, 1971; McHugh et al., 1996) see Fig. 2-2, but also have been reported in non-human primates (Courellis et al., 2019; Mao et al., 2021), and humans performing 2D, laptop-based navigation (Ekstrom et al., 2003). Place cells are thought to receive organizing information from another population of spatially-selective cells, grid cells, located in the medial entorhinal cortex. Grid cells fire in multiple positions in an environment with firing fields that occupy the vertices of a hexagon that tile an entire environment as illustrated in Fig. 2-2 (Hafting et al., 2005; Sargolini et al., 2006). Unlike place cells, which change their preferred firing location in a new environment, grid cells maintain a characteristic spatial relationship and location of their firing fields independent of an environment (Fyhn et al., 2007) and as such grid cells are thought to provide a grid map of an environment which guides place cell firing field selection as has been theorized by computational models (Whittington et al., 2020). A related population of spatially-selective cells are referred to as spatially periodic band (or stripe) cells fire with firing fields that create stripes which tile a spatial environment. These cells have been reported in rodents

predominantly in the medial entorhinal cortex but also in smaller proportions in the hippocampus (Krupic et al., 2012) and also were predicted based on computational models (Grossberg and Pilly, 2012; Whittington et al., 2020).

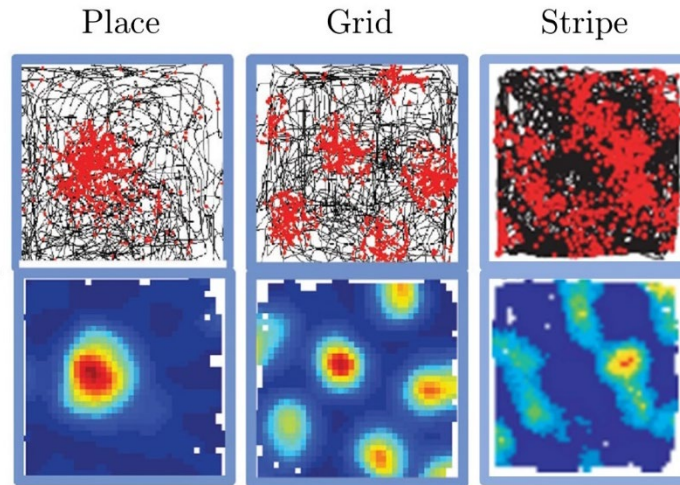


**Figure 2-2. Spatially Periodic MTL Cells.** Top row shows a bird's eye view of an open field with black lines showing a rodent's trajectory in an environment and red dots indicating the rodent's position in the environment when a particular single-unit was firing. Bottom row illustrating the firing rate map for the same unit shown in the top row over all positions within the open field. Three spatially periodic cell types are depicted in each column, from left to right: place cell, grid cell (both reproduced from Moser et al., 2015), and stripe cell (reproduced from Krupic et al., 2012).

### 2.2.2 Memory codes

Memory processing has been linked to the MTL through numerous approaches, including previously mentioned lesion case studies in humans, neuroimaging and neurophysiology approaches in humans and animal models (for reviews, see Squire et al., 2004b; Opitz, 2014). However, the precise neurophysiology underlying memory processing remains an open question, especially since determining the internal memory processes (such as declarative memory retrieval) can be difficult to ascertain in animal studies. Even still, single-unit MTL populations that tune to memory have been identified in rodents,

including a population of so-called object trace cells in the lateral entorhinal cortex which fire in spatial positions associated with previously encountered objects (Tsao et al., 2013). Entorhinal cortex single neurons with similar properties have been identified in humans as well. Memory-trace cells fire in association with arrival at location of previously-learned object positions (Qasim et al., 2019) and egocentric bearing cells encode egocentric position in relation to environmental anchor positions and are modulated by memory recall (Kunz et al., 2021).

### 2.2.3 Remapping

A core component of episodic memory is the integration of context and spatial information. Context describes the cues and expectations that organize information to guide retrieval and the hippocampus is thought to bind the context of an episodic memory (Stark et al., 2018). Although much has been learned about context in rodents (Fyhn et al., 2007; Colgin et al., 2008; Alexander et al., 2016; Latuske et al., 2018; Kubie et al., 2019), ecologically-meaningful context changes in ambulating humans have not been studied. The MTL has been linked to contextual encoding, based on fear conditioning studies in which optogenetic reactivation in the hippocampus recreates a contextual memory (Ramirez et al., 2013). Context changes in rodents result in place cell remapping, i.e. rapid changes in receptive fields and thus the ensemble firing rate map (Colgin et al., 2008; Alexander et al., 2016). Hippocampal place cell remapping in rodents is thought to reflect the intrinsic statistics of experiencing a particular context (Plitt and Giocomo, 2019). Frequent alternation of contexts leads to a gradient change between the two place cell representations, versus a binary flipping between representations when contexts alternate infrequently (Plitt and Giocomo, 2019). Meanwhile, grid cells maintain the same firing maps across different contexts while reflecting a degree of flexibility (e.g. grid realignment in novel environments) (Hafting et al., 2005). Preliminary studies suggest

that the human encoding of context may be more complex. In humans performing view-based 2D VR in four different environments, some properties of single-unit grid-like cells were found to adapt: scaling of grid period, grid orientation, and rotational symmetry (Nadasdy et al., 2017). A recently proposed model of the MTL suggests the ERC encodes the environmental statistics as a basis function flexibly applied by the hippocampus to reflect specific environmental features (Whittington et al., 2020). This model predicted many experimental findings of the MTL, including place, grid, and object-vector cells. It also predicts that grid cells maintain a correlational structure across different environments. Altogether, how the human MTL encodes complex spatial memories in different contexts is a complicated, open question.

## 2.3 Oscillations

Intracranial neurophysiology experiments also record local field potential (LFP) that reflects the summative activity of a population of neurons in a small volume of tissue. In human intracranial recordings, LFP is recorded from small diameter (40  $\mu\text{m}$ ) micro-wire electrodes. Filtering of LFP activity into frequency bands has highlighted rhythmic oscillations that have been linked to the processing of distinct cognitive functions.

### 2.3.1 Theta oscillations support spatial and memory processes

Theta oscillations ( $\sim$ 3-12 Hz, broadly) are thought to support both spatial navigation and memory based on studies in rodents as well as in humans (Buzsáki et al., 1983; Wang et al., 2014; Aghajan et al., 2017; Zutshi et al., 2018). In contrast to continuous theta oscillations present in rodents, theta oscillations in humans are present in non-continuous bouts, both during real-world ambulation and in virtual navigation (Ekstrom et al., 2005; Watrous et al., 2013; Aghajan et al., 2017). It has also been proposed that there exist two types of theta: type I is a low-frequency ( $\sim$ 2-5 Hz)

oscillation related to spatial navigation while type II is a higher-frequency (~6-9 Hz) oscillation related to episodic memory (Jacobs, 2014; Watrous and Ekstrom, 2014; Bush et al., 2017; Foo and Bohbot, 2020). A study in humans suggests that frequency of theta oscillations is lower during virtual reality relative to real-world stimuli/navigation (Bohbot et al., 2017), which is consistent with studies in rodents (Ravassard et al., 2013; Watrous et al., 2013).

Theta oscillations are modulated by spatial navigation variables. For example, oscillatory power in the MTL was elevated during successful virtual spatial navigation compared to inactivity or virtual stillness (Caplan et al., 2003; Ekstrom et al., 2005; Kaplan et al., 2012). Furthermore, there is a higher prevalence of theta bouts during fast ambulation compared to slow ambulation in humans (Aghajan et al., 2017). The power of theta oscillations is also modulated by proximity to boundaries, such as room walls (Stangl et al., 2021). Theta oscillations also organize assemblies of MTL neurons by binding cell assemblies into separable groups that can be reinstated to support spatial navigation and memory (Buzsáki and Moser, 2013). Single neurons in these assemblies fire at critical points in alignment with ongoing theta oscillations. For example, a place cell may have a preferred theta phase at which it fires, or conversely, a place cell may fire during earlier phases of theta oscillations over consecutive theta cycles (theta precession) as a rodent navigates through the cell's preferred place field (O'Keefe and Recce, 1993). Theta oscillations also thought to reflect the coordinated activity of grid cell populations. Multiple studies have identified a relationship between theta oscillations and walking direction, such that there is hexadirectional modulation of the power of theta oscillations based on forward-heading direction, where power is elevated when a participant is virtually navigating in accordance with one of six directional peaks that are thought to reflect the intrinsic axes of grid cell populations (Chen et al., 2018; Maidenbaum et al.,

2018; Chen et al., 2021). As such, theta oscillations are critically related to the activity of spatially selective MTL neurons.

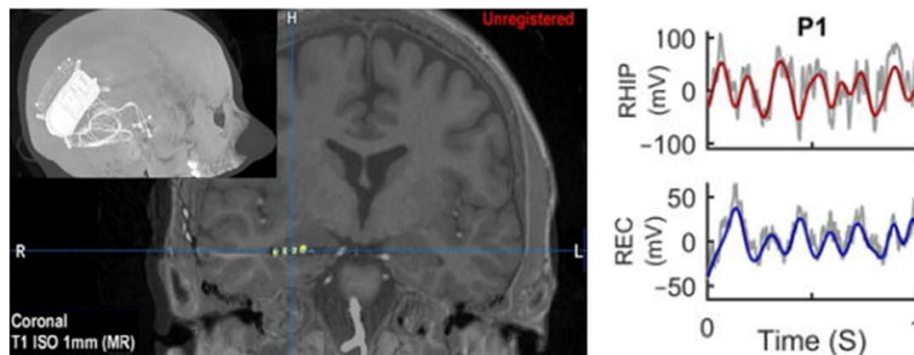


**Figure 2-3 MTL theta oscillations.** Theta oscillations (3-12 Hz) recorded from a freely-ambulating human. Post-operative high-resolution MRI scan (left) with four electrode contacts shown in the yellow. A CT scan depicting the position of the Neuropace Responsive Neurostimulator System embedded in the skull to record intracranial electroencephalographic (iEEG) activity is shown in the left inset. An example 1-second raw iEEG trace is shown in gray in two electrode contacts with filtered theta oscillation overlaid in red (RHIP, right hippocampus) and blue (REC, right entorhinal cortex). Reproduced based on (Aghajan et al., 2017).

Episodic memory encoding and retrieval depend on fluctuations in theta oscillations (Kahana et al., 1999; Long et al., 2017; Solomon et al., 2019b; Kota et al., 2020; ter Wal et al., 2021) and they exhibit reinstatement of retrieved items associated with their environmental context (Pacheco Estefan et al. 2019). Furthermore, theta oscillations support the subsequent memory effect, which is the observation that stronger oscillatory power (or brain activation) during encoding predicts improved memory retrieval at a later timepoint (Lin et al., 2017). Taken together, MTL theta oscillations play a crucial role in supporting memory and associated spatial representations in humans.



## 2.4 Overview

Despite progress in identifying the neural substrates of spatial navigation in rodents, non-human primates, and humans, an open and pressing question remains of how MTL neurophysiology dynamically represents episodic memories and spatial maps in humans during naturalistic experiences. How spatial and contextual information is embedded in episodic memories and dynamically accessed during complex experiential learning and memory retrieval in real-world settings remains largely understudied due to the inherent challenges in recording intracranial signals from deep brain structures during real-world spatial navigation and memory paradigms.

In Chapter 3, we present a discussion of cutting-edge methods to investigate MTL neurophysiology at two scales: (1) intracranial EEG (iEEG) during real-world ambulation and (2) single-unit and LFP recordings during immersive, head-mounted display 3D virtual reality. These methods provide an opportunity to bridge human and animal studies and highlight fundamental differences.

In Chapter 4, we present our findings highlighting how theta oscillations in freely moving humans dynamically encode momentary cognitive task demands, specifically relating to episodic memory retrieval and spatial navigation which also provides a first study utilizing 3D virtual reality in freely moving humans during iEEG recordings.

In Chapter 5, we present our results highlighting the contextual changes in mobile iEEG spatial representations and supporting observations from single-unit neuron populations that relate to spatial navigation and memory retrieval. Critically, we utilize the same 3D virtual reality spatial memory paradigm, allowing us to leverage insight gained in freely moving humans (Ch. 4) with rare single-unit recordings.

# CHAPTER 3:

## Intracranial neural recordings in humans

### 3.1 Introduction

Traditional approaches to recording deep brain activity in humans require participants to remain immobile, limiting the ecological validity and breadth of cognitive neuroscience questions that can be asked. Rare clinical opportunities to record intracranial brain activity from individuals, by capitalizing on electrophysiology recordings collected for clinical purposes, have advanced our understanding of the neurophysiology of human cognition. In this chapter, we will introduce two electrophysiological methodologies in humans that provide complimentary insight into (1) population-level and (2) single neuron brain activity by leveraging cutting-edge neural interfaces (such as electrodes and implanted brain sensing technologies) that are implanted in neurosurgical patients for clinical treatment.

The first approach, or intracranial electroencephalography (iEEG) recordings from chronic neurostimulator devices, are now possible in mobile human participants interacting with their environment in a natural way, thus providing unique insight into spatial navigation and memory during real-world ambulation. Research-related benefits of such chronic neurostimulator devices include resistance to motion artifacts, access to deep brain structures, measurement of neural activity with high temporal resolution, as well as the possibility to perform closed-loop neuromodulation through stimulation that can be associated with specific behavioral or neurophysiological features.

The second approach, or single-unit recordings, provides high-temporal resolution signals that allow for the study of individual neurons and their specific firing properties. Although these participants tend to be stationary, access to single-unit neural activity in humans is an unparalleled window into the basic unit of human cognition.

Recent technical developments have streamlined the integration of numerous wearables with both wireless iEEG and single-unit recordings, including virtual and augmented reality (VR/AR) headsets, which substantially broaden the scope of possible cognitive neuroscience experiments that can be implemented. Furthermore, use of these AR/VR headsets to develop stimuli allows a platform to present identical stimuli across these two recording approaches and thus draw conclusions about iEEG activity during real-world ambulation along with single-unit firing properties in response to the same set of stimuli. Here, we provide an overview of the methodological and technical aspects of these intracranial brain recordings in human research participants and discuss associated promises and challenges.

### 3.2 Mobile iEEG recordings

The human brain undergoes complex cognitive processes throughout our daily lives by integrating proprioceptive and kinesthetic cues with rich sensory stimuli and information. Understanding how complex behaviors are encoded in the brain thus requires the ability to study human cognition and record brain activity during naturalistic paradigms and behaviors. Traditional methods of recording neural activity in humans are limited by large recording equipment and motion artifacts. Specifically, functional magnetic resonance imaging (fMRI), magnetoencephalography (MEG), and intracranial stereo-electroencephalographic (sEEG) recordings all require patients to be still, within or tethered to large recording equipment, or at the very least that their heads remain motionless.

Notable progress, however, has been made in mobile brain and body imaging technology using scalp electroencephalography (EEG) recordings, which has advanced our understanding of cognitive variables in conditions of naturalistic movement. Recent studies have used mobile scalp EEG to explore questions such as how walking modulates task switching (Richardson et al., 2021), how movement speed modulates neural

representations of focusing on a visual target (Lee et al., 2021), how attention varies across stationary vs walking conditions (Ladouce et al., 2019), how cognitive motor interference is modulated by movement complexity (Reiser et al., 2019), and how the dynamics of cortical brain regions support specific features of active spatial navigation (Do et al., 2021), among many others. Although these studies provide first-insight into how movement modulates human cognition, scalp EEG signals are also complicated by motion-induced artifacts and limited to recording broad neural population signals primarily from cortical structures and with limited spatial resolution. Thus, these constraints reduce the breadth and ecological validity of behavioral, neural, and cognitive processes and relationships that can be studied.

Recently approved implantable medical devices for treating neurological diseases (Table 3-1) have created a unique clinical opportunity to record more localized deep brain activity via iEEG recordings in humans who can be mobile and behave in naturalistic settings. These chronically implanted neural devices that enable wireless iEEG recording and neurostimulation are surgically implanted intracranially and can remain there permanently throughout a person's lifetime. Patients with such implants can enjoy day-to-day life as these devices are not externally visible nor do they interfere with any standard activities of daily living, including freely-moving activities of interest. Thus, the opportunity to record from such chronically implanted neurostimulation devices provides a unique window into cognition allowing for a broad – rather endless – range of ambulatory activities and cognitive tasks to be explored.

	<i>Responsive Neurostimulator (RNS)</i>	<i>Percept</i>	<i>RC + S</i>
<i>Company</i>	Neuropace	Medtronic	Medtronic
<i>Sampling frequency (Hz)</i>	250	250	1000
<i>Battery life</i>	~8 years (320 model); ~4 years (300 model)	~ 5 years	rechargeable
<i>Location of battery</i>	Intracranial	Intrathoracic	Intrathoracic
<i>Synchronization method</i>	Use of the “Mark” or “Magnet” signal to inject an artifactual signal across devices	Stimulation to inject an artifactual signal across devices (e.g., Scalp EEG and iEEG)	Conversion to Unix time on each data stream
<i>Example studies</i>	Scangos 2021(a,b) Stangl et al, 2021 Topalovic et al, 2020 Henin et al, 2019 Rao et al, 2019 Meisenhelter et al, 2018 Molina et al, 2018 Aghajan et al, 2017	Shirvalkar et al, 2020	Gilron et al, 2021 Sellers et al, 2021
<i>Clinical trials</i>	MDD, PTSD, LOC, OCD, epilepsy	MDD, OCD, SCI	MDD, epilepsy
<i>Typical electrode regions</i>	Hippocampus, amygdala, entorhinal cortex, parahippocampal cortex	Subthalamic nucleus, ventral intermediate nucleus of thalamus	Determined by investigational use criteria
<i># of implanted patients</i>	Few thousand	Several hundreds	Less than 30

**Table 3-1. Overview of Implantable Neurostimulator Devices.** Shown are the general characteristics of three of the most commonly available human-use chronic implantable neurostimulator devices. MDD: Major Depressive Disorder, PTSD: Post-traumatic stress disorder, LOC: Loss of control (obesity), OCD: obsessive-compulsive disorder, SCI: Spinal cord injury.

### 3.2.1 Chronically implanted neural sensing devices

While deep brain stimulation (DBS) devices have been used in over a hundred thousand patients for over thirty years to treat neurological disorders such as Parkinson's disease, essential tremor, and dystonia, it is only within the last decade that there has been an increase in the availability of DBS devices that allow for sensing of neural activity. The first of these devices, the Responsive Neurostimulator System (RNS, Neuropace, Inc.), was approved by the FDA in 2013 for the treatment of intractable epilepsy and has since been implanted in over 2500 patients and increasing by several hundred individuals each year. The FDA-approved clinical use of the RNS System is to detect seizure-related activity and subsequently deliver neurostimulation to reduce seizures frequency and pathological symptoms. The RNS System can support up to two intracranial depth or cortical strip electrode leads each of which have four contacts and are implanted in hypothesized seizure-onset zones. Exact locations of the RNS System electrodes vary by patient with both cortical (e.g., orbitofrontal, lateral temporal) and subcortical locations (e.g., amygdala, hippocampus, entorhinal cortex) as common targets. Contact-spacing on electrodes can also vary based on clinical needs, ranging from 3.5 mm to 10 mm (center-to-center). The RNS System also includes a hermetically-encased neurostimulator which is implanted in the skull and is thus shielded and resistant to movement artifacts and externalized electrical noise sources. This neurostimulator package contains the battery and stores iEEG data in small units (~240 seconds) with a sampling rate of 250 Hz on four bipolar channels until it is downloaded wirelessly (via an external wand device, Fig. 3-1A-B) to a server that can be accessed by researchers or clinicians. The RNS System can also be programmed to initiate stimulation on selected channels based on real-time analysis of incoming neural activity (e.g., seizure activity or other clinical/behavioral neurophysiological biomarkers).

The second FDA-approved DBS device that allows for recording of iEEG activity is the Percept PC Neurostimulator (Medtronic, Inc.) used to treat Parkinson's disease. Since its approval in 2020, it has been implanted in a few hundred patients and expected to increase rapidly as patients with older DBS non-sensing devices are upgraded during battery replacement procedures. The Percept can record iEEG activity with a sampling rate of 250 Hz and on up to 6 bipolar channels with the neurostimulator package and battery implanted in the chest near the clavicle in the thoracic cavity. FDA-approved electrode placement sites for the Percept include the subthalamic nucleus (STN) and ventral intermediate nucleus of the thalamus (VIM) (Goyal et al., 2021), however, other sites can be targeted with FDA investigational device exemption (IDE) approval. Brain activity can be recorded in two formats: 1) 10-minute windows, which are then averaged over time and reported, or 2) continuously while connected to the implantable pulse generator (IPG) which provides power.

The Activa PC+S and RC+S Neurostimulators (Medtronic, Inc.) are also available and allow for much more research flexibility (e.g., higher sampling rates, increased programmability of closed-loop capability and wider variety of stimulation parameters), however, are only available with FDA IDE approval and thus have been used in only a small number of patients (< 30 total) across various clinical trials for epilepsy, depression, essential tremor, obsessive-compulsive disorder (OCD), dystonia, and Parkinson's disease.

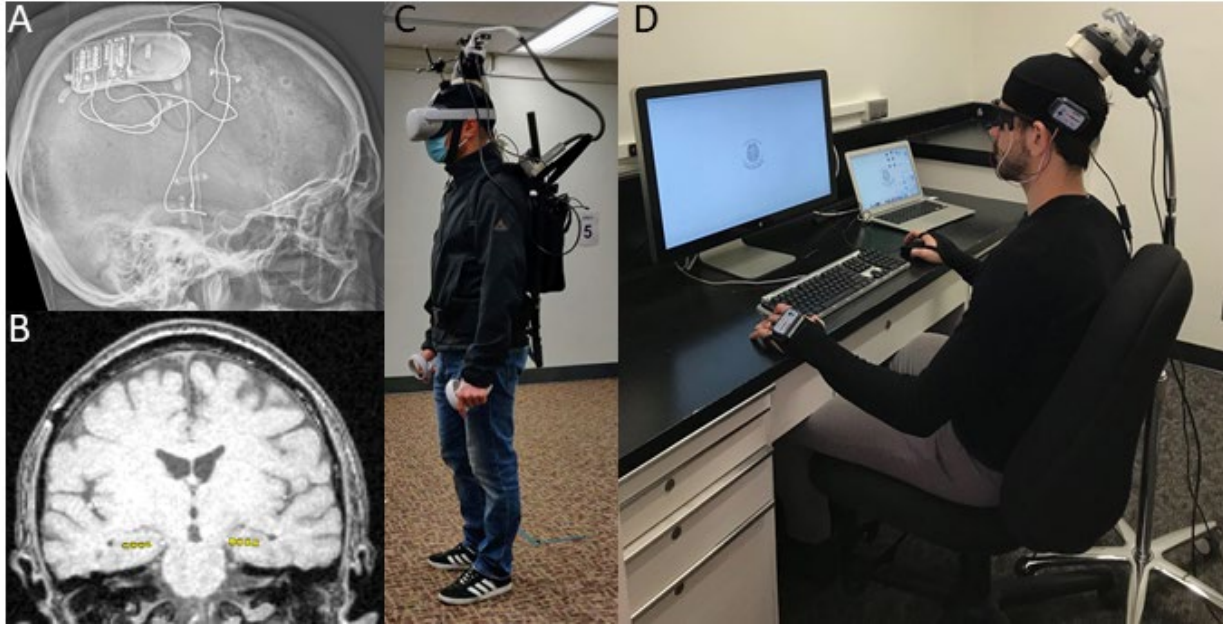


**Figure 3-1. Ambulatory Intracranial Recording Set Up.** An example CT (A) and MRI (B) showing the RNS System implanted intracranially with two leads implanted in the medial temporal lobe. (C) Mobile iEEG recording set-up. As part of the mobile deep brain recording and stimulation (Mo-DBRS) platform, a backpack can be worn, which includes a malleable metal arm holding the wand in place above the participant's RNS implant and is connected to a metal-framed backpack (Topalovic et al., 2020). The participant shown is wearing a VR headset, carrying the associated hand-held controllers, and has a rigid body motion sensor antenna fixed to the top of their head for precise motion tracking. Full-body motion capture suits can also be worn. (D) Stationary iEEG recording set-up. Participant shown is wearing biometric sensors for recording heart rate and skin conductance (on hands), as well as an eye tracking headset that allows for pupillometry and eye-gaze tracking, all of which can also be worn during mobile studies. The wand is placed above the RNS implant using a portable wand holder.

### 3.2.2 Limited sampling of brain regions

Another constraint in mobile iEEG recordings is the limited number of electrode channels available per participant (up to 6 channels) and thus brain regions which can be sampled given that the placement of electrodes is driven solely by clinical criteria. Nonetheless, there exists a large pool of potential participants (thousands) from which to select from in order to acquire sufficient amounts of data from a given brain region while



minimizing variability. Currently, studies with hypotheses related to medial temporal and striatal function are understandably the most common given electrodes are implanted most often in these brain regions. Furthermore, as the types of neurologic and psychiatric conditions treated by implanting chronic neurostimulators expands, a greater diversity of brain regions will likely be accessible, which in turn will open the door to a greater variety of cognitive and clinical neuroscience research questions that can be answered.

The spatial resolution of mobile iEEG data is another important variable to consider when designing a study using chronic neurostimulators, which is limited by the diameter of the implanted electrodes (1.5 mm), spacing of electrode contacts (up to 10 mm) if using bipolar recordings, and the spatial resolution of neuroimaging-based localization procedures (e.g., co-registration of MRI and CT images). However, in contrast to most intracranial neurophysiology studies performed in acute epilepsy monitoring units, mobile iEEG study participants are able to complete experiments of longer durations (up to 6-8 hours per day, and over multiple days with flexible timelines) since they have not recently undergone neurosurgery or have any other competing medical/surgical procedures that co-occur. Finally, participants are often eager to contribute to research and are highly motivated, especially if they report positive clinical outcomes due to their chronic neurostimulator treatment and thus large sample studies are indeed possible to counteract the limited number of brain sites that can be sampled within a single participant.

### 3.3 Stationary single-unit recordings

Neurons are the fundamental units of the brain that can develop highly specialized response patterns to stimuli and work in concert with other neurons to develop circuits supporting cognition by communicating through the firing or action potentials. An action potential is a result of the bulk ion movement across the neuronal membrane of ions including Na<sup>+</sup>, K<sup>+</sup>, Ca<sup>+</sup>, and Cl<sup>-</sup>. Each of these ions perturb the membrane potential, to a degree weighted by the number of ions moving and the difference between the Nernst

potential of that ion and the current membrane potential. Action potential firing is all-or-none, meaning that an action potential will only propagate from one neuron to the next when the presynaptic dendrites depolarize sufficiently to cross a threshold of -45 mV, on average. The action potential concludes with repolarization which has a characteristic hyperpolarization before returning to baseline (J. Gordon Betts, Kelly A. Young, James A. Wise, Eddie Johnson, Brandon Poe, Dean H. Kruse, Oksana Korol, Jody E. Johnson, Mark Womble, 2013). During the repolarization phase, there is a relative and absolute refractory period during which the neuron cannot, or infrequently will fire. These refractory periods correspond to a minimal so-called interspike interval. Neuronal firing of a single putative neuron typically displays an minimal interspike interval of 2.5 ms, in order to obey the biological principle of an absolute refractory period (Quiroga, 2012).

A critical approach in modern developed around studying action potentials and firing properties of putative single neurons (referred to as single neurons) using extracellular recordings (Dayan, 2005). Extracellular single-unit recordings are obtained from electrodes placed in neural tissue that can record the summative electric field potentials of a small volume of tissue that can include a small number of neurons surrounding an electrode. Although extracellular recordings are a common and useful neuroscience methodology in animal models, ethical considerations preclude their analogous use in humans. However, the rare opportunity to record single-unit activity from extracellular electrodes in humans is possible through collaboration with epilepsy patients who are transiently implanted with multiple depth electrodes for clinical purposes. Specifically, this cohort of epilepsy patients undergo neurosurgical placement of 6-12 electrodes in numerous MTL and broader brain regions for multiple-week (typically 1-4 weeks) monitoring of brain activity so that the neurological team can determine the focus of these patients' seizures. While undergoing in-patient monitoring of their intracranial brain activity for clinical purposes, patients can also consent to participate in research in which they complete cognitive tasks while researchers record single-unit and

LFP brain activity, in accordance with an institute's Institutional Review Board procedures.

Single neuron and LFP activity can be recorded from micro-wire electrodes. A widely used and well known electrode is the Behnke-Fried electrode which contains 8 clinical macro contacts and 8 micro-wire electrodes that bore through the macro contacts and splay off of the tip (Fried et al., 2014). The micro-wires are  $\sim 40 \mu\text{m}$  in diameter and can record extracellular activity. Importantly, studies investigating the safety of recordings utilizing these Behnke-Fried electrodes have reported no increases in complications associated with these recordings (Chari et al., 2020).

### 3.3.1 Spike sorting

Since extracellular electrodes record summative electrical activity from multiple neurons surrounding the recording site, a critical analytical step is spike sorting, or the process of decomposing spiking activity into distinct putative neurons (Dayan, 2005; Lefebvre et al., 2016). Principles of spike sorting capitalize on the principle that each neuron has a distinct spike waveform template. This is a result of the unique dendrite arborization that every neuron develops. As such, a particular neurons' unique firing properties, combined with the exact distance and orientation of the neuron relative to the electrode recording location results in a unique and distinct waveform that can be used as a template to distinguish spiking events from different putative neurons, from a neural recording trace. Templates are typically defined by extracting features of waveforms and clustering them into distinct waveform templates. A range of spike sorting methods are frequently used which typically employ feature extraction methods ranging from principle component analysis, wavelets, independent component analysis, among others. Once templates have been established, all detected spikes are compared to templates and a distance metric is optimized to match spikes to the nearest template. Cluster cutting, or spike sorting, can be performed via an algorithm and in combination with user input.

Common clustering methods range from Euclidean distance, superparamagnetic clustering, template matching, K-means, gradient ascent, and others.

One challenge and limitation of spike sorting approaches is that during single-unit recordings from individual micro-wires, in some cases of single neuron recordings from single microwires, activity may be recorded from multiple nearby neurons that cannot be further isolated into single neurons. Evaluation of various parameters are not sufficient to distinguish between the multiple units in these cases. These so-called “multi-units” may be characterized by displaying a greater number of violations of the interspike interval, a noisy baseline, and a broader spike waveform peak. One approach that can minimize the detection of multi-units which cannot be further isolated into single neurons is the use of tetrode electrodes. These four-pronged electrodes record activity from multiple reference points and improve the ability to isolate single neurons based on comparisons of electrical recordings across these four recording sites which are separated by a known, and pre-determined physical distance. However, these tetrodes are not yet available for use in humans. When performing studies of cognitive neuroscience in human single neuron recordings, it is important to identify and remove multi-unit clusters from analysis of tuning properties of single neurons.

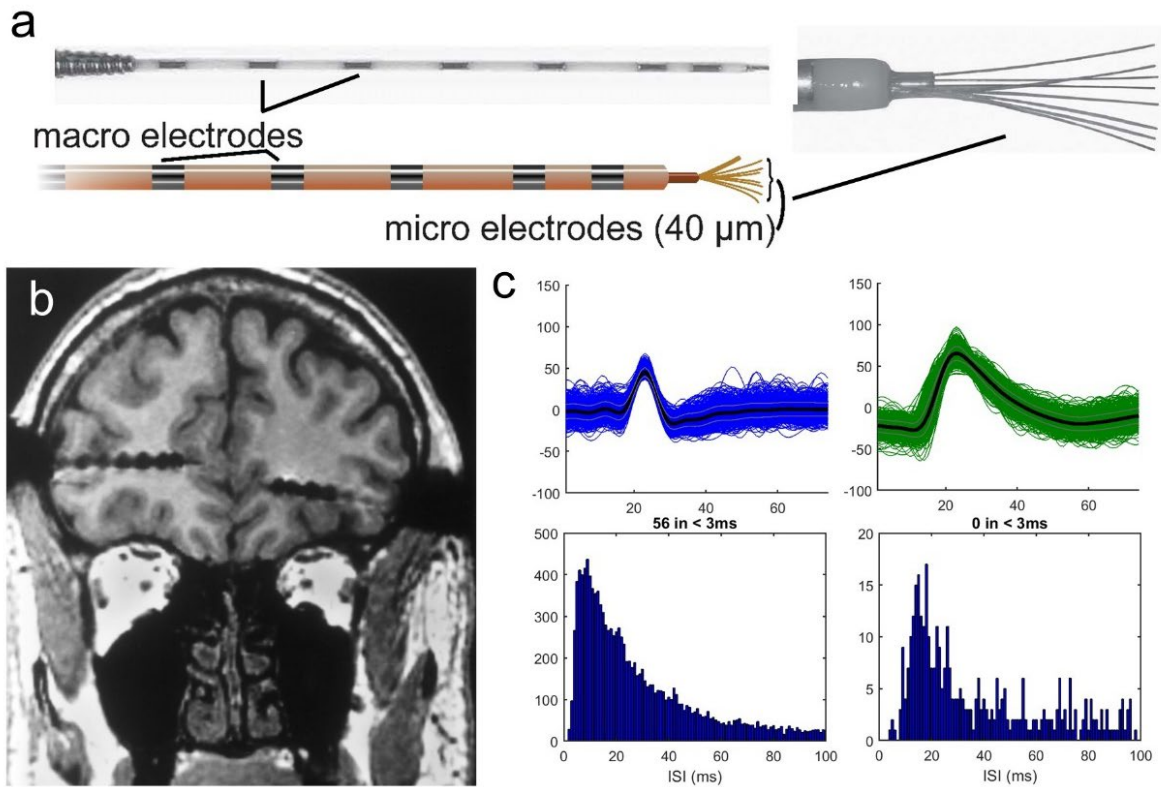


**Figure 3-2. Electrodes used to record human single neurons.** (A) Example Behnke-Fried depth electrode with close-up view of macro contacts used for clinical iEEG recordings and micro-wires protruding off the tip (adapted from Staba, 2014; Mankin et al., 2021). (B) Coronal MRI demonstrating iEEG depth electrodes with microwires protruding from the distal end of the tip, adapted from (adapted from Fried et al., 1999). (C) Two example single neurons. Top, spike waveform. Bottom, histogram of interspike intervals (ISI) for all spikes for each single-unit.

### 3.3.2 Advantages and limitations

Single-unit recordings in humans provide a critical opportunity to observe the natural firing dynamics of single neurons in the brain, which is a rare opportunity to test theories developed in other animal models to identify the differences and similarities in neuron encoding of cognitive processes. Further, single-unit recordings also allow for researchers to investigate the relationship between spikes and ongoing LFP. However,

these recordings are subject to a few notable constraints. Participants must remain immobile during single-unit recordings, since the recording equipment and electrodes involve bulky equipment and long cables that are also subject to significant motion artifacts. Additionally, human single-unit recordings occur in hospital rooms, oftentimes in intensive care units, where extensive medical equipment can introduce electrical noise that can be difficult to isolate from precious single neuron firing. Although post-hoc noise cleaning techniques can minimize the contamination of neural signal, spike sorting can still be influenced by noise in the form of algorithms categorizing noise as putative units. Spike sorting is also limited by the strength of the feature extraction algorithms and template development since there a ground truth is not available, isolated clusters can be treated as putative neurons (thus referred to as single neurons). Further, micro-wire electrodes provide huge insight into single-unit firing, however they do not offer the opportunity to investigate large populations of neurons, rather a single electrode may yield ~5-20 neurons and precluding the ability to study the concerted firing dynamics of a neural population. However, technological advances to develop high-density neural probes are underway and may improve the single-unit recording yield of electrodes in the future.

### 3.4 Virtual Reality

Studies of human cognition traditionally use laptop or screen-based 2-dimensional experimental task designs to present videos or images as stimuli used to interrogate internal processes. How human cognition is represented in the brain during more naturalistic experiences remains an open question. In this chapter, we have described technological advances that are now enabling the study of iEEG in freely walking human participants, ushering in a new era of research studying human cognition in the “real world” and outside of laboratory settings. However, human single-unit recordings still require immobility in the hospital setting. Although efforts are underway to record single-

unit activity in a mobile framework (Topalovic et al., 2023), it can be difficult to generate complex and rich environmental settings in the hospital environment in order to investigate human cognition. As such, VR is a valuable tool for human cognitive neuroscience.

Head-mounted VR displays offer a 3-dimensional and immersive experience with continuously improving and realistic graphics. Head movements and body motion on the display are matched to body movement in the real world to create a seamless interactive experience. Numerous VR headsets are available on the market including the Pico Neo, Meta Quest, HTC Vive, among others. Experimental tasks in VR can be built using readily available and open-source game engines, such as Unity, in which every aspect of an immersive experiment can be controlled by the researcher – from the placement of room landmarks and stimuli, to the consistency and uniformity of environmental textures. Furthermore, VR allows experimenters to deliberately distort reality or to rapidly subject participants to very different environments, tasks, or experiments in a controlled manner. Given the virtual and computer-driven nature of the experience, VR also provides access to quantitative behavioral metrics with a high-temporal resolution. For example, in the real-world it could be challenging to precisely determine the positional accuracy of participant completing an object-location task, while in VR, positional accuracy can be readily accessed, and performance can even trigger alternative game sequelae.

Different VR headsets offer different additional features, such as integrated pupil and gaze tracking or the option of performing VR in both stationary or ambulatory formats. This common dual-movement functionality provides a valuable opportunity to develop experimental tasks that can be used across different neurophysiology recording modalities, such as during both single-unit and also mobile iEEG recordings. As such, VR is a valuable tool for the modern cognitive neuroscientist to deliberately construct environmental tasks in a controlled-reality, providing detailed and quantitative metrics of behavior, and the versatility of being used with multiple neuroimaging approaches.

## 3.5 Current findings

### 3.5.1 Findings from mobile iEEG recordings

Multiple studies have validated long-term recordings obtained from chronically implanted devices by comparing findings of cognition to those identified using acute iEEG recordings (Rao et al., 2017; Henin et al., 2019). A rapid increase in the number of individuals chronically implanted with sensing DBS devices over the past decade has enabled scientists the ability to use mobile iEEG recordings in humans to carry-out, for the first time, cognitive and clinical neuroscience studies in freely moving humans. One such area of study has been to determine whether findings from freely moving rodent studies of spatial navigation translate to humans. The first research study of this kind investigated whether oscillatory activity in the medial temporal lobe (MTL) was modulated by walking speed (Aghajan et al., 2017) (Fig. 3-2A) given that decades of findings emphasized a critical role for rodent MTL theta oscillations (4-8 Hz) in spatial navigation and memory (Bland, 1986). While this study was the first to discover the presence of speed-modulated theta oscillations in the human MTL during freely-moving walking behavior, it also highlighted fundamental species-specific differences between rodents and primates (including humans) worthy of additional investigation in future mobile iEEG studies: Theta oscillations were found to increase in prevalence during faster compared to slower walking speeds in ambulating humans, but their overall presence was less prominent (~10% of the time) compared to that found in freely-moving rodents, a result consistent with recent findings in freely-moving non-human primates (Mao et al., 2021) and replicated in an additional study (Stangl et al., 2021). Another more recent mobile iEEG study found similar levels of theta activity during walking (~10%), but further identified separate behavioral and environmental variables that also modulate MTL theta activity, such as one's own (or another person's) proximity to environmental boundaries (e.g. walls). Furthermore, this spatial modulation of theta power was dependent on cognitive state (Stangl et al., 2021). Future studies are needed to determine



the complex relationship between MTL oscillatory activity and cognitive (e.g., task goal), behavioral (e.g., movement speed, direction, position) and environmental variables (e.g., boundaries, presence of others), which are now enabled with mobile iEEG recordings in humans.

Other research groups have recorded remotely from these chronically implanted devices while participants are going about their daily lives in their home environments. One study explored patient-specific neurophysiological biomarkers relating to inadequate or excess movements in Parkinson's disease in five participants implanted with the Summit RC+S device with electrodes in the motor cortex and subthalamic nucleus. Streaming of neural activity in the home setting was collected and decoded in relation to movement state information obtained from wearable monitors. During data recordings, participants performed normal activities of daily living while wearing a watch that measured movement activity to distinguish bradykinesia and dyskinesia. The authors found that individual patients had unique neural biomarkers (e.g. frequency band associated with movement state) for changes between active and inactive movement states. Across participants, many exhibited coherence between the motor cortex and subthalamic nucleus that discriminated between mobile and immobile states (Fig. 3-2B) (Gilron et al., 2021).

Moreover, there is an ever-increasing scope of research areas that can be investigated using mobile iEEG recordings to advance our understanding of other neurologic and psychiatric diseases. Research studies have begun exploring new clinical applications for chronically implanted sensing and stimulation devices that pave the way for future opportunities to record mobile iEEG from a broader range of brain regions. One group implanted the RNS System in the centromedian-parafascicular region of the thalamus in a case of medically-refractory Tourette syndrome (Molina et al., 2018). A review proposed a possible approach to treat chronic pain by implanting a chronic sensing and stimulating device in a number of potential target thalamic, cingulate, and other

regions (Shirvalkar et al., 2020). Recent efforts have used responsive neurostimulation for the treatment of loss of control of eating in participants with treatment-refractory obesity by implanting the RNS System in the nucleus accumbens (Wu et al., 2020). Another group implanted the RNS System in the amygdala and striatum to significantly improve depressive symptoms in a case of treatment resistant-depression (Scangos et al., 2021a, 2021b). The RNS System has even been implanted in the occipital lobe of blind patients and used to investigate whether stimulation could be used to induce visual percepts (Caspi et al., 2021).

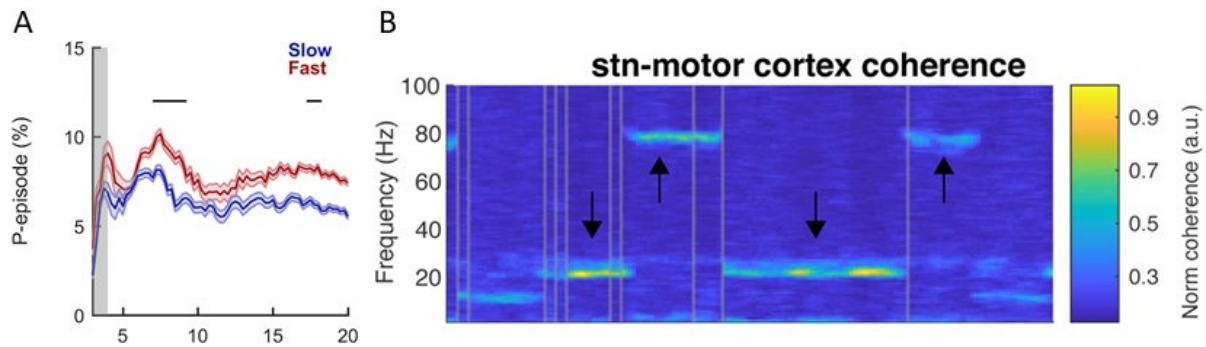


**Figure 3-3. Example findings from mobile iEEG studies.** (A) Theta oscillations increase in prevalence during fast versus slow walking speeds in the medial temporal lobe (MTL, adapted from (Aghajan et al., 2017)). (B) Beta-gamma coherence between the subthalamic nucleus (STN) and motor cortex distinguishes mobile (low dyskinesia, upward arrows) from immobile states (high dyskinesia, downward arrows) in an example participant. Adapted from (Gilron et al., 2021).

Altogether, these results are an exciting foundation highlighting the utility and versatility of a new generation of neurostimulator devices for advancing cognitive neuroscience research. These studies have capitalized on mobile iEEG during a variety of naturalistic behaviors. Additionally, an increasing number of studies are exploring the use of chronic sensing and stimulating devices for the treatment of a broad range of other neurologic and psychiatric disorders. Looking ahead to the future, these studies foreshadow an increasing diversity of brain regions that can be wirelessly recorded from in

naturalistic and chronic environments, expanding the possible scope of cognitive neuroscience research using chronic sensing and stimulating devices.

### 3.5.2 Findings from single-unit electrophysiology

Using view-based VR in a hospital-bed setting, invasive electrophysiological recordings from implanted micro-wires (Fig. 3-2) in patients with epilepsy have identified single neurons that respond in a variety of spatially-selective ways during virtual spatial navigation. In one of the first of these studies, single-unit activity within MTL regions was recorded while participants completed a VR taxi cab driver task where they picked up and delivered virtual passengers to various stores in the environment. Results showed a significant proportion of hippocampal neurons that increased in firing rate at specific locations within the environment (Ekstrom et al., 2003), resembling the activity of place cells in rodents (O'Keefe and Dostrovsky, 1971). A follow-up human single-unit study discovered cells in the entorhinal cortex, which increased in firing rate when a participant was in multiple locations across the environment with activity peaks separated by 60-degree angles making up a hexagonal grid and thus resembling grid cells found in non-human animals (Hafting et al., 2005). Numerous other human single-unit studies using view-based VR have identified cells within the MTL that encode spatial information such as specific locations in the environment (e.g., one's own location or the location of goals), spatial view, path direction, direction and distance to reference points in the environment (e.g., via so-called egocentric bearing cells), or heading direction (Jacobs et al., 2010; Miller et al., 2013; Nadasdy et al., 2017; Tsitsiklis et al., 2020; Kunz et al., 2021). The spatial distribution of these neurons across different brain regions suggests distinct roles for MTL subregions in navigation. For example, while place and grid cells seem to be more prevalent in the hippocampus and entorhinal cortex respectively, other cells such as

those that are view-responsive, egocentric bearing, or responsive to reference points in the environment are more prevalent in the parahippocampal cortex.

A portion of spatially-selective cell types (e.g., place, direction, and egocentric bearing cells) show positive relationships with memory performance, suggesting a general link between spatially-selective cells in the human MTL and episodic memory (Miller et al., 2013; Qasim et al., 2019; Kunz et al., 2021). One study found that place-responsive cells reactivated during episodic memory retrieval of items associated with a specific location in the VR environment that they responded to, supporting the idea that spatially-selective cells in the human MTL contribute more generally to episodic memory (Miller et al., 2013). Another study found a population of cells (i.e., memory-trace cells) in the ERC that increased in firing rate immediately prior to the retrieval of a previously learned VR object-location association even in the absence of the visible object itself (Qasim et al., 2019). Further, these memory-trace cells were significantly active during the retrieval cue period prior to movement towards the remembered location, suggesting a broader role for these neurons in memory representations independent of movement.

Altogether, these findings suggest that many of the single-unit mechanisms discovered in freely-moving rodents are also present in the human brain during stationary view-based virtual navigation, thus bridging decades of findings across species. However, given humans can declare their recollections, these studies have also been able to provide unique insights into human behavior and episodic memory, specifically. Some of these specific findings are noteworthy of discussion such as the increased types of visually-responsive cell types, wider distribution of spatially selective cells across brain areas (i.e., outside of the MTL), and modulation by additional environmental and/or behavioral variables (e.g., task goal or memory recall) in humans.

### 3.6 Technical challenges

Designing and carrying out studies during intracranial human recordings come with several technical challenges. In single-unit recordings, notable challenges include noise, limitations of spike sorting as discussed above, and developing experiments that can be completed within a short (~1 hr time frame). Specifically, completing single-unit recordings in neurosurgical patients in the hospital setting poses a unique set of challenges as the study participants are in a post-operative, post-anesthetic, and sometimes post-ictal state during studies. Given the arduous and tiring nature of these patients' experience in the hospital setting, it is important to design a task that is simple, direct, and short enough (~ 1 hr) that it can maintain the participant's attention without causing unnecessary fatigue. Given the dynamic and complicated nature of completing an experiment in the hospital setting, it is critical to test an experimental task multiple times in pilot participants and to develop a repertoire of quick solutions to common problems that can arise (Mamalek, 2014).

In mobile iEEG studies, challenges include wireless recording of data from the implanted device, integration with other biometric data streams. In mobile iEEG studies, current FDA-approved devices are designed primarily with clinical- and not research-needs in mind. For example, the RNS System and Percept devices themselves do not allow for real-time wireless access and/or control of the implanted neurostimulator, which is critical for designing and carrying out well-controlled mobile iEEG studies. There have, however, been externalized platforms recently developed that allow for external wireless control of and communication with chronic neurostimulation devices (Meisenhelter et al., 2019; Topalovic et al., 2020; Gilron et al., 2021). For example, one such platform is the mobile deep brain recording and stimulation (Mo-DBRS) platform (Topalovic et al., 2020), which provides researchers with open-source tools to enable real-time wireless control of the timing of stimulation, start/stop of iEEG recording, and accurate synchronization of iEEG data with wearable sensors and equipment (e.g., VR/AR

headsets, eye trackers, motion sensors). While the Mo-DBRS platform has been primarily tested with the RNS System (Fig. 3-1A-B), most features including integration with wearable sensors can be extended for use with other implantable neurostimulation devices. Another such system has been developed and shared with the scientific community to enable similar features using the RC+S System, including an open source toolbox that supports pre-processing of raw data, time-alignment across data streams, and basic power calculations (Gilron et al., 2021; Sellers et al., 2021).

Here, we briefly discuss the technical features of one of these platforms, specifically, the Mo-DBRS platform, which includes a Wand (Fig. 3-1C-D) that continuously communicates with the intracranially implanted device via near-field telemetry. With this platform, the Wand is physically connected to a laptop or tablet programmer (carried by the participant in a backpack) to allow for wireless user-based control (e.g., to start and stop iEEG recordings). A custom-built programmer tool interfaces with the laptop or tablet programmer so that the user can programmatically control the Wand to stop/start iEEG data storage and deliver stimulation or synchronization pulses. The programmer tool and consequently the Wand can then be controlled using a wireless control device (e.g., Raspberry Pi) that can be wirelessly controlled by the researcher (manually) or researcher's program. During mobile iEEG experiments, the Wand can be affixed to the participant's head via mechanical solutions that relieve its weight and allow for several hours of comfortable ambulatory movement (Fig. 3-1C) or stationary experiments (Fig. 3-1D). All of the other Mo-DBRS accessories and tools (e.g., laptop or tablet programmer, programmer tool, Raspberry Pi) can fit comfortably within a backpack (Fig. 3-1C) along with any other wearable equipment (e.g., mobile scalp EEG amplifier) during ambulatory behavioral tasks. With these capabilities, the Mo-DBRS platform can thus be fluidly combined and synchronized with wearable sensors for physiological recordings (e.g., heart rate, respiration, skin conductance), eye tracking (for gaze and/or pupillometry), scalp



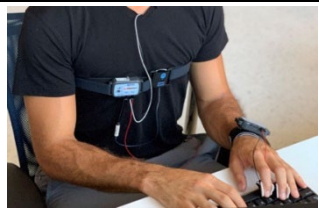
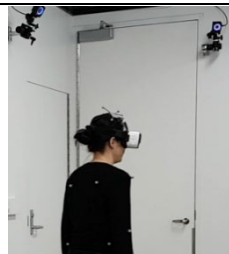
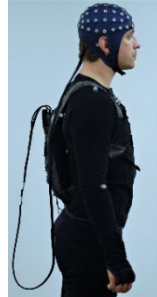



EEG, precise kinematic tracking, and virtual reality (VR) or augmented reality (AR) headsets (see Table 3-2). Precise kinematic tracking, including head position and rotation, as well as information about arm, leg, and torso movements can be captured by wearing a full-body motion capture suit or placing motion capture markers at body joints or appendages of interest.

A critical challenge of experimental design in mobile iEEG studies using any platform is accurate and precise synchronization of neural recordings with behavioral task features and other data streams. For example, a single experiment may incorporate a task delivered on a VR headset with simultaneous full-body motion and eye tracking on independent devices. Such an experiment would result in several separate data streams (iEEG activity, VR task, positional and kinematic variables, and gaze positions), each of which would be recorded with unique time clocks and data acquisition start/stop times. Aligning these separate data streams into the same time scale is critical for relating the behavioral and neural variables that occur at any given point in time. To facilitate data alignment, it is therefore useful to deliver synchronization pulses simultaneously across all data streams. One approach is to use brief electrical deflections (“Mark” artifacts) or stimulation artifacts that are reflected in the iEEG that can be used as synchronization pulses to note the same timepoint as it occurs on all data streams. In the case of Mo-DBRS, the Mark command can be wirelessly initiated by an externalized wireless control device (e.g., Raspberry Pi) and delivered to the implanted device via the head-mounted Wand. In the above example, the same control device can send simultaneous signals to other data streams (e.g., VR task, motion tracking software) to synchronize the corresponding timepoints across all data streams. Previous studies have characterized sufficiently accurate and precise synchronization latencies using this method (Topalovic et al., 2020).

Lastly, the recording of numerous data streams through the use of wearables, audiovisual recordings, and mobile iEEG or single-unit electrophysiology can result in

enormous and complex data sets that are difficult to parse. The use of deep learning and artificial intelligence strategies to analyze these resulting large datasets during complex naturalistic behavioral studies will likely be beneficial for future mobile iEEG studies in humans (Mobbs et al., 2021). Furthermore, synchronization of multiple data streams can be challenging and result in unknown temporal latencies that make relating neural activity to precise behavioral events difficult. Future studies that add/adopt novel data types should characterize synchronization latencies prior to collecting data in participants with chronic sensing neurostimulators.



	Example product	
Eye tracking	<i>Pupil Core (Pupil Labs GmbH)</i> <i>Eyetracking (Tobii AB)</i>	
Heart rate	<i>Smart center bionomadix (Biopac Systems Inc.)</i>	
Respiratory rate	<i>Smart center bionomadix (Biopac Systems Inc.)</i>	
Skin conductance	<i>Smart center bionomadix (Biopac Systems Inc.)</i>	
Motion tracking	<i>OptiTrack Cameras and Motive software (NaturalPoint, Inc.)</i> <i>(Xsens Inc.)</i>	
Scalp EEG	<i>eego sports (ANT Neuro)</i>	
Audiovisual	<i>GoPro 360 (GoPro Inc.)</i>	
Virtual reality	<i>Meta Quest 2 (Facebook Technologies, LLC)</i> <i>Pico neo 2 (Pico Interactive, Inc.)</i> <i>Vive Pro (HTC Corporation)</i>	
Augmented reality	<i>MagicLeap (MagicLeap, Inc.)</i> <i>Hololens (Microsoft)</i>	

**Table 2. Wearable Sensors and Accessories.** Example wearable sensors and accessories that can be integrated with mobile iEEG recordings. From top to bottom: Eye-tracking headsets can record pupillometry, saccades and gaze positions. Other on-body sensors can record heart rate, respiration, skin conductance. Wall-mounted motion capture cameras can track position, speed and other movement variables. Mobile scalp EEG set up is shown with a lightweight backpack carrying the amplifier and connected to the scalp EEG cap. A wearable camera can be used to capture audiovisual data such as for comprehensive documentation of participants' field of view and visible or auditory events. Example virtual and augmented reality headsets are also shown.

### 3.7 Clinical confounds

While recording human brain activity on a single-unit level or during natural ambulation presents a significant scientific opportunity, it is important to be cognizant of the limitations associated with doing such studies. Currently, individuals are implanted with chronic or transient electrodes solely for clinical purposes and thus electrodes are often placed within disease-modified brain tissue. For example, in patients with epilepsy, electrodes are implanted in hypothesized seizure-onset zones. However, because electrode contacts can span up to 10 mm of tissue and often in bilateral brain regions, some contacts may be implanted in tissue that is less affected by disease. One way researchers attempt to characterize the presence of aberrant disease-related neural activity is by isolating any abnormal samples, for example interictal epileptiform discharges (IEDs) in the case of epilepsy. There are several methods currently used to detect IEDs and exclude the affected iEEG, LFP, or single-unit data (Gelinas et al., 2016; Aghajan et al., 2017; Stangl et al., 2021). Additionally, multiple studies have found that neural activity patterns outside the seizure onset zone are unaffected and that normal neural activity patterns occur between epileptic events (Gelinas et al., 2016; Parvizi and Kastner, 2018; Liu and Parvizi, 2019; Akkol et al., 2021). Another way to mitigate the potential contamination of neural recordings with disease-related episodes is by selecting participants that have a low frequency of these events, which can be characterized in

advance given these patients have long-term at-home recordings available to the researcher and/or clinician. In the case of epilepsy, IED event frequency in the recent months preceding the study can thus be available to the researcher and used as a selection criterion for recruiting participants with less disease-related events for mobile iEEG studies.

It is also important to recognize that human studies of intracranial neurophysiology involve working with patient groups who may suffer from cognitive (e.g., memory impairments in epilepsy) and behavioral (e.g. difficulty walking in PD) deficits, and other comorbidities (e.g., depression in epilepsy or PD). This can introduce variability in a study and limit the generalizability of findings. However, as the number of approved indications for which the use of chronic sensing neurostimulation devices increases, the sample of individuals from which to select from will also increase. Thus, those individuals who are better suited for a given study can be preferentially selected in order to minimize variability across the study sample. Further, findings replicated across different clinical groups can lessen the probability that results are due to specific disease-related abnormalities and consequently increase confidence in the generalizability of findings to healthy individuals.

### 3.8 Ethical considerations

Research with patients who have implanted neural electrodes require a protocol approved by an IRB (internal review board) and should minimize risks associated with informed consent. Additional risks associated with mobile iEEG studies should be minimized including to prevent substantial battery drainage, frequency of seizures during the study, and discomfort during behavioral tasks. Across mobile iEEG and single-unit recordings, it is imperative to maintain confidentiality and data security during recording and data transfers. Participants should be made aware of the risks through a fully informed consent process. In the case of mobile iEEG recordings, it is good practice to

allow participants to choose whether stimulation therapy remains on during the recordings. While mobile iEEG studies are ideally carried out without the confound of artifacts due to responsive neurostimulation, the potential risk of increased symptoms (e.g. seizures) can be reduced by inviting participants who have an overall lower frequency of seizure-related activity in the months prior to the research study and thus lower the likelihood of stimulation events occurring during a given research study. Additionally, it is good practice to have a neurologist on the research team that can be available during the study to monitor iEEG activity for the presence of pathological events (e.g., IEDs) or behavioral symptoms. For neurostimulation studies, the level of stimulation administered should be controlled, ideally with a charge density lower than that used for treatment (e.g., less than 10  $\mu\text{C}/\text{cm}^2$ ) (Suthana et al., 2012, 2018). Finally, there is a risk of battery depletion associated with mobile iEEG studies that would lead to the need for more frequent battery-replacement surgeries, especially for research studies that use stimulation and/or real-time data viewing of iEEG data. To minimize this risk, research studies should limit the number of study visits per participant (especially if using stimulation and/or real-time recordings) and/or sample more widely from the population of patients who have chronic sensing neurostimulation devices implanted to prevent the same group of patients from participating repeatedly. In the case of RC+S and other existing and/or future rechargeable battery-powered devices, battery drainage associated with participation in research studies is not a concern.

### 3.9 Promises and future opportunities

Human iEEG single-unit studies provide an exciting and unique opportunity for first-in-human exploration of behavior and cognition in mobile and naturalistic settings and on the level of single neurons. Such studies will help to bridge the gap between findings in freely-moving single-unit and LFP studies in animal models to understand the human neural mechanisms that underlie everyday behaviors such as spatial navigation,

physical movement, and social interaction. Importantly, mobile iEEG studies in humans provide an avenue for cognitive neuroscience studies to no longer be constrained by immobility and limited to artificial laboratory environments. Single-unit studies, though still typically constrained to immobility, provide insight into the single neuron dynamics of human cognition. Future research studies can thus use more realistic environments with higher ecological validity, either by constructing them using advanced 3D-modeling and VR/AR technologies to allow for experimental control or by simply having participants step into novel and complex real-world environments (e.g., outdoor or complex indoor spaces, social experiences) that may be difficult to reconstruct in lab settings. Intracranial recordings, especially combined with VR/AR and the opportunity to enter real-world situations opens the door to countless new questions across countless fields and topics in neuroscience: spatial navigation, episodic memory, emotion, social interaction, exercise, activities of daily living, psychiatric conditions, and sleep, to name a few.

Additionally, ongoing clinical trials using chronically implanted sensing neurostimulators for neuropsychiatric conditions foreshadow increased implantation of these devices in areas relating to altered emotional processing and pathological brain states (e.g., depression, PTSD, OCD, loss of control, panic disorder). This future opportunity opens the field up to many new questions that can be answered to better understand the pathophysiology underlying neuropsychiatric disease without relying only on animal models, as well as advance theories related to how emotional states shape cognition in everyday life experiences.

Finally, chronic neurostimulator devices and single-unit recordings also provide an opportunity for the development of novel closed-loop stimulation paradigms in relation to neural or behaviorally relevant cues. A closed-loop approach allows the experiment to program a change in stimulation pattern in response to a condition that is met. This condition could be detection of a particular neural feature of interest, by online and real-time analysis of neural signals, or it could be more complex and relate a neural feature

with a behavior that is detected. With the increasing data from available from human intracranial recordings paired with multiple biometric data streams, there is a broad range of questions that can be investigated using closed-loop approaches that compare neural activity and behavioral states with and without the presence of stimulation of a particular brain region. This notable methodological advance provides researchers with the ability to test causal questions relating neural activity and behavior under naturalistic settings.

# CHAPTER 4:

## Dynamic neural representations of memory and space in freely moving humans

### 4.1 Introduction

The ability to learn and recall personal experiences, or episodic memories, is critical for everyday life and guiding of future behaviors. Encoding of the environmental (spatial) context in which an episode takes place is important for its successful subsequent recall. The medial temporal lobe (MTL) has long been identified as a brain region essential for successful episodic memory formation within a spatiotemporal context across rodents, non-human primates, and humans alike (Squire, 1992; Squire et al., 2004; Buzsáki and Moser, 2013; Jutras et al., 2013). Current evidence from rodent studies suggests that oscillatory activity in the theta frequency band ( $\sim 6-8$  Hz) (Quirk et al., 2021) in the MTL supports spatial navigation (Winson, 1978; Hasselmo, 2005) and successful memory retrieval (Buzsáki and Moser, 2013; Colgin, 2020) through its ability to temporally organize neural activity locally and across brain regions (Buzsáki and Moser, 2013; Colgin, 2020). However, studies in humans show mixed results (Hanslmayr et al., 2016; Herweg et al., 2020b) regarding the presence of theta activity and its temporal dynamics during retrieval and encoding of subsequently recalled items (Guderian and Düzel, 2005; Kaplan et al., 2012; Herweg et al., 2016). Specifically, a majority of human memory studies identify that lower frequency theta ( $\sim 3$  Hz) activity increases/decreases during encoding/retrieval, thereby also calling into question the role of higher frequency theta oscillations, analogous to those found in rodents, in human memory (Hanslmayr et al., 2016; Herweg et al., 2020b).

Given the difficulty of recording human deep brain activity during physical movement, it is currently unknown if and how MTL theta oscillations flexibly support memory during ambulatory spatial navigation and/or during complex experiences that

involve dynamically changing cognitive demands. Human neuroimaging studies of spatial memory during navigation have traditionally used view-based virtual reality (VR) to simulate movement through an environment while participants remained immobile and restricted due to large recording equipment that is susceptible to motion artifacts. Recent technological advancements in human mobile neuroimaging (Topalovic et al., 2020), however, have enabled the discovery of MTL higher frequency ( $\sim 7$  Hz) theta oscillations that are modulated by physical movement (e.g., walking) (Aghajan et al., 2017; Stangl et al., 2021) and proximity to environmental boundaries (Stangl et al., 2021). Nonetheless, it remains unclear if and how these theta oscillations support successful memory retrieval during ambulatory spatial navigation, and further, how to reconcile their role in flexibly representing both memory and space during a complex behavioral experience.

The current study capitalized on a recently developed mobile neuroimaging platform (Topalovic et al., 2020) that enables wireless recording of intracranial electroencephalographic (iEEG) activity from the MTL during unrestricted ambulatory movement in humans. Freely moving participants performed a spatial memory task in immersive VR environments while movement was simultaneously tracked to examine how memory-related processes and spatial features within the environment dynamically modulated MTL activity. Our results suggest that MTL theta activity reflects both successful memory retrieval and spatial environmental features in a temporally dynamic and flexible manner that can remap based on environmental context and momentary task goals.

## 4.2 Methods

### 4.2.1 Participants

There were 6 participants in the study (33-54 years of age, 4 female, mean = 43.3  $\pm$  s.e.m. = 3.1). All the participants had pharmaco-resistant epilepsy treated with a chronically implanted FDA-approved RNS System (Neuropace, Inc; 320 Model) that



continuously records iEEG activity across 8 contacts (4 bipolar channels). Participants with at least 2 bipolar channels in MTL regions (i.e. hippocampus or entorhinal cortex) were recruited for the study (example electrode placement shown in Fig. 4-1b). The sites of electrode implants were determined by clinical criteria. Further, participants with low seizure activity and thus fewer average daily stimulation therapies were recruited for the study. Informed consent approved by the UCLA Medical Institutional Review Board (IRB) was obtained from all participants.

#### 4.2.2 Spatial memory task in immersive virtual reality

Participants completed an ambulatory spatial memory task in two different immersive VR environments (room dimensions were 5.84 x 5.84 m) where they learned and retrieved various positions of translucent colored cylinders (halos) as discussed in the main text. All VR environments were matched in size to the real-world environment and constructed using the Unity game engine. VR headsets used included the Quest 2 VR headset (Meta, Inc., as seen in Fig. 4-1a) or the Pico Neo 1 and Pico Neo 2 VR headsets (Pico Immersive Pte. Ltd.). Prior to performing the task, participants completed a 5-minute practice version of the task in a distinct virtual environment to provide them familiarity with the immersive VR headset and to engage them in normal walking behavior. The first retrieval block included several repeated sets of retrieval and visible halos, until the participant met a learning criterion (completing 15 consecutive trials with error < 1.5 m). Retrieval block #1 was completed in an identical manner in the second context, immediately following completion in the first context. The starting context (stone or wooden) was counterbalanced across participants. The total number of trials in retrieval block #1 varied across participants (15-30 trials in participants 1-5, Fig. 4-2a, see details in Table 4-1). P6 was unable to learn all halos to meet the learning criterion in retrieval block #1 in both contexts, and as such, was manually advanced to retrieval

block #2 after 40 minutes in each context (69 trials in the stone context, 60 trials in the wooden context). For retrieval block #2 and above there were a fixed number of trials (15 in each block), with the context per block alternating until a total of 2-11 retrieval blocks were completed depending on the time available for each participant (see number of block details by participant in Table 4-1). Total task time took approximately 30 - 200 minutes across participants.

Location and orientation tracking of participants was collected throughout the experiment using submillimeter resolution with the Opitrack motion tracking system using twenty-two high-resolution infrared wall-mounted cameras and MOTIVE application (Natural Point, Inc., see Fig. 4-1a). The cameras sampled the position of a collection of uniquely oriented rigid body position markers located atop the participants head at 120 Hz (Fig. 4-1a). Positional data was compared across VR headsets and Opitrack data collection, and analysis proceeded using VR headset data since positional accuracy was comparable. Movement speed was computed as the change in position between consecutive samples divided by the time lapse between samples. Angular velocity was computed as the change in head rotational dimension (radians) of consecutive samples divided by the time lapse between samples.

#### 4.2.3 iEEG data acquisition

The RNS System continuously records iEEG activity and delivers stimulation in a closed-loop fashion upon detection of abnormal (i.e., epileptic) activity patterns to prevent imminent seizure activity, and is implanted in the skull to support two penetrating electrode leads, 1.27 mm in diameter, with up 4 platinum-iridium electrode contacts spaced either 3.5 mm or 10 mm apart. In each participant, 4 bipolar channels were recorded at a sampling rate of 250 Hz. In accordance with the IRB protocol and with

participant consent, closed-loop stimulation was turned off during the experimental recordings in order to remove potential stimulation artifacts from the data.

For the duration of the experiment, amplifier settings on the RNS System (320 model) were programmed to apply a 1 Hz high pass filter and a 90 Hz low pass filter. Wireless iEEG data was recorded from the RNS System as previously described (Topalovic et al., 2020). Briefly, a ‘Wand’ accessory wirelessly recorded iEEG from the implanted RNS System using near field telemetry. The Wand was positioned on the head, immediately above the implanted RNS System on the patients’ head and secured in a custom-made Wand holder and attached to a backpack to allow for free movement (Fig. 4-1a). Data was stored as a continuous timeseries across channels and storage was remotely triggered wirelessly at the end of each session of continuous blocks. Of note, since there was no wired connection between the implanted RNS System (the recording apparatus), the VR headset, and an external power source, the iEEG data was free from power line noise.

To synchronize iEEG with behavioral data, the Unity application executed on the VR headset was programmed to trigger a signal (mark) wirelessly at specific time points inserted into the iEEG data. These synchronization marks were sent at specified times in the tasks, specifically at the start of each block (see Topalovic et al. (Topalovic et al., 2020) for synchronization details of the setup).

#### 4.2.4 Electrode localization

Precise localization of electrode contacts was performed by co-registering post-operative head CT scans with pre-operative MRI scans (T1 and/or T2-weighted sequences). One example localization of the four contacts on one electrode lead can be seen in Figure 4-1B. Across the six participants, there were nineteen total channels localized to the MTL in regions including the hippocampus, parahippocampal cortex,

perirhinal cortex, and entorhinal cortex. No recording contacts were located in the amygdala. For list of electrode contact localizations of all participants, see Table 4-1.

#### 4.2.5 Detection of epileptic events

Inter-epileptic discharges (IEDs) are abnormal electrical distortions related to epilepsy that can occur intermittently and on an individual basis. IEDs were removed from all iEEG channels prior to normalization of power and all additional neurophysiological analyses. We applied IED detection methods previously described (Gelinas et al., 2016; Aghajian et al., 2017, 2019; Stangl et al., 2021). Briefly, IED detection used a double thresholding approach where for the first threshold, each sample was tested against two criteria to identify IEDs to be removed from analysis: (1) whether the envelope of the unfiltered signal was 6.5 standard deviations away from baseline, and (2) whether the envelope of filtered signals (15-80 Hz bandpass filtered after signal rectification) was 6.5 standard deviations away from baseline activity. Once these IED samples were detected, a second threshold was applied to remove samples surrounding detected IED samples. Specifically, a smoothing gaussian filter with a moving kernel range of 0.1 s was applied to a binary vector with 1's denoting detected IEDs and a threshold of 0.01 was applied to the smoothed vector to identify all samples around and including detected IEDs, all of which were excluded from analysis in order to remove potential residual epileptic activity. In order to remove a wider window around high-amplitude IED events, this method was applied a second time with a higher 7.25 standard deviation cutoff for the first threshold and a wider 0.25 second smoothing window for the second threshold. Using this method, an average 3-7% of samples were removed per channel, similar to previous results (Aghajian et al., 2017; Stangl et al., 2021). We specifically recruited participants with low baseline IED activity based on their historical data from

the RNS System (i.e., average daily number of stimulation events delivered in recent months).

#### 4.2.6 Behavioral analyses

Memory performance was computed as the distance error, or the distance between the position at which the participant pressed the button during retrieval trials to indicate the recalled halo position and the center position of the halo. Immediately after the button press, the participants received visual on-screen feedback of either “Correct!” (if they were within 0.75 m of the halo’s center) or “Incorrect”. To determine whether participants successfully learned halo positions over each experimental session, learning was evaluated by comparing each participants’ mean error (e.g., memory performance) in retrieval block #1 across both contexts (excluding the last 15 trials which met the learning criterion threshold necessary to advance past retrieval block #1 for P1-5) to mean error during their last retrieval block in each context. The mean error performance across the last retrieval block compared to that during retrieval block #1 (before meeting the learning criterion) was evaluated for significance using a pairwise permutation test across participants.

For memory retrieval analyses, correct and incorrect trials were defined from when the participant received instructions to retrieve a particular halo (no visible halo cue was present) until the instance at which they recalled the halo position (button press). Visible halo (feedback) periods were defined from the instance of recall (button press), at which point the halo appeared in its correct location, until the instance at which the participant navigated to the visible halo. Visible halos occurred immediately following both correct and incorrect trials; feedback appeared after correct trials even when participants were within 0.75 m of the halo and thus participants were still required to navigate to the center of the visible halo.

For boundary versus inner room area analyses, we used a method similar to a previous study(Stangl et al., 2021). Since the same room dimensions used in this study were identical to those used in a previous study, the same 1.2 m proximity to boundary (i.e., wall) cutoff was used to separate “boundary” versus “inner” room areas. Furthermore, it is worth noting that the previous study found that the cutoff threshold for separation of boundary (range 0.8 – 1.6 m) did not change the overall boundary modulation observed(Stangl et al., 2021).

#### 4.2.7 iEEG data analysis

Time frequency analysis was performed by computing the oscillatory power at individual frequency steps (1 Hz) between 3-120 Hz using the BOSC toolbox (Seager et al., 2002; Whitten et al., 2011) with a third order Morlet wavelet. Specifically, a 3-cycle Morlet wavelet convolution was applied to every frequency step by using it as a kernel for convolution with the iEEG signal. Amplitude and power were extracted from the resulting signal consisting of complex values. We repeated all analysis with a sixth order Morlet wavelet and the results were qualitatively and quantitatively the same, suggesting the robustness of the results with regards to analysis parameters. Next, each channel’s power timeseries was normalized for each frequency step using the MATLAB “zscore” function (after excluding IED samples).

For bar graphs comparing mean power across a bandpower range (i.e. 6-8 Hz), normalized power was summed over frequency steps (1 Hz) for all samples that fell within a particular task condition of interest (e.g., any sample that occurred during any correct or incorrect trial). Mean normalized power was then computed over the summed bandpower timeseries.

To evaluate the prevalence of significant theta oscillations, we used the BOSC toolbox to detect bouts of at least 2 cycles above 95% chance for 1 Hz frequency steps

between 3-25 Hz as has been done previously (Aghajan et al., 2017; Stangl et al., 2021). Theta prevalence was computed as the percentage of detected bouts out of all relevant task condition samples.

Theta-gamma phase-amplitude coupling was computed using the “modulation index” (MI) between the phase of low frequency (theta) and amplitude of high frequency (gamma) according to the methods described previously (Tort et al., 2009). Specifically, the timeseries was split into two task conditions (samples during correct and incorrect retrieval trials). Phase-amplitude coupling was computed independently on each task condition in 1 Hz frequency steps between 3-12 Hz (low frequency oscillations) and 3 Hz frequency steps between 40-90 Hz (high frequency oscillations) on a channel-by-channel basis. MI was computed for each possible theta-gamma frequency pair (e.g., 3 Hz theta and 40 Hz gamma represents one possible frequency pairing). Each theta-gamma frequency pair modulation index was then normalized to a surrogate distribution for that specific pairing generated by computing 100 iterations in which gamma amplitudes were coupled with randomly shuffled 1-second theta phase segments, as was done previously (Tort et al., 2010; Stangl et al., 2021). For each comparison (e.g. strength of phase-amplitude coupling during retrieval relative to arrow trials), we applied a data subsampling approach (see below) to compare the same number of samples across conditions. The visualized heat map reflects the mean difference between two conditions of the normalized MI across channels and was smoothed for visualization (Fig. 4-8A). To visualize the specific low-frequency phase that high-frequency amplitudes were coupled to, we computed the high-frequency amplitudes across a broad range of high frequencies (40-90 Hz), normalized to a surrogate distribution as described above, and computed the mean amplitude over 18 phase bins ( $20^\circ$  each) ranging from  $0-360^\circ$  of the low frequency oscillations (Fig. 4-8B-C). To evaluate differences in phase-amplitude coupling between task conditions across gamma frequencies, the difference in surrogate-normalized MIs

between retrieval and arrow trials was computed on a channel-by-channel basis. To determine if theta-gamma coupling was significantly stronger between conditions over a broad range of low frequency and high frequency oscillations, we computed permutation tests for the difference in MI between correct and incorrect trials for each possible theta-gamma coupling pair, across channels. Significant differences were shown in yellow and an FDR correction was applied across all comparisons with significant FDR-corrected differences shown in red (Fig. 4-8D). Then, the mean phase-amplitude coupling for theta bandpower and gamma bandpower was computed across MIs for each channel was plotted (Fig. 4-8E, F). The heatmaps depicting differences in MI between conditions and also those illustrating the preferred phase of high frequency oscillatory coupling were smoothed for visualization purposes (using the `interp2` MATLAB function with a smoothing factor of  $k = 7$ , Fig. 4-8A-C).

#### 4.2.8 Statistical comparisons & data subsampling

Statistical comparisons were completed using two-sided permutation tests with 1000 iterations. For comparisons of bandpower arrays between two conditions, the permutation test calculated whether the mean difference between value pairs was significantly different from zero. For comparisons of bandpower ranges across three conditions, one-way ANOVA was used to evaluate differences between conditions, followed by Tukey's test for multiple comparisons. When multiple comparisons were used (i.e., multiple frequency steps in a bandpower analysis), p values were adjusted using the false discovery rate (FDR) (Benjamini and Hochberg, 1995; Benjamini and Yekutieli, 2001).

For top-down maps of theta bandpower (e.g., Fig. 4-5), the room was divided into 19 x 19 bins. Mean bandpower over condition was computed for each bin, specifically the bandpower for all samples in which the participant was positioned in a bin was summed,



then divided by the number of samples the participant occupied in that bin. A gaussian smoothing kernel of 0.2 standard deviations was applied to this heatmap, normalized to the peak power and finally, interpolated (using MATLAB function 'interp2' with  $k = 7$ ) for visualization.

For analyses comparing oscillatory power or theta prevalence between conditions that had a differing number of samples, we performed all calculations on 500 iteratively generated, equally sized subsets of data. Specifically, we first compared the number of samples for all conditions to be compared (e.g., correct, incorrect, and visible halo conditions). For the condition with the fewest number of samples, we applied no correction. For the other conditions, we randomly selected the same number of samples for the fewest-sample condition from the longer timeseries and repeated this step iteratively 500 times, with replacement (using the MATLAB "datasample" function). For each iteration, we computed the parameter of interest (e.g., bandpower), then averaged this parameter of interest across all 500 iterations. We did this on a channel-by-channel basis and used the averaged result for all statistical comparisons and plotting of data.

### 4.3 Results

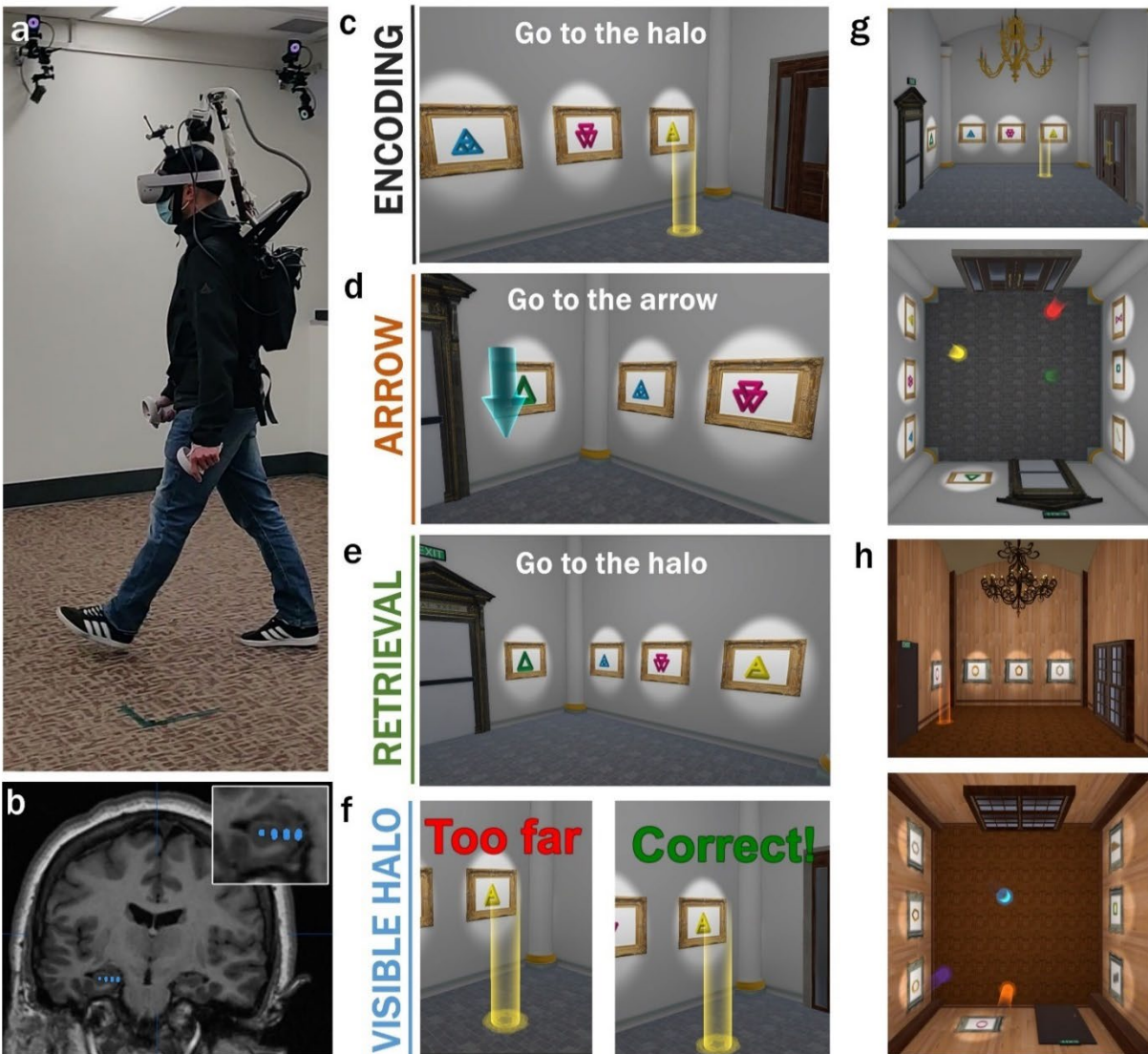


**Figure 4-1. Experimental setup and ambulatory spatial memory task.** (a) Equipment worn by participants including the Mobile-Deep Brain Recording and Stimulation (Mo-DBRS) system that enables recording of intracranial MTL activity (Topalovic et al., 2020), a virtual reality (VR) headset and associated handheld VR controllers. Also shown are wall-mounted motion capture cameras. (b) An example participant’s intracranial electrode contacts (blue circles) localized to the left hippocampus from a post-implant CT registered to a pre-surgical MRI. (c-f) Ambulatory spatial memory VR task showing different types of trials: (c) Encoding trials, which consisted of navigation to multiple distinct visible halos, each presented one at a time (instructions: “Go to the [color] halo”), (d) Arrow trials, which consisted of navigation to a visible arrow randomly positioned along the perimeter of the room (instructions: “Go to the arrow”), (e) Retrieval

trials, which consisted of navigation to previously learned halo positions (halos not visible; instructions: “Go to the [color] halo location & press the button when you arrive”) followed by (f) visible feedback and instructions to navigate to the correct halo position (halo is visible; feedback/instruction: “Too far away!/Correct! Walk to the [color] halo”). (g,h) Each participant completed the task in two different environmental contexts: (g) stone and (h) wooden. Perspective and top-down views of each context with halos visible. Contexts differed in terms of visual appearance (e.g., color/shape of wall artwork, doors, chandeliers, flooring, walls, etc.) but were matched in their geometric layout and placement of visual (wall) artwork. The three halo colors and positions were different between contexts.

#### 4.3.1 Measuring spatial memory using ambulatory VR and motion tracking

We developed a novel ambulatory VR spatial memory task which six participants completed while MTL iEEG activity was recorded (Fig. 4-1a) from a chronically-implanted responsive neurostimulator (RNS) system (Fig. 4-1b, see detailed information in Table 4-1). The spatial memory task was carried out in an immersive room-scale VR environment (5.84 x 5.84 m, Fig. 4-1c-h) during which participants interactively navigated to, learned, and later recalled the position of uniquely colored visible translucent cylinders (halos). The physical movement of participants in the real room was mapped to body position in VR space such that the scene was updated according to each participants’ motion in a one-to-one-manner. The spatial memory task consisted of learning (encoding) trials, arrow trials, and memory recall (retrieval) trials (Fig. 4-1c-f). During encoding trials, participants were instructed to navigate to a halo (Fig. 4-1c, Supplemental video 1) and learn its spatial location. During arrow trials, participants were instructed to navigate to an arrow (Fig. 4-1d) located in the perimeter of the room, which appeared at a new randomized position in each trial. The task began with encoding trials (each repeated with unique halo colors and positions, Fig. 4-1g-h) interleaved with arrow trials. After one encoding and arrow trial was completed for each halo, participants began retrieval trials, during which they were instructed to navigate to a previously learned halo position from

memory and indicate their arrival (recall position) using a button press on a wireless handheld VR controller (Fig. 4-1e). After each retrieval trial, visual feedback (“correct” or “incorrect”) appeared specifying whether the participant responded correctly or incorrectly. At the end of this feedback and regardless of performance, the halo became visible (visible halos, Fig. 4-1f) in its correct position until the participant navigated to its center, providing an opportunity to re-learn the halo position. Arrow trials were also interleaved in between retrieval trials similar to encoding trials. See supplemental video 2 for example retrieval, feedback, and arrow trials. Participants completed the task with 15 retrieval and arrow trials (constituting one retrieval block) and alternated between two environmental contexts (stone room: Fig. 4-1g, wooden room: Fig. 4-1h) each of which contained three halos with unique colors and positions. For further details see *Methods*.

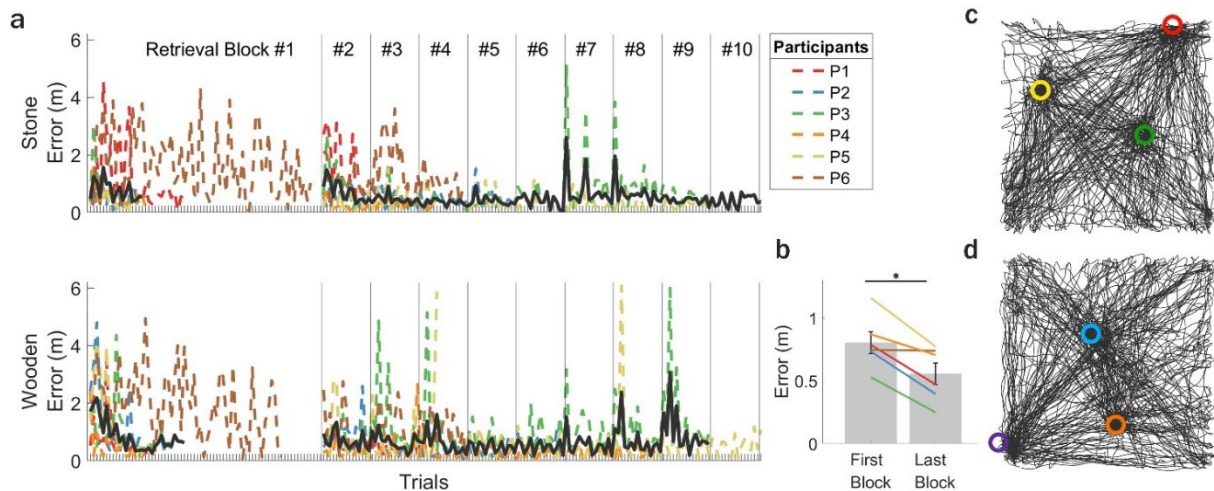


**Figure 4-2. Memory performance during the ambulatory spatial navigation task.** (a) Mean memory performance (error) was measured for each of the six participants (P1-6, colored lines,  $n_{\text{halos}} = 3$  halos) by calculating the average distance between recalled and correct halo locations across trials. The 1<sup>st</sup> retrieval block included a variable number of trials for P1-5 (15-30 trials) depending on when a learning criterion (error for 15 consecutive trials  $< 1.5$  m) was reached. P6 did not show learning during retrieval block #1 and thus was manually advanced to subsequent retrieval blocks. Mean performance across participants is also shown (black line,  $N_{\text{participants}} = 5$  participants, P1-5; P6 excluded due to inability to meet learning criterion). The total number of retrieval blocks varied across participants (5-10 blocks). (b) Difference in

mean error between the first (trials before learning criteria was met) and last retrieval block. Lines show data from individual participants. \* =  $p < 0.05$ . (c-d) Top-down view of an example participant’s walking trajectory collapsed over all encoding, retrieval, and arrow trials in the (c) stone and (d) wooden context. Halo colors and positions are indicated in each of the two environments.

Participant Number		P1	P2	P3	P4	P5	P6
Age		50	38	43	54	33	42
Sex		female	male	male	female	female	female
Total retrieval blocks (stone + wooden contexts):		6	12	18	17	20	8
# of trials in retrieval block #1 Stone		30	15	18	18	15	69
# of trials in retrieval block #1 Wooden		21	30	27	18	21	60
Recording duration (minutes):		32	143	114	103	155	135
Electrode 1	Hemisphere	left	left	left	left	left	left
	Contact Spacing (mm)	3.5	10	3.5	3.5	10	10
	# of MTL channels	2	1	2	2	1	2
	Channel 1 localization	HPP/HPP	HPP/HPP	HPP/HPP	HPP/HPP	ERC/PRC	HPP/HPP
	Channel 2 localization	HPP/HPP	Extra-MTL	HPP/HPP	HPP/PRC	Extra-MTL	HPP/HPP
Electrode 2	Hemisphere	right	right	right	left	right	right
	Contact Spacing (mm)	10	10	3.5	10	10	3.5
	# of MTL channels	1	1	2	2	1	2
	Channel 1 localization	HPP/PRC	HPP/HPP	HPP/HPP	HPP/HPP	ERC/PRC	ERC/ERC
	Channel 2 localization	Extra-MTL	Extra-MTL	HPP/HPP	HPP/HPP	Extra-MTL	PRC/PRC

**Table 4-1. Participant demographics, experimental task info, and localizations of electrodes.** The number of retrieval blocks and trials for the six participants (P1-6) who completed the ambulatory spatial navigation task in the stone and wooden contexts. Localizations of electrode contact pairs for each bipolar recording channel: hippocampus (HPP), perirhinal cortex (PRC), entorhinal cortex (ERC). Extra-MTL indicates contacts that were localized to regions outside of the MTL.

Memory performance during retrieval trials was measured by computing the distance (error) between the recalled position (button press) and the actual halo position (Supplemental video 2). Across participants, mean error was significantly reduced during the last compared to the first retrieval block (see *Methods* for further details,  $p = 0.021$ , pairwise permutation test, Fig. 4-2a-b). The complete trajectory of an example participant over the course of the entire task in each VR environment is shown in Figure 4-2c-d, illustrating adequate and evenly distributed sampling of positions across the room as was

seen in all participants. After retrieval block #1, mean error across participants was 0.56 m ( $\pm 0.01$ , standard error of the mean, s.e.m.). Accuracy was also computed during the same retrieval blocks based on a 0.75 meter (m) radial distance threshold (from the center of the halo), which was used to provide visual feedback to the participant (“correct” or “incorrect”). Accuracy was calculated to be 65% ( $\pm 8.5\%$  s.e.m.) on average across participants. Altogether, these behavioral findings showcase the ability of ambulatory immersive VR combined with motion tracking to be used to precisely assess spatial memory performance in freely moving human participants with simultaneous iEEG recordings.

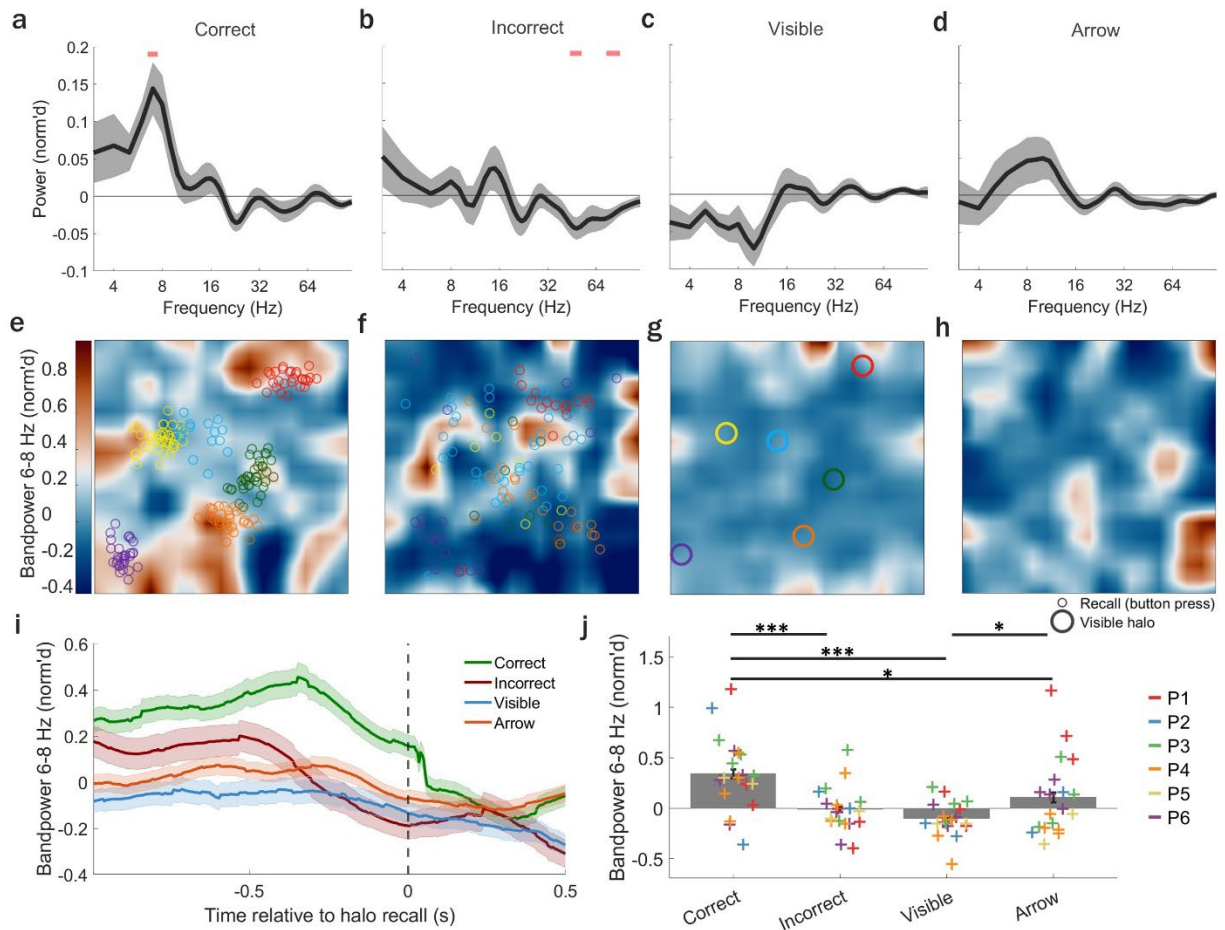


**Figure 4-3. MTL theta bandpower increased during correct compared to incorrect retrieval, visible halo, or arrow trials.**

(a-d) Mean ( $\pm$  standard error of the mean [s.e.m.]) normalized (norm'd) power across MTL channels ( $n_{\text{channels}} = 19$ ) for frequencies 3-120 Hz during the 0.5 s period prior to either the button press during (a) correct or (b) incorrect recall during retrieval trials, (c) arrival at visible halos during feedback, or (d) in the 0.5 seconds prior to arrival at arrows during arrow trials. MTL theta bandpower significantly increased during correct but not incorrect retrieval, visible halos, or arrow trials. Horizontal pink bar indicates significant power increase/decrease ( $p < 0.05$ , 2-sided permutation test, corrected using false discovery rate [FDR] (Benjamini and Hochberg, 1995; Benjamini and Yekutieli, 2001)). (e-h) Top-down view of theta bandpower (6-8 Hz) in an example MTL channel of participant 5 averaged across all samples during retrieval trials (e, correct; f, incorrect) when halos were not visible and during (g) visible feedback when halos were visible and (h) during arrow trials, excluding the 0.5 meters prior to arrival at halos. (e-f) Colored circles reflect recalled locations during retrieval for all correct and incorrect trials. (g) Colored circles reflect locations of halos during visible feedback. (i) Mean ( $\pm$  s.e.m.) norm'd theta bandpower across

MTL channels ( $n_{\text{channels}} = 19$ ). Note, halos were not visible during correct (green) or incorrect (red) retrieval trials. Arrow trials and arrival at arrow (orange). Vertical gray dotted line (time = 0) indicates the moment (button press) when participants arrived at the remembered halo position (correct/incorrect) during retrieval trials or arrived at the visible halo (visible, blue) during feedback, or arrow (orange) during arrow trials. (j) MTL theta bandpower significantly increased during the 0.5 s prior to recall for correct compared to incorrect retrieval trials, visible trials and arrow trials. Circles represent the mean norm'd bandpower across all trials for an individual channel. \* =  $p < 0.05$ , \*\* =  $p < 0.01$ , \*\*\* =  $p < 0.0001$ , FDR corrected.

#### 4.3.2 Successful memory retrieval is associated with increased MTL theta bandpower

We next investigated whether MTL oscillatory activity was modulated by successful memory retrieval. To do this, we first examined power across a range of oscillatory frequencies (3-120 Hz) during the time period around the instant of recall (button press). During this time period, MTL oscillatory power significantly increased only at theta (6-8 Hz) frequencies (6-8 Hz: all individual frequencies  $p < 0.05$ , after correcting for multiple comparisons using the false discovery rate [FDR](Benjamini and Hochberg, 1995; Benjamini and Yekutieli, 2001),  $n_{\text{channels}} = 19$ , Fig. 4-3a-d). Specifically, this theta (6-8 Hz) bandpower was significantly elevated during correct but not incorrect retrieval trials, arrival at visible halos during feedback, or arrival at arrows during arrow trials (Fig. 4-3e) and this increase was specific to the 0.5 s prior to recall ( $p < 0.001$ ; correct vs. incorrect,  $p = 0.015$ ; correct vs. visible halo,  $p < 0.001$ ; incorrect vs. visible halo,  $p = 0.009$ ; correct vs. arrow,  $p = 0.050$ ; arrow vs. incorrect,  $p = 0.339$ ; arrow vs. visible,  $p = 0.012$ ; FDR corrected,  $n_{\text{channels}} = 19$ , Fig. 4-3j, FDR corrected; Supplemental video 3).

Successful memory-retrieval-related increases in MTL theta bandpower were not present over the entire retrieval period (6-8 Hz: all individual frequencies  $p > 0.05$ , FDR corrected,  $n_{\text{channels}} = 19$ ), and further, only occurred in MTL not non-MTL channels (Table



4-1). Specifically, in non-MTL channels ( $n_{\text{channels}} = 5$ ), there were no significant theta bandpower changes during successful (6-8 Hz: all individual frequencies  $p > 0.05$ , FDR corrected) or unsuccessful memory retrieval trials (6-8 Hz: all individual frequencies  $p > 0.05$ , FDR corrected), or during arrival at visible halos during feedback (6-8 Hz: all individual frequencies  $p > 0.05$ , FDR corrected). MTL memory-related theta bandpower increases could not be explained by the presence of a virtual object since halos were not visible during retrieval trials (Fig. 4-3a-b,f-g). An example channel illustrating the effect is shown in Figure 4-3, where MTL theta bandpower peaked near correctly (Fig. 4-3f) but not incorrectly (Fig. 4-3g) recalled halo positions nor visible halo positions (Fig. 4-3h) nor in association with halo positions during arrow trials (Fig. 4-3i).

Given prior studies showing that movement speed modulates the prevalence of theta oscillations (Whishaw and Vanderwolf, 1973; Winter et al., 2015; Aghajan et al., 2017), we evaluated whether there were differences in speed profiles during correct versus incorrect retrieval trials. We found no significant differences in movement speed during correct compared to incorrect retrieval trials nor between retrieval trials and visible feedback during the same 0.5 s prior to recall/arrival at a virtual halo, ( $p = 0.370$ ,  $p = 0.862$ ,  $n_{\text{participants}} = 6$ , Fig. 4-4), suggesting that the observed memory-related effects were not driven by differences in movement speed between conditions. Additionally, there were no significant differences in movement speed between navigation in the stone and wooden context nor between the first-encountered and second-encountered context (since starting context was counterbalanced across participants,  $p = 0.589$ ,  $p = 0.502$ ,  $n_{\text{participants}} = 6$ ). Furthermore, given prior results illustrating that MTL theta oscillations occur in non-continuous bouts in freely ambulating humans (Aghajan et al., 2017; Stangl et al., 2021), and that these bouts are modulated by behavioral variables (e.g., movement speed), we examined whether differences in the prevalence of theta bouts could explain memory-related effects on MTL theta bandpower (Fig. 4-5). We found that MTL theta bandpower

increases did occur in transient bouts and occurred at similar rates compared to previous studies (Aghajan et al., 2017; Stangl et al., 2021), however, the prevalence of these bouts did not significantly differ between task conditions (retrieval vs. arrow vs. visible halo trials,  $p > 0.05$ ; correct vs. incorrect,  $p > 0.05$ ; across all individual frequencies between 3-25 Hz,  $n_{\text{channels}} = 19$ , Fig. 4-5a-c), suggesting successful memory retrieval results in increased MTL theta bandpower in the absence of changes in its prevalence.

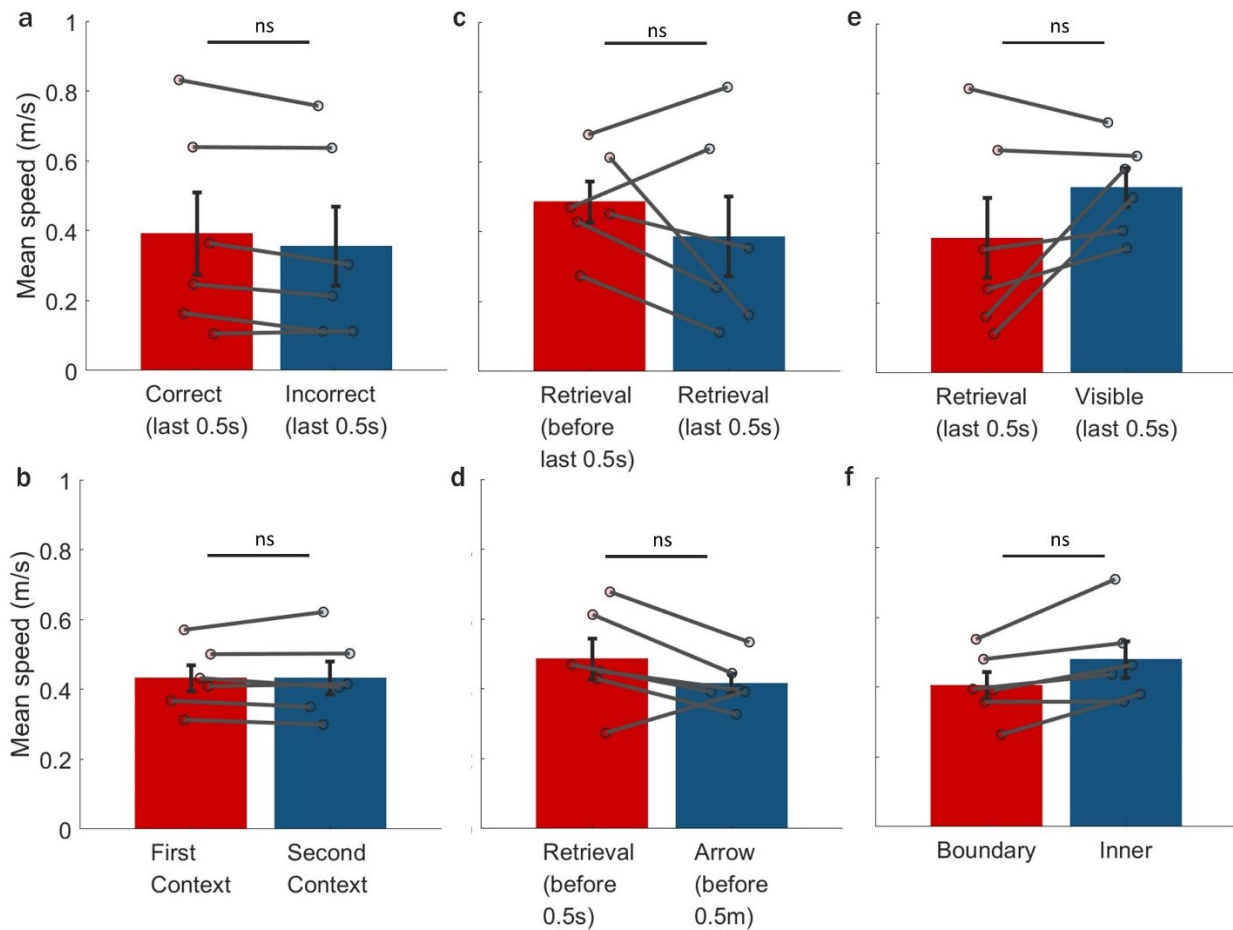


**Figure 4-4. Movement speed during different task conditions.** Mean speed ( $\pm$  standard error of the mean [s.e.m.]) across participants (open circles,  $n_{\text{participants}} = 6$ ), with each gray line indicating participant's mean speed across conditions, compared during (a) correct versus incorrect retrieval trials during the 0.5 s prior to recall, (b) first versus second context, (c) before versus during the 0.5 s prior to recall, (d) retrieval (excluding 0.5 s prior to recall) versus arrow (excluding 0.5 m preceding arrival at arrow) trials, (e) retrieval (excluding 0.5 s prior to recall) versus visible feedback (excluding 0.5 s preceding arrival at visible halo

position), and (f) positions in the boundary ( $< 1.2$  m from walls) versus inner area ( $> 1.2$  m from walls) of the room.  $ns = p > 0.05$ .

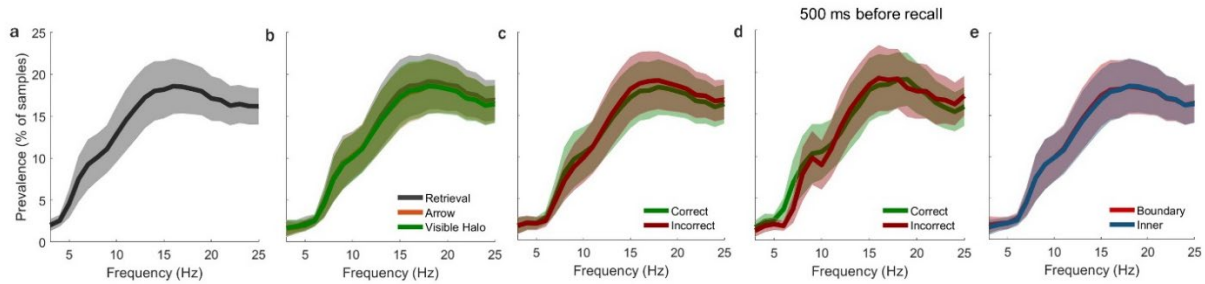


**Figure 4-5. Oscillatory prevalence across task conditions.** Mean ( $\pm$  standard error of the mean [s.e.m.]) oscillatory prevalence across frequencies (3 – 25 Hz) and MTL channels ( $n_{\text{channels}} = 19$ ) during (a) the entire task, (b) retrieval, arrow, and visible halo trials, (c) correct and incorrect retrieval trials, (d) correct and incorrect retrieval trials specifically during the last 500 ms prior to recall, and (e) boundary ( $< 1.2$  m from room walls) and inner ( $> 1.2$  m from room walls) room positions. No significant differences were found in oscillatory prevalence across frequencies (3 – 25 Hz) for any conditions shown (b-e).

#### 4.3.3 MTL theta bandpower is modulated by spatial position

Next, we investigated whether MTL theta oscillations were modulated by one's location in the environment. To do this, we used data from both contexts (stone and wooden) and computed MTL theta bandpower across positions, separately in each room, during retrieval (when halos were not visible) and arrow trials (when arrival positions at arrows were excluded). We first excluded iEEG data from retrieval periods that showed memory-related modulation (last 0.5 s before recall). In this way, we could determine whether MTL theta bandpower was modulated by spatial position, independent of the moment of recall or arrival at a target goal halo position. Excluding the last 0.5 s prior to recall in this way, resulted in exclusion of the time window (as well as proportional spatial distance) preceding the physical arrival at the target (goal) halo on any given retrieval trial. Thus, this analytic approach retained instances when participants incidentally

traversed non-visible previously-learned (non-target) halo positions along the participants' trajectory to the goal halo location.

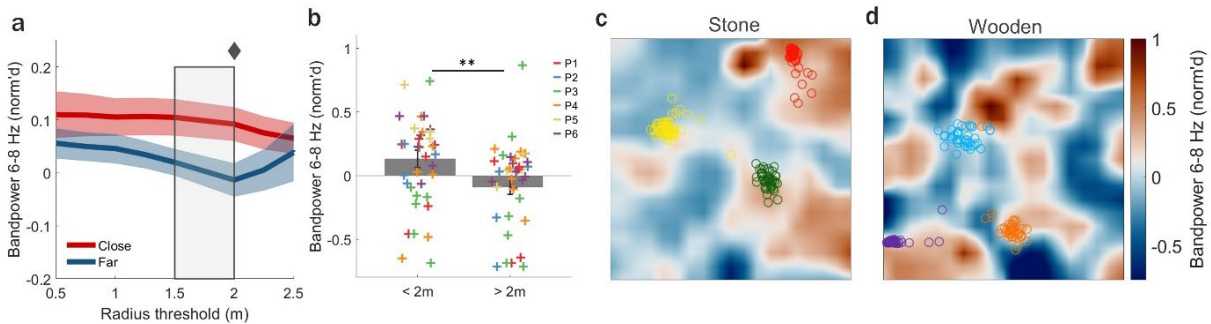


**Figure 4-6. MTL theta bandpower increased at non-target halo positions.** (a) Mean normalized (norm'd) theta (6-8 Hz) bandpower during retrieval trials (excluding last 0.5 s prior to recall of target halos) in positions close versus far from non-target halo positions shown across varying radius (distance to halo) thresholds used to determine the cutoff between 'close' and 'far' positions. Gray box highlights radius thresholds where theta bandpower significantly differed between 'close' and 'far' positions ( $p < 0.05$ ). Diamond indicates significant radius threshold (2 m) after correcting with false discovery rate [FDR]. (b) Mean norm'd theta bandpower significantly increased in positions close to ( $< 2$  m, red) versus far away ( $> 2$  m, blue) from non-target halo centers. Crosses represent mean norm'd bandpower for each channel during retrieval trials, excluding the last 0.5 s prior to recall of a target halo with colors corresponding to individual participants. (c-d) Top-down view of theta bandpower in an example channel across room positions, during retrieval trials, when no visible halos were present, and excluding the 0.5 s preceding recall of target halos. Circles represent positions where target halos were recalled (button press), split by stone (c) and wooden (d) contexts. \* =  $p < 0.05$ .

We examined MTL theta bandpower when participants were in positions that were classified as 'close' to or 'far' from the non-visible non-target halos during participants' trajectories to the target halo (of which the 0.5 s prior to target halo arrival was excluded). MTL theta (6-8 Hz) bandpower was significantly increased at 'close' compared to 'far' distances relative to the non-visible non-target halo positions. The difference in MTL theta bandpower between 'close' and 'far' positions peaked at a distance threshold of

2 m from non-target halo positions (distance thresholds of 1.5 and 2 m: both  $p < 0.05$ ,  $n_{\text{channels} \times \text{conditions}} = 38$ , Fig. 4-6a-b). Furthermore, the spatial distribution of theta (6-9 Hz) bandpower increases was specific to relevant positions within each context separately (stone:  $p = 0.033$ ; wooden:  $p = 0.044$ ,  $n_{\text{channels}} = 19$ ) suggesting that MTL spatial representations can remap based on the perceived environment (see example channel showing theta activity in the stone (Fig. 4-6c) and wooden (Fig. 4-6d) context). Since halos were not visible for the duration of the examined period, and since the 0.5 s leading up to recall and arrival at the to-be-retrieved target halo were removed, these results suggest that MTL theta bandpower increased incidentally at meaningful spatial positions within a familiar environmental context.

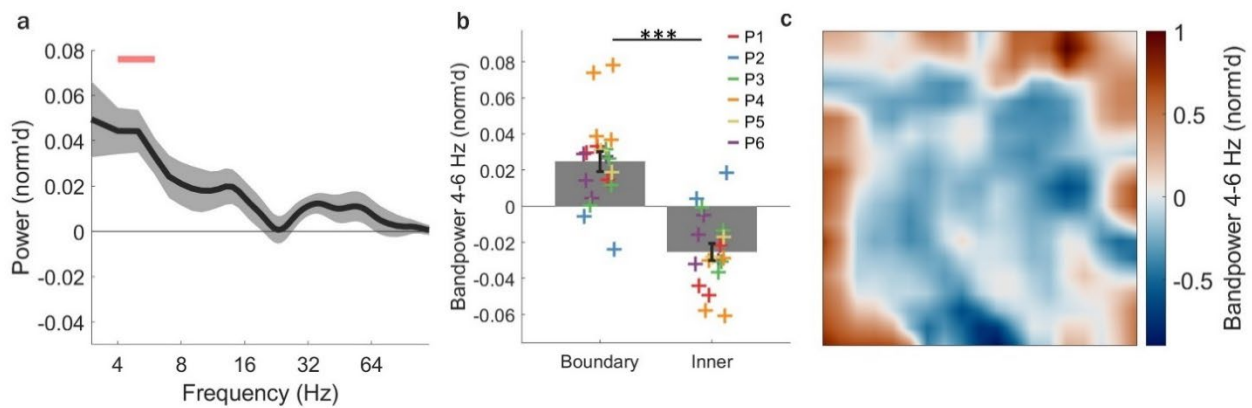


**Figure 4-7. MTL theta bandpower is modulated by position relative to environmental boundaries.** (a-b) Analysis performed over arrow trials, excluding the 0.5 m leading up to arrival at arrows. (a) Mean ( $\pm$  s.e.m.) normalized (norm'd) difference in power across frequencies (3-120 Hz) and MTL channels ( $n_{\text{channels}} = 19$ ) between positions near (within 1.2 m of walls, based on prior work(Stangl et al., 2021)) versus away from boundaries. Significant differences in norm'd power in boundary compared to inner positions occurs for theta frequencies (4-6 Hz, horizontal pink bar =  $p < 0.05$ , corrected using false discovery rate [FDR]). (b) Mean  $\pm$  s.e.m.) norm'd theta bandpower (4-6 Hz) across MTL channels ( $n_{\text{channels}} = 19$ ) for boundary and inner positions. Crosses represent individual channels with colors corresponding to individual participants.

\*\*\* =  $p < 0.001$ . (c) Top-down view of norm'd theta (4-6 Hz) bandpower in an example channel for data across the entire task, excluding the 0.5 leading up to arrival at arrows.

We next examined how MTL oscillatory power was modulated by spatial positions near room boundaries (e.g., walls), based on evidence of boundary-related representations identified in a prior ambulatory spatial navigation study in humans (Stangl et al., 2021). Since the VR room dimensions in our study were identical to those in this previous navigation study (Stangl et al., 2021), we used the same boundary-inner room area cutoff of 1.2 m from the wall. Across widespread (3-120 Hz) oscillatory frequencies examined, mean power significantly increased at boundary compared to inner-room positions only for theta frequencies (4-6 Hz) during arrow trials (excluding 0.5 m prior to arrow arrival: 4-6 Hz: all individual frequencies  $p < 0.05$ , FDR corrected,  $n_{\text{channels}} = 19$ , Fig. 4-7a; boundary versus inner:  $p < 0.001$ , Fig. 4-7b;  $n_{\text{channels}} = 19$ ). Conversely, there were no significant differences in mean theta bandpower between boundary and inner room positions during memory retrieval trials (4-6 Hz: all individual frequencies  $p > 0.05$ , FDR corrected,  $n_{\text{channels}} = 19$ ). Boundary-related power increases were also observed at higher frequencies during arrow trials (12-14, 31-35 Hz, all individual frequencies  $p < 0.05$ , FDR corrected,  $n_{\text{channels}} = 19$ ) similar to a previous study (Stangl et al., 2021). The boundary-related theta bandpower increase was also present when looking at data over the *entire* task (again, excluding data from positions within 0.5 m of arrow arrival, 4-6 Hz bandpower,  $p < 0.001$ ) and can be seen in an example channel in Figure 4-5C. Importantly, boundary-modulation of theta bandpower was not due to changes in movement speed, given that there were no significant differences in mean movement speed when participants were in the “boundary” compared to “inner” room positions, across participants ( $p = 0.852$ ,  $n_{\text{participants}} = 6$ , Fig. 4-4f). Also, theta prevalence was not significantly different between “boundary” and “inner” positions ( $p > 0.05$ , across all individual frequencies 3-25 Hz,  $n_{\text{channels}} = 19$ , Fig. 4-5d)

similar to a previous study (Stangl et al., 2021). Notably, boundary-related modulation of MTL theta bandpower was not present during retrieval trials, with or without the 0.5 s of data preceding recall included (all retrieval trials:  $p = 0.152$ ; excluding 0.5 s preceding recall:  $p = 0.188$ ; boundary versus inner, 4-6 Hz bandpower,  $n_{\text{channels}} = 19$ ), potentially due to competing modulation of theta activity by non-visible non-target halo positions during retrieval search periods as discussed previously. Taken together, these results illustrate that MTL theta bandpower can be dynamically modulated by critical positions (e.g., that previously contained relevant objects or were closer to walls) depending on environmental context or task goal.

#### 4.3.4 Theta bandpower fluctuations are robustly driven by memory accuracy or proximity to boundaries and not by movement variables

Although the greatest modulation of theta bandpower during correct, relative to incorrect, trials was observed at 0.5 seconds prior to retrieval, we evaluated the robustness of this memory modulation across a broad 3-120 Hz frequency range and over time windows leading up to retrieval (Fig 4-8a,b). Across time windows of 0.25, 0.5, 0.75, 1, and 2 seconds prior to recall, we found that correct trials exhibited significant increases in theta bandpower ( $\sim 6$ -8Hz, all individual frequencies  $p < 0.05$ , FDR corrected, Fig 4-8a) while there were no significant increases in theta bandpower in the 0.25 – 2 s time window during incorrect trials (all individual frequencies  $p > 0.05$ , FDR corrected, Fig 4-8b).

Although theta oscillations were not modulated by correct or incorrect memory performance over the entirety of retrieval trials (6-8 Hz: all individual frequencies  $p > 0.05$ , FDR corrected,  $n_{\text{channels}} = 19$ ), we next investigated whether theta power was modulated by subsequent memory performance across time windows immediately after cue presentation. Across 0.25 – 2 s time windows immediately following cue presentation, there were no significant deflections of theta bandpower in correct or incorrect trials (6-8

Hz: all individual frequencies  $p > 0.05$ , FDR corrected,  $n_{\text{channels}} = 19$ , Fig 4-8c-d). In the 2 second time window following cue presentation, low frequency oscillations were significantly elevated in both correct and incorrect trials (3-4 Hz: all individual frequencies  $p > 0.05$ , FDR corrected,  $n_{\text{channels}} = 19$ ). In addition to the observation that theta oscillations were not modulated in the 0.5 s prior to arrival to visible halos or arrows (Fig 4-3c-d), we did not find significant modulation of theta bandpower in the 0.25 – 1 second prior to arrival at visible halos/arrows (6-8 Hz: all individual frequencies  $p > 0.05$ , FDR corrected,  $n_{\text{channels}} = 19$ , Fig 4-8e-f).

Next, we examined the robustness of the boundary modulation of theta bandpower effect (Fig. 4-7a) over a wide range of boundary definition thresholds. Across boundary thresholds of 0.8 – 1.8 m away from walls, theta oscillations were significantly elevated in boundary relative to inner positions over the entire task (4-6 Hz: all individual frequencies  $p < 0.05$ , FDR corrected,  $n_{\text{channels}} = 19$ , Fig. 4-8g). During arrow trials in which the 0.5 m prior to arrival at an arrow was excluded, theta bandpower was also significantly higher in boundary relative to inner positions for boundary thresholds of 0.8 – 1.4 m (excluding 0.5 m prior to arrow arrival: 4-6 Hz: all individual frequencies  $p < 0.05$ , FDR corrected,  $n_{\text{channels}} = 19$ , Fig. 4-8h).



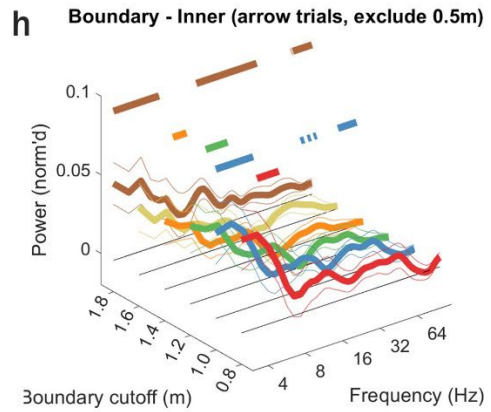
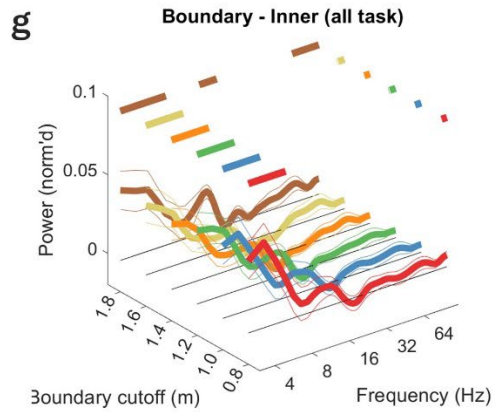
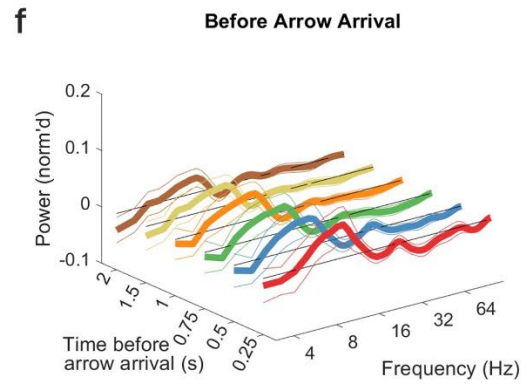
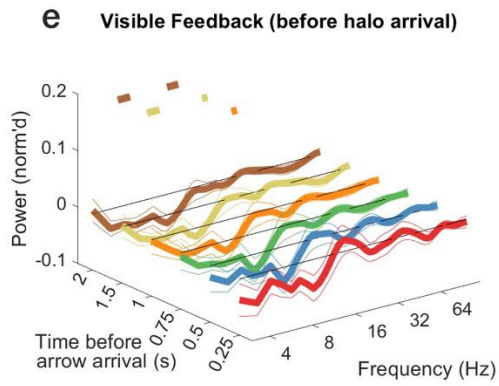
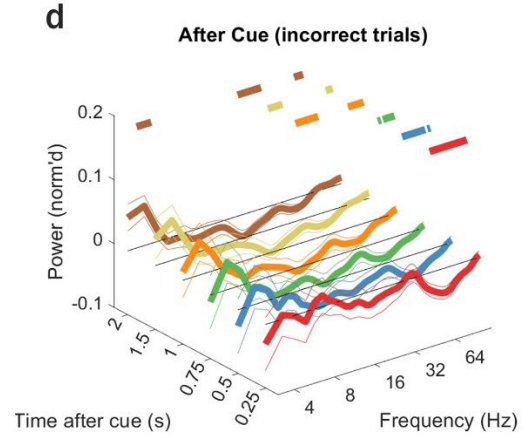
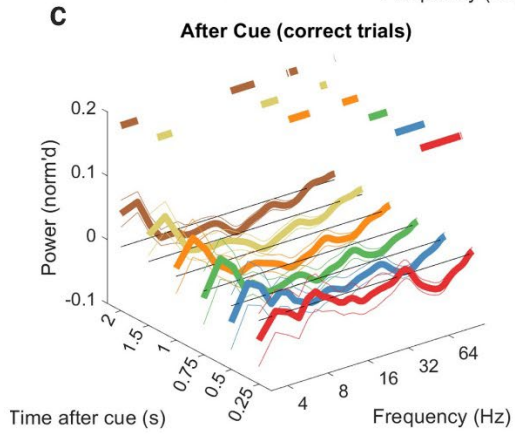
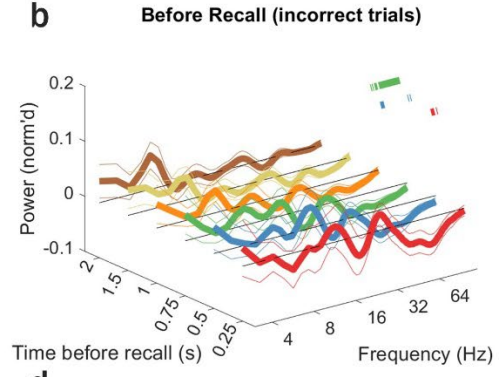
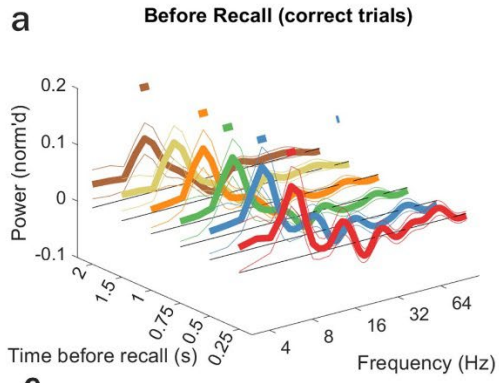


**Figure 4-8. Robustness of memory and spatial modulation of theta power.** Mean ( $\pm$  standard error of the mean [s.e.m.]) normalized (norm'd) power across MTL channels ( $n_{\text{channels}} = 19$ ) for frequencies 3-120 Hz for varying time windows relative to task periods of interest. ) 0.25 – 2 seconds (a-b) prior to recall in (a) correct and (b) incorrect trials, (c,d) after cue presentation in (c) correct and (d) incorrect trials, (e) before arrival at the visible halo during visible feedback periods and (f) before arrival at an arrow during arrow trials. Varying over boundary threshold cutoffs ranging between 0.8 – 1.8 m away from walls for (g) entire task and (h) arrow trials, after excluding the 0.5 meters before arrival at an arrow. Horizontal bar indicates significance,  $p < 0.05$  for all frequency steps, corrected using false discovery rate [FDR].

Many movement variables have been linked to variations in theta power. One key advantage of VR is that it provides access to quantitative and instantaneous movement metrics including speed, angular velocity, and head rotation. To evaluate whether speed, angular velocity, or head rotation significantly explained the variation in theta bandpower fluctuations, we developed a linear mixed-effects model approach. We also incorporated variables reflecting the memory and spatial encoding effects previously seen. Specifically, we included a measure of the momentary distance to position of recall, distance to nearest boundary, quantitative final distance error for the current trial ('Trial Error') and a binary 'Correct' versus 'Incorrect' label for each trial in line with previous analyses presented in this chapter (Fig. 4-9a). During memory retrieval, memory-related cognitive variables were statistically significant predictors of the variation in theta bandpower (distance to recall:  $\beta$  coefficient -0.0915,  $p < 0.001$ ; trial accuracy (error):  $\beta$  coefficient -0.0717,  $p = 0.0340$ ;  $n_{\text{participants}} = 6$ , Fig. 4-9a).

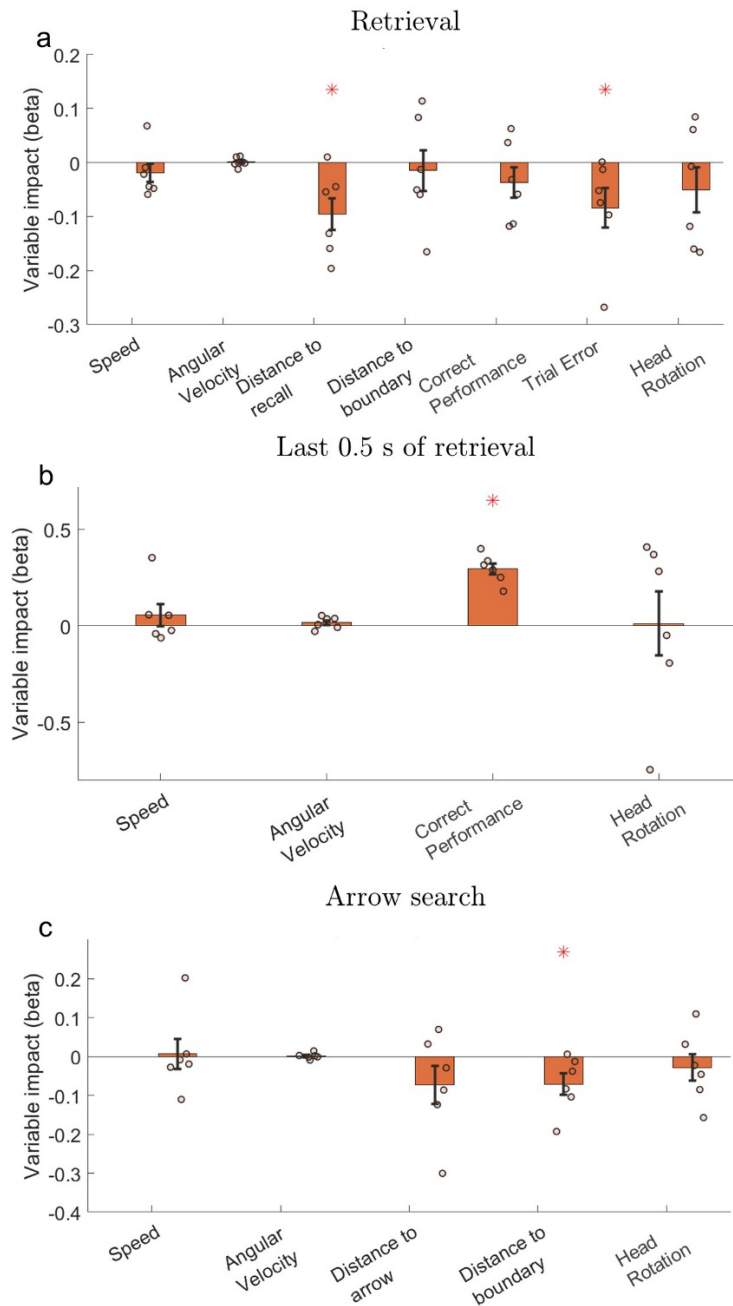


**Figure 4-9. Memory accuracy and proximity to boundaries drive theta bandpower fluctuations.** Linear mixed-effects models were calculated to predict each participant's normalized theta bandpower timeseries by a range of predictor variables that were fixed effects with samples blocked according to channel identity. (a) The models developed for the retrieval period (when no halos were visible) are summarized. Speed, angular velocity, distance to recall (position of button press), distance to boundary (nearest wall), and trial performance (distance error at position of recall) were continuous variables. Correct and incorrect was a

binary variable and head rotation was a categorical variable comprised of 12 possible binned movement directions (with the mean beta coefficient over all 12 levels depicted). (b) The models developed for the last 0.5 seconds of the retrieval period (when no halos were visible) are summarized. (c) The models developed for the arrow search period are depicted. All variables are defined as in (a), with the addition of the continuous distance to arrow variable reflecting momentary proximity to the visible and target arrow position. Asterisks denote a significant impact of a variable on theta power ( $p < 0.05$ , uncorrected). Significance was determined for each variable by testing whether the variable's beta weight was significantly different from zero in a one-sided permutation test across participants. Error bars show the standard error of the mean across  $n_{\text{participants}} = 6$ .

We also developed a separate model to evaluate the impact of speed, angular velocity, and head rotation movement variables on the memory effect observed in the last 0.5 seconds prior to recall during retrieval trials by incorporating these variables with trial performance (binary correct vs incorrect; Fig. 4-9b). This model confirmed that correct relative to incorrect memory performance drives theta bandpower fluctuations in the 0.5 second window prior to recall, and notably other movement variables were not significant predictors.

We developed a separate model, following the same principles, to determine the driving variables during the arrow search trials that represented the non-memory phase of the task. For this model, we incorporated a metric of the instantaneous distance to position/arrival to the visible arrow (Fig. 4-9c). During arrow search periods, proximity to the nearest boundary was a significant predictor of theta bandpower (distance to boundary:  $\beta$  coefficient -0.0706,  $p = 0.0320$ ,  $n_{\text{participants}} = 6$ ). Interestingly, proximity to the visible arrow targets was not a significant predictor of fluctuations in theta bandpower in this model (distance to arrow:  $\beta$  coefficient -0.0728,  $p = 0.116$ ,  $n_{\text{participants}} = 6$ ), suggesting that in the memory retrieval model, the memory demands is a critical component to significant drivers of theta bandpower fluctuations.

Taken together, linear mixed-effects modelling revealed that during memory retrieval, memory accuracy, binary memory performance, proximity to recall position and during arrow search, proximity to boundaries were important drivers of fluctuations in theta bandpower. In both models, the movement variables were not significant predictors of theta bandpower, emphasizing that memory and spatial variables dominated during memory- or arrow search- phases of the task, respectively.

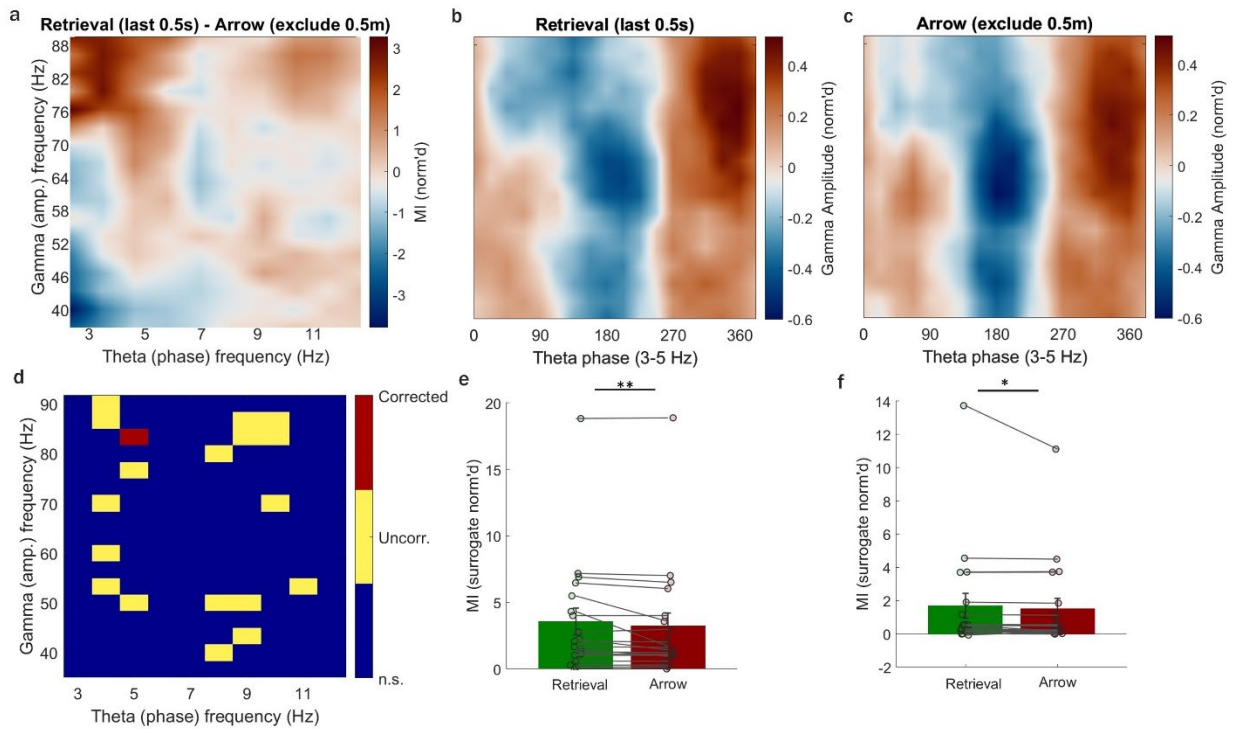


**Figure 4-10. Theta-gamma phase-amplitude-coupling is increased during correct retrieval trials.** (a) Phase-amplitude coupling was calculated using a modulation index (MI) between phases of low-frequency (theta) oscillations and the amplitude of high-frequency (gamma) oscillations normalized (norm'd) to a surrogate distribution per frequency pair. The heatmap reflects the difference in normalized MI values during the retrieval trials (last 0.5 seconds) and arrow trials (excluding the last 0.5 m prior to arrival at arrows), in an example channel. (b,c) Mean gamma amplitude (normalized to a surrogate distribution) over phases of theta (0-360°; segmented into 18 phase bins of 20° each) for theta bandpower (3-5) Hz during retrieval trials (last 0.5 seconds; B) and arrow trials (excluding the last 0.5 m prior to arrival; c). (d) Permutation tests were performed to test whether pairwise comparison of retrieval (last 0.5 s) minus arrow (excluding 0.5 m) phase amplitude coupling was significantly different from 0 for each theta-gamma pairing across all channels with

statistically significant ( $\alpha = 0.05$ ) pairings shown in yellow (uncorrected) and red (corrected using false discovery rate [FDR]). Significant theta-gamma coupling was observed at (82 Hz) gamma amplitudes coupled to (5 Hz) theta phases after FDR correction. (e) Significant (pairwise) difference in normalized MI between retrieval compared to arrow trials is shown for theta (3-5 Hz) phase and gamma (50-90 Hz) gamma amplitude, with circles indicating average values from individual channels ( $n_{\text{channels}} = 19$ ). (f) Significant (pairwise) difference in normalized MI between retrieval compared to arrow trials is shown for theta (6-11 Hz) phase and gamma (40-60 Hz) gamma amplitude, with circles indicating average values from individual channels ( $n_{\text{channels}} = 19$ ). \*  $p < 0.05$ , \*\*  $p < 0.01$ .

#### 4.3.5 Coupling between theta and gamma oscillations during retrieval and directed search

Prior work has highlighted that synchronous theta and gamma oscillations (around 40-90 Hz) are associated with memory retrieval (Hanslmayr et al., 2016) and that theta-gamma phase-amplitude coupling occurred during a freely-moving spatial navigation task (Stangl et al., 2021). We sought to determine if similar theta-gamma phase-amplitude coupling was associated with memory retrieval during freely moving navigation and if phase-amplitude coupling during retrieval trials was stronger than during task periods without a memory demand (arrow trials). We computed a Modulation Index (MI) to measure whether theta (phase) and gamma (amplitude) cross-frequency coupling increased during retrieval trials (specifically in the last 0.5 s where there was a memory effect) and in arrow trials (excluding the 0.5 m prior to arrival at arrow positions). MI values were computed for each theta-gamma frequency pair and normalized to a surrogate distribution (Tort et al., 2010), and the difference between the MI during retrieval and arrow trials on each channel was computed (difference in MI in an example channel shown in Fig. 4-10a). Gamma amplitude specifically coupled to a theta phase of  $90^\circ$  and  $270^\circ$  during retrieval and arrow trials (Fig. 4-10b-c). We found that theta-gamma coupling was stronger during retrieval relative to arrow trials after correcting multiple comparisons (5 Hz and 82 Hz,  $p < 0.001$ , individual permutation tests per frequency pair, FDR corrected,  $n_{\text{channels}} = 19$ , Fig. 4-10d). Specifically, coupling of theta and gamma oscillatory bands was significantly

stronger during retrieval compared to arrow trials for low theta (3-5 Hz) and gamma (50-90 Hz) frequencies ( $p = 0.009$ ,  $n_{\text{channels}} = 19$ , pairwise permutation test, Fig. 4-10d) and for high theta (6-11 Hz) and gamma (40-60 Hz) frequencies ( $p = 0.045$ ,  $n_{\text{channels}} = 19$ , pairwise permutation test, Fig. 4-10f).

#### 4.4 Discussion

We have shown that human MTL theta bandpower is modulated dynamically by successful memory retrieval and spatial position depending on environmental context and momentary behavioral demands. This study is the first to our knowledge to combine simultaneous ambulatory iEEG recordings and immersive VR, thereby providing proof-of-concept data for a novel behavioral paradigm for use in freely moving humans. Using this platform, we were able to investigate how MTL oscillations represent memory and space flexibly during an ambulatory spatial navigation task that involves changes in context and behavioral demands. Our findings highlight two phenomena, one related to memory recall and the other to spatial position.

First, we find that MTL theta bandpower is elevated 0.5 s prior to the moment of recall when the item being remembered (halo) is not visible and only when it is recalled correctly. This specific temporal pattern of theta bandpower increase, albeit of a higher frequency, echoes a previous finding in stationary humans showing hippocampal reinstatement of low frequency theta oscillations during early retrieval time windows, specifically within the first 0.5 s after a retrieval cue was presented (Griffiths et al., 2021). Additionally, our findings that theta bandpower is elevated only during successfully recalled trials is in line with prior reports from human iEEG studies that identify low-frequency theta activity being modulated by memory performance during stationary view-based spatial memory tasks (Miller et al., 2018; Solomon et al., 2019a; Herweg et al., 2020a; Vivekananda et al., 2021). It is possible that the higher frequency theta effects seen

here are due to the fact that participants were physically navigating to recalled locations. Importantly, we found no significant differences in speed profiles during correct versus incorrect memory retrieval trials or task conditions (memory retrieval, or arrival at arrows or visible cues) and speed was not a significant predictor of theta bandpower fluctuations in any of the models for retrieval or arrow search periods, suggesting MTL high-frequency memory-related theta bandpower changes were not driven by changes in movement speed. Further, while prior work in ambulatory humans has shown that theta prevalence (not power) is modulated by movement speed during a non-mnemonic walking task (Aghajani et al., 2017) our findings here suggest successful memory retrieval modulates high-frequency theta bandpower in the absence of changes in its prevalence. Interestingly, we found that differences in theta bandpower was specific to the 0.5 seconds prior to recall and not present over the entirety of retrieval. The effect was replicated using a modeling approach, confirming that correct performance drives theta bandpower increases in the 0.5 seconds pre-recall and that movement variables (e.g., speed, head rotation, angular velocity) were non-contributory. However, modeling over the entire retrieval period highlighted that while correct performance did not significantly predict increases in theta power (confirming our initial results), improved performance (reduced error) was a significant predictor of increases in theta power throughout memory retrieval. These results are in line with prior discussions suggesting that mixed literature on the direction of theta oscillation power changes in humans could be clarified by relating a continuous memory performance metric to theta power oscillations (Herweg et al., 2020b). Thus, our results emphasize the importance of investigating memory and spatial representations during ambulation, while highlighting the need for future studies to determine how higher frequency memory-related theta changes differ between ambulatory compared to stationary (virtual) navigation.

Second, we found that MTL theta bandpower increased near previously learned object (halo) positions or environmental boundaries depending on context and momentary



task goals. Specifically, MTL theta bandpower increased near non-target halos when participants were actively searching for and recalling a separate non-visible target halo. This ‘spatial map’ of relevant halo positions was specific to each context (stone or wooden) and alternated as participants switched between environments, consistent with the idea of context reinstatement during memory retrieval (Herweg et al., 2020a). Further, MTL theta bandpower increased at positions close to environmental boundaries (walls) but only when searching for boundary-positioned cues (arrows). This spatial remapping of oscillatory activity based on the behavioral goal (memory recall versus cue-driven navigation) suggests that MTL theta bandpower can dynamically reflect multiple spatial and mnemonic variables in an “on/off” and flexible manner. One possibility is that transient theta power increases may reflect relevant neural representations that are momentarily engaged during dynamic mind-wandering states in humans. Specifically, a momentary increase in power of theta bouts may reflect the relevant neural representations (e.g. for memory or space) that are recruited for a particular cognitive/behavioral goal, in contrast with rodents, where more continuous theta activity occurs during freely moving navigation. Thus, these findings provide a possible explanation for non-continuous theta bouts in humans (Aghajani et al., 2017) where behavioral/cognitive variables may play a more critical role in their modulation as compared to continuous movement-related theta oscillations in rodents (Vanderwolf, 1969; Winson, 1978).

Mechanistically, remapping of MTL theta bandpower across different cognitive tasks could reflect coordinated remapping of local single neuron activity, although the relationship between oscillatory and single neuron remapping in humans requires further exploration. Rodent studies have shown that place cells, which encode particular positions in an environment, globally remap in different contexts and environments (Hafting et al., 2005; Colgin et al., 2008). It is thus plausible that nearby local theta bandpower

remapping may reflect or organize place cell remapping, or that changes in theta bandpower may reflect the summation of populations of nearby remapped place cells. Prior studies recording MTL single neuron activity in stationary humans showed firing rate changes that dynamically changed during free recall tasks (Gelbard-Sagiv et al., 2008) when virtually approaching the position of a previously learned object (Qasim et al., 2019), and in relation to egocentric directions while navigating towards local reference points (Kunz et al., 2021). Given that these MTL neuronal populations each exhibit characteristic tuning to memory and spatial features, it is possible that their summative activity may be coordinated in relation to broader regional theta oscillations to support successful memory retrieval and anchoring positions of spatial targets. Indeed, environmental (contextual) remapping of population-level neuronal signals identified with fMRI has also been shown in a stationary view-based virtual navigation study in humans where hippocampal-entorhinal cortex activity ‘flickered’ between two contexts during incorrect memory retrieval trials as the participant struggled to identify the environment they were in (Julian and Doeller, 2021).

Traditional human neuroimaging studies of memory retrieval and spatial navigation have been done in stationary participants viewing stimuli on a computer screen. Many of these studies were also designed to evaluate neural activity changes during brief stimulus presentations (e.g., 1-2 s when a cue is presented), which limits the ability to disentangle more complex neural dynamics related to multidimensional spatiotemporal experiences in an immersive environmental setting. In contrast, by utilizing 3D ambulatory VR, our study presents a critical advancement for future human behavioral studies measuring brain activity during freely moving behavior by creating a more ecologically-valid setting that enables participants to physically explore, learn, and recall experimentally-controlled stimuli in their environment. Furthermore, the use of VR in this way still allows for deliberate experimental control of the environmental context, as well as the timing and placement of stimuli.

In summary, our results provide novel insights into how human MTL oscillatory dynamics support cognitive maps that could dynamically represent both memory and space in an ecologically-valid setting that involves physical movement through distinct spatial environments. These findings suggest that MTL theta oscillations contain memory- and spatial contextual-related information that may enable transient changes in cognitive states during complex real-world experiences. Our combined deep brain recording and immersive VR approach also presents a unique opportunity for future cognitive and clinical neurosciences studies of naturalistic behavior in humans to unravel underlying mechanisms during complex freely moving behaviors that may be further impaired in patients with neurologic and psychiatric disorders.

# CHAPTER 5:

## Contextually-changing spatial representations

### 5.1 Introduction

Spatial navigation studies recording neural spiking activity in freely moving rodents have identified spatially selective cells in the medial temporal lobe (MTL), such as place (O’Keefe and Dostrovsky, 1971; McHugh et al., 1996), grid (Hafting et al., 2005; Sargolini et al., 2006), and stripe cells (Krupic et al., 2012; Mhatre et al., 2012). Rare single-unit recordings in humans performing spatial navigation in stationary, view-based 2D virtual navigation enable comparisons to animal studies and provide early evidence of spatially selective units (Ekstrom et al., 2003; Jacobs et al., 2013; Nadasdy et al., 2017). However, recent technological developments in 3D and immersive virtual reality (VR) enable a more direct comparison between human studies with those in freely moving rodents; 3D compared to 2D offers a more ecologically valid experience. While 2D VR studies in humans have found a smaller proportion of single neurons compared to that in rodents that display place-like (Ekstrom et al., 2003; Jacobs et al., 2013), and grid-like (Jacobs et al., 2013; Nadasdy et al., 2017) activity, the results may be more comparable to rodents when using 3D compared to 2D navigation, supported by evidence comparing these two in rodents (Aghajian et al., 2015). Moreover, the coordinated activity of one of these spatially-modulated cell populations, grid cells, is thought to drive hexadirectional modulation of BOLD signal and theta bandpower in intracranial electroencephalography (iEEG) and functional magnetic resonance imaging approaches (Doeller et al., 2010a; Chen et al., 2018; Maidenbaum et al., 2018; Staudigl et al., 2018; Stangl et al., 2019). Our study builds on prior work by investigating the neural substrates using rare human recordings by capitalizing on two participant cohorts that provide access to both single-unit and mobile iEEG episodic and spatial memory representations and bridges insights

from these multi-scale neural mechanisms by using the same immersive VR spatial memory task.

A core component of episodic memory is the integration of context and spatial information. Context is defined as the cues and expectations that organize information to guide retrieval (Stark et al., 2018). Although much has been learned about context in rodents (Fyhn et al., 2007; Colgin et al., 2008; Alexander et al., 2016; Latuske et al., 2018; Kubie et al., 2019), ecologically-meaningful context changes in ambulating humans have not been studied. Context changes in rodents result in place cell remapping, i.e. rapid changes in receptive fields and thus the ensemble firing rate map (Colgin et al., 2008; Alexander et al., 2016). Place cell remapping in rodents is thought to reflect intrinsic statistics of experiencing a particular context (Plitt and Giocomo, 2019). Meanwhile, entorhinal cortex grid cells maintain the same firing maps across different contexts while reflecting a degree of flexibility (e.g. grid realignment in novel environments; Hafting et al., 2005). Preliminary studies suggest that the human encoding of context may be more complex. In humans performing view-based 2D VR in four different environments, some properties of single-unit grid-like cells were found to adapt: scaling of grid period, grid orientation, and rotational symmetry (Nadasdy et al., 2017). A recently proposed model of the MTL suggests the entorhinal cortex encodes the environmental statistics as a basis function flexibly applied by the hippocampus to reflect specific environmental features (Whittington et al., 2020). Importantly, flexible accessing of differential spatial representations between contexts have also been demonstrated in humans in a recent fMRI study identifying that contextual representations flicker during dynamic retrieval (Julian and Doeller, 2021). This model predicted many experimental findings of the MTL, including place, grid, and stripe cells, as well as that grid cells maintain a correlational structure across different environments. How the human MTL encodes complex spatial memories in different contexts during real world navigation is a complicated, open

question. Here, we interrogate how ecologically meaningful contextual changes modulate spatial memory representations using a dual single-unit and mobile iEEG approach in two complimentary participant cohorts using a single immersive VR spatial memory task.

## 5.2 Methods

### 5.2.1 Participants

Two cohorts of participants were included in the study, all of whom had pharmaco-resistant epilepsy. The first cohort included 13 participants who were undergoing diagnostic neurosurgical evaluation in the hospital epilepsy monitoring unit setting. Participants were surgically implanted with depth electrodes for epilepsy diagnostic evaluation in a range of global brain regions using Behnke-Fried electrodes containing microwires (for detailed discussion, see Chapter 3.3). The second cohort included 6 participants that all were chronically implanted with an FDA-approved RNS (responsive neurostimulator) System (Neuropace, Inc; 320 Model). The RNS System continuously records ongoing iEEG from 8 contacts across 2 electrode leads implanted in MTL regions (resulting in 4 bipolar channels per participant). For further details, please see the *Methods* section in Chapter 4.2.1. In both cohorts of participants, sites of electrode contacts were determined by the clinical team based on each participant's individual clinical needs and participant recruitment was based on maximizing the number of participants with electrode contacts located in MTL regions. All participants completed written informed consent as approved by the UCLA Medical Institutional Review Board (IRB).

## 5.2.2 Spatial memory task in immersive VR in stationary and ambulatory movement formats

Participants completed a virtual reality spatial memory task in two different virtual environments (room dimensions were 5.84 x 5.84 m) where they learned and retrieved 6 uniquely colored and positioned translucent cylinders (halos) across the two environments. The task began in the first context with encoding trials in which a single halo appeared in its correct location and the participant navigated to the visible halo. After all encoding trials for each of the 3 halos in that context was completed, the participant completed repeating retrieval trials in which written instructions cued the participant to navigate from memory to a particular halo's position and indicate the recalled position by button press. Regardless of performance, the halo then appeared in its correct location and if the participant navigated to the visible halo ('visible feedback period') in order to advance to the next trial. During the first retrieval block, trials repeated until the participants met a learning threshold or completing a set number of trials correctly as defined by recalling the halo within a set radius surrounding the halo's actual position. During subsequent retrieval blocks, participants completed a pre-defined number of trials per block regardless of performance and all retrieval trials were followed by visible feedback periods. All retrieval and encoding trials were interleaved with so-called "arrow trials" in which participants navigated to a visible arrow that appeared at a random position along the perimeter of the virtual environment. Since the position of the arrow was randomized in each trial, there was no memory component to arrow trials. Further, arrow trials encouraged participants to thoroughly sample the environment, including navigation to positions not associated with the fixed positions of halos. The starting environmental context was counterbalanced across participants. Each block alternated between the two contexts. The total number of blocks and total task time completed varied across participants. All participants completed a 5-minute practice

version of the task in a distinct virtual environment to provide a basic familiarity of the VR environment and task structure.

The cohort of participants that were undergoing neurosurgical evaluation of epilepsy in the hospital epilepsy monitoring unit were constrained to their hospital bed due to the wired clinical recording equipment and thus completed the task in a stationary format (as such, this participant cohort will be referred to as “stationary participants”). These participants completed the task using an immersive head-mounted display VR (HTC Vive, HTC Corporation) with embedded eyetracking (Tobii). Participants navigated through the environment and pressed buttons either using the participant controllers or a wireless keyboard with arrow keys corresponding to navigational directions. Five of the thirteen stationary participants were unable to complete the training module in head-mounted VR due to difficulty navigating in the immersive VR environment, discomfort wearing the headset with glasses and head bandage interference, or nausea, and as such these participants completed the task in a 2D-virtual navigation format on a laptop. Across the 13 stationary participants, the number of blocks completed varied between 2 – 12 blocks and the total task time ranged from 20 min – 1 hour.

The cohort of participants that had the RNS System implanted were able to freely ambulate since there was no additional clinical recording equipment (see Chapters 3.2, 4.2.1-3, and 4.3.1-2 for more details). These participants will be referred to as “ambulatory participants” since they completed the VR task in an ambulatory format. These ambulatory participants completed the task using immersive head-mounted VR (Quest 2, Meta; or Pico Neo 2, Pico). Across the 6 ambulatory participants, the number of blocks ranged from 8 – 22 blocks and the total task time ranged from 32 – 135 minutes.

Given the limited attention span and available time of stationary participants in the epilepsy monitoring unit, each block consisted of 3 trials (compared to 5 in the



ambulatory setting). Additionally, given the increased challenges associated with navigating in a virtual environment using V, and the decreased memory of participants in the post-anesthesia state, the learning criteria applied in retrieval block #1 was less stringent in the stationary format (correct retrieval, based on an error radius of  $< 2$  m, in 9 consecutive trials) relative to the ambulatory format (correct retrieval, based on an error radius of  $< 1.5$  m, in 15 consecutive trials).

### 5.2.3 Single-unit or iEEG data acquisition

Stationary participants were implanted with Behnke-Fried electrodes that continuously recorded single-unit activity from 8 microwires, 40- $\mu$ m in diameter, on each depth electrode (see Chapter 3.3 for details). Data was recorded using the Blackrock Neuroport System or the Neuralynx recording systems at 30 kHz or 32 kHz, respectively. Spike templates were automatically determined by using a super paramagnetic clustering algorithm, sorted automatically using the wave clus algorithm (Wave clus 3, Quiroga et al., 2004) and manually confirmed. Low firing units (less than 500 total spikes) and units which had greater than 2% of spike events violating the interspike interval expectation were excluded. For further details, see Chapter 3.3.

iEEG activity was recorded from the continuously recording RNS System in ambulatory participants. Electrode leads are 1.27 mm in diameter and electrode contacts were spaced either 3.5 mm or 10 mm apart. A backpack containing equipment supporting wireless telemetry to continuously obtain iEEG activity was worn by participants during the task (see Fig. 5-1b,d,f,h). Further details can be found in Chapter 3.2 and 4.2.3-5.

#### 5.2.4 Behavioral analysis

Behavioral metrics including continuous position and head rotation were collected from the VR headset. Memory performance was computed as the distance error, defined as the distance between the recalled position and the actual center position of the halo. After pressing a button, participants received written feedback on-screen stating “Correct!” if their error was within 1 m in stationary participants or 0.75 m in ambulatory participants or “Incorrect!” if not.

Data was synchronized by Unity triggering a signal (mark). In single-unit recordings, a BNC cable connected the Unity application to the neural recording system and provided an analog recording of the times that a mark was sent. In ambulatory recordings, Unity wirelessly transmitted a signal to inject a characteristic mark deflection in the iEEG signal which occurred at the transitions between blocks. For greater detail, refer to Chapter 3, Chapter 4.2.3, and Topalovic et al., 2020.

#### 5.2.5 Single-unit data analysis

To quantify the spatial modulation of single-unit activity, firing rates and occupancy time (time spent across virtual 2D positions) were computed across 2D positions in the virtual environment based on binning the environment into 15 cm x 15 cm bins, resulting in a 38 x 39 binned virtual environment. A smoothing kernel (0.2) was applied to the map of binned spike counts and occupancy times and the firing rate map was computed by dividing the resulting spike count array by the occupancy time array. Firing rate maps were only computed for instances when the participant was actively moving by applying a minimum instantaneous speed threshold of 0.1 m/s.

Grid cells were classified by computing the autocorrelation of the firing rate map. The autocorrelation map was rotated in 30° increments and the cross-correlation of the

rotated and original autocorrelation maps were used to compute a widely-used gridness score using the formula (Jacobs et al., 2013):

$$g = \min(\text{cor}(r, r^{60^\circ}), \text{cor}(r, r^{120^\circ})) - \max(\text{cor}(r, r^{30^\circ}), \text{cor}(r, r^{90^\circ}), \text{cor}(r, r^{150^\circ}))$$

The orientation of a grid cell was determined by using the MATLAB function ‘extrema2’ to find the six peaks of the autocorrelation map and the inverse tangent was computed for each peak. The grid cell orientation was defined as the smallest angle of the six peaks.

Stripe cells were classified according to previously described methods (Krupic et al., 2012) by computing the 2D Fourier transform of the firing rate map (using the MATLAB function ‘fftshift’, padded to 256 x 256), applying a normalization factor, and using the maximum Fourier power as the metric quantifying the spatial periodicity of the unit.

Place cells were categorized by computing the sparsity of the firing rate map and by computing the information content of the firing rate map. If either the sparsity or the information content was significant, then the unit was classified as a place cell.

Spatial metrics (gridness score, maximum Fourier power, sparsity, and information content) were evaluated in relation to a shuffled distribution to determine whether a single-unit was classified as a grid cell, stripe cell, or place cell. Specifically, spike times were randomly shifted in time in a circular manner to generate 100 shuffled spike trains. Each shuffled spike train then underwent calculation of the gridness score, the maximum Fourier power, the sparsity and the informational content. If a unit’s spatial metrics exceeded the 95<sup>th</sup> percentile of the shuffled distribution, then it was classified as a spatially-modulated unit.

### 5.2.6 iEEG data analysis

Inter-epileptic dischargers (IEDs) were detected and removed as described in Chapter 4.2.5. Oscillatory power was computed over time points at individual frequency (1 Hz) steps using the BOSC toolbox (Seager et al., 2002; Whitten et al., 2011) with a six cycle Morlet wavelet. Each channel’s power timeseries was normalized (MATLAB function ‘zscore’) over task periods. For more details, refer to Chapter 4.2.7.

To determine whether channels exhibited hexadirectional modulation of theta bandpower, we followed widely used methods (Doeller et al., 2010b; Stangl et al., 2019). Briefly, theta bandpower (6-8 Hz) was normalized over the entire task period per channel. A timeseries of normalized theta bandpower over task timepoints and an aligned timeseries of heading direction for corresponding time points were divided into training and test subsamples. First, a GLM (GLM 1) was fit on the training dataset to determine the grid orientation with the best fit of a sinusoidal model of hexadirectional modulation of theta bandpower. Next, the grid orientation determined was applied to the test dataset and a second GLM (GLM 2) was fit to determine the strength (e.g.,  $\beta$  weight) of the hexadirectional modulation. To determine the reliability of the  $\beta$  weight, we constructed a surrogate distribution by shuffling the heading directions with respect to the theta band power over time points and computed the  $\beta$  weight for each shuffle over 500 iterations. The significance quantified by a p value was determined by comparing the actual  $\beta$  weight to the 95<sup>th</sup> percentile of the shuffled distribution. These steps were repeated over five-fold cross-validation steps. For each fold, one-fifth of the data was used as the test set and the remaining four-fifths of the data were used to train GLM 1 and the remaining four-fifths were used to test the dataset using GLM 2. From each fold, a grid orientation and a  $\beta$  estimate describing the fit of the testing data to the grid orientation were computed. The overall grid orientation and strength of hexadirectional modulation were determined by

averaging over folds the grid orientation determined from GLM 1 and the  $\beta$  estimate from GLM 2, respectively. In order to account for the possibility that each environmental context elicited a distinct grid orientation based on realignment across contexts, both GLMs were fit with two separate regressor variables to allow for two separate regressions to occur, with each regressor corresponding to a unique context.

To compare the change in orientation within a context compared to across contexts, hexadirectional modulation was computed after dividing all the data into four parts: for each context, data was divided into samples falling into the first half of a block or the second half of a block. Then, hexadirectional modulation strength and orientation were computed for each context, in both the first half and second half of blocks. In channels and conditions that exhibited significant hexadirectional modulation (greater than the 95th percentile of the shuffled distribution), change in grid orientation was compared in a pairwise fashion on a channel-by-channel basis between the first half and second half of a block (“within” condition) and between the first half of one context and the second half of the other context (“across” condition). Critically, since the contexts were alternated between each block, and since different blocks were collapsed into a single context grouping, the time delays between samples were comparable in the “within” context and “across” context conditions.

## 5.3 Results

### 5.3.1 Measuring spatial memory using VR during human single-unit and mobile iEEG recordings

We developed a novel VR spatial memory task which was completed by nineteen participants while MTL iEEG activity was recorded. There were two cohorts of participants. The first cohort (Fig. 5-1a,c,e,g) was comprised of thirteen participants that

were enrolled in the study while undergoing a diagnostic neurosurgical procedure in the hospital setting that involved implantation of numerous Behnke-Fried depth electrodes (Fig. 5-1c) with the capability of recording single-unit activity (Fig. 5-1g). These participants were required to remain in their hospital bed due to bulky wiring of clinical recording equipment, and thus completed the VR spatial memory task in a “stationary” format (as this cohort of patients will be referred to; Fig. 5-1a). The second cohort (Fig. 5-1b,d,f,h) was comprised of six participants that already had the FDA-approved Responsive Neurostimulator System (RNS; Fig. 5-1f) implanted intracranially for the clinical treatment of their epilepsy with typically four bipolar channels that continuously record intracranial EEG (iEEG) activity (Fig. 5-1h). These participants were recruited to participate in the study based on the location of their RNS electrodes in the MTL region (Fig. 5-1d).

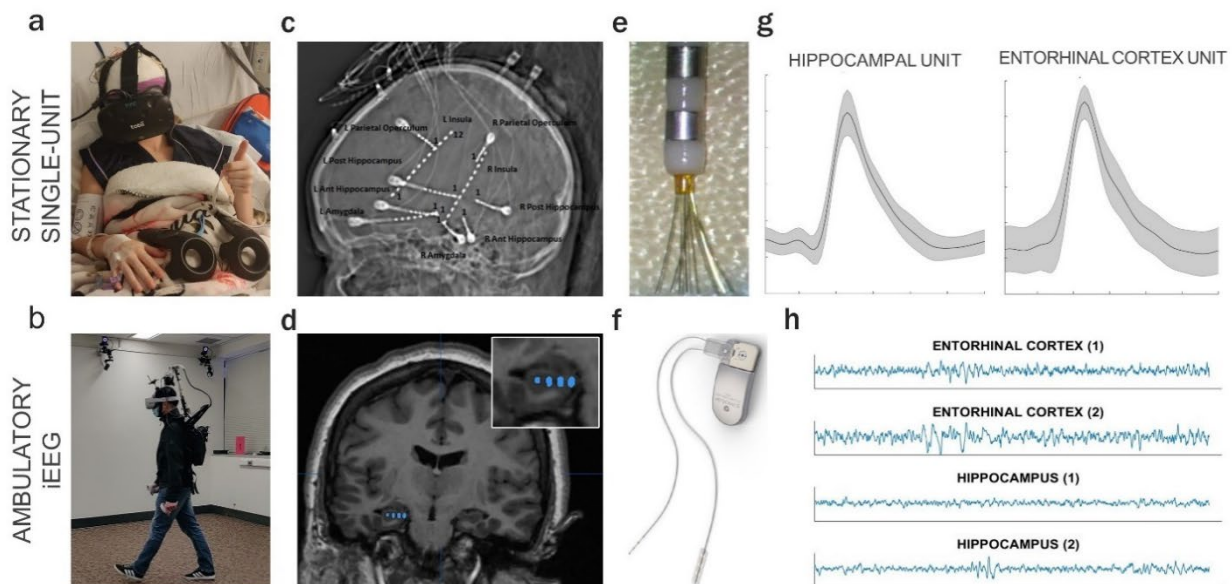


**Figure 5-1. Experimental and neurophysiology recording set up in ambulatory and stationary task formats.**

(a) Stationary participant wearing Vive virtual reality (VR) headset, and (b) ambulatory participant wearing a Quest VR headset while freely walking with recording telemetry equipment in backpack (for more details, see Chapter 4 and Topalovic et al., 2020). (c,d) Example participants' post-implant CT registered to a pre-surgical MRI illustrating intracranial recording electrodes. (c) An example 'stationary' participant is

implanted with multiple Behnke-Fried depth electrodes for an epilepsy diagnostic procedure in the hospital setting and (d) an example ‘ambulatory’ participant with electrode leads implanted in the left hippocampus. (e) Tip of Benke-Fried depth electrode with 8 microwires. (f) Responsive Neurostimulator System is depicted with a hermetically encased recording device that is implanted inside the skull and two depth electrodes. (g) Example hippocampal and entorhinal cortex unit waveforms that are recorded from the microwires shown in (e). (h) Four example bipolar channels recorded from an example participant implanted with the RNS device shown in (f).

The same VR spatial memory task was completed in both cohorts of patients across two virtual environments (5.84 x 5.84 m). Eight of the thirteen stationary participants completed the task using a head-mounted VR headset with navigation controlled by either hand controller or keyboard buttons and five participants completed the task on a 2D laptop set up due to physical constraints including glasses or larger head wrappings that precluded the use of the VR headset. All ambulatory participants ( $N_{\text{participants}} = 6$ ) completed the task in room-scale VR in which physical movements were matched the virtual stimuli in the VR environment.

In each environment, participants interactively learned and later retrieved the locations of six uniquely-colored and positioned translucent cylinders (halos) located across the two environments (Fig. 5-2). The task consisted of encoding trials, in which participants were instructed to navigate to a visible halo (see Chapter 4, Fig. 5-1c) and learn its position. After completing three encoding trials (one for each halo in the environment), participants proceeded to retrieval and arrow trials (Fig. 5-2a-c). Participants were cued to navigate to a particular halo’s position from memory and indicated their recalled position with a button press, which was immediately followed by visible feedback both written as (“Too far” or “Correct!”) and regardless of performance, the halo became visible in its correct position and the participant navigated to the center of the halo to advance to the arrow trial. During arrow trials, the participant navigated to a visible arrow located in a random position along the room perimeter. Retrieval and

arrow trials in a single environment alternated to constitute a block and each block alternated between contexts. The first retrieval block in each context contained a variable number of retrieval trials (Fig 5-3a), depending on how many trials a participant required to meet a learning criterion, in order to advance through the task. The learning criterion varied in the stationary (9 consecutive correct trials with error < 2m) and ambulatory (15 consecutive correct trials with error < 1.5m) format, to accommodate constraints of the hospital setting (study durations limited to a 1-hour timeframe) and participants' stamina level in a post-surgical state. All other retrieval blocks were comprised of a set number of trials regardless of performance (9 retrieval and arrow trials/block in the stationary format and 15 retrieval and arrow trials/block in the ambulatory format). Further details can be found in the Methods section and Chapter 4.

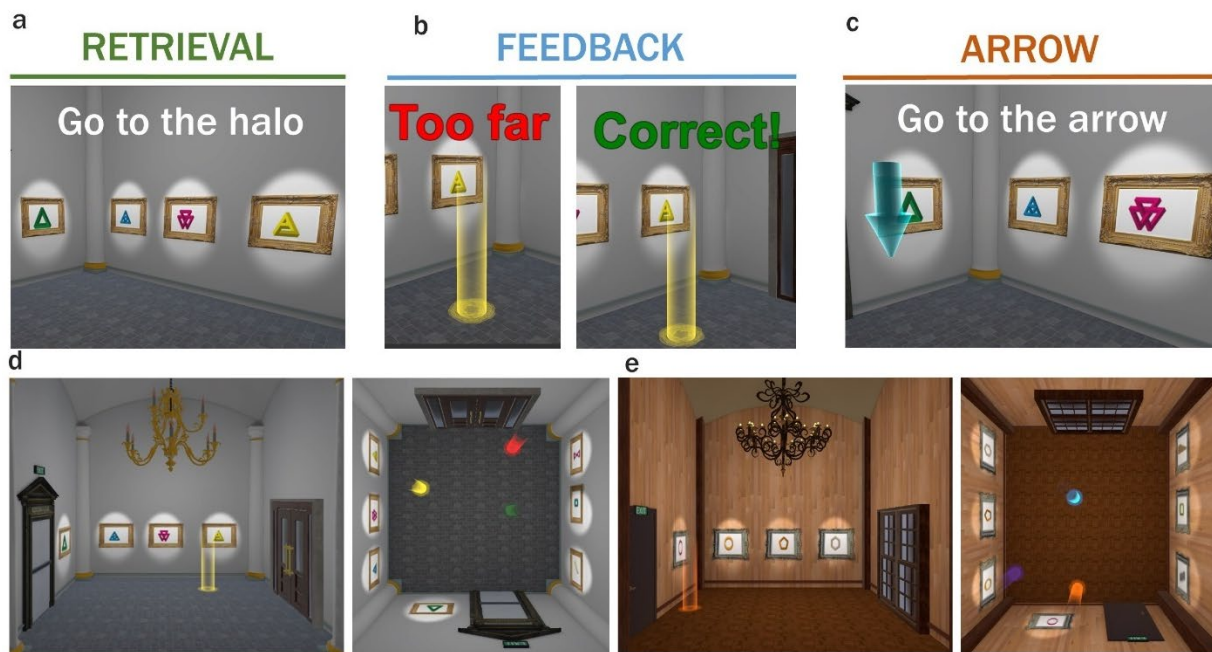


**Figure 5-2. VR spatial memory task.** (a) Retrieval trials consisted of written instructions to navigate to the position of a particular [colored] halo and indicate recalled position by button press. (b) Immediately after the participant pressed a button to indicate recall, visible feedback appeared with written text indicating that the participant was either “Too far” (left) or “Correct!” right. In either case, participants were still



required to navigate to the center of the visible halo. (c) Arrow trials were interleaved with all retrieval and encoding (not shown; refer to Fig. 4-1 for depiction) trials and consisted of participants navigating to a blue arrow that appeared at a random location along the perimeter of the environment. The task was completed in two environments with identical dimensions and landmark positions, each with three uniquely colored and positioned halos. Side-angle and top-down views of the (d) Stone and (e) Wooden environments are shown.

Memory performance was assessed using an error metric defined as the distance between recalled position (button press) and actual halo center point. Performance across stationary participants ( $N_{\text{participants}} = 13$ ) is shown for the Stone (top) and Wooden (bottom) contexts in Fig. 5-3a with mean performance over participants shown in black and individual performance of participants shown as colored lines. Across participants, mean improvement in performance between participants' first block and last block was 0.188 m (reduction in trial error;  $p = 0.036$ ,  $N_{\text{participants}} = 13$ , Fig. 5-3b). An example participant's trajectory over the course of the task is shown as a black line and divided into each context in Fig. 5-3c,d. Performance of ambulatory participants is shown in Chapter 4 (Fig. 4-2 and section 4.3.1). Altogether, these results indicate that a single VR spatial memory task can be used across stationary and ambulatory participants and learning and maintained memory is observed across both participant cohorts. Further, this dual-cohort approach provides the opportunity to probe neurophysiology on two mechanistic levels: single-unit activity in the stationary cohort and mobile iEEG activity in the ambulatory cohort. Importantly, utilizing the same VR task across both cohorts can bridge findings from different mechanistic scales of neurophysiology recordings.

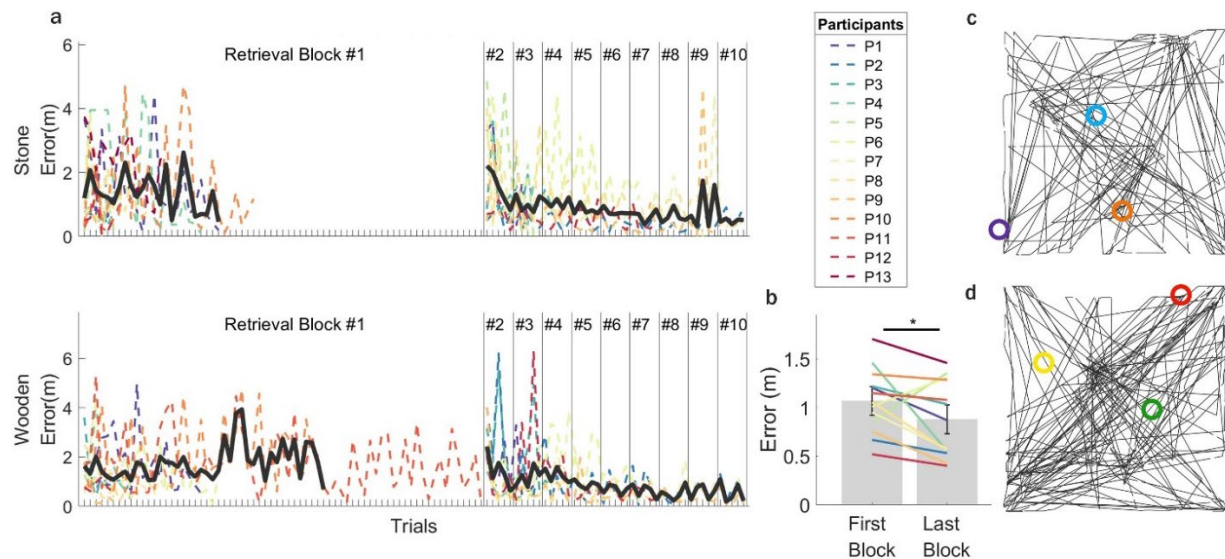


**Figure 5-3. Memory performance during the stationary spatial navigation task.** (a) Mean memory performance (error) was measured for each of the thirteen participants (P1-13, colored lines,  $n_{\text{halos}} = 3$  halos) by computing the average distance between the recalled and correct halo position across trials. The first retrieval block included a variable number of trials (1-45) across participants based on when a learning criterion was reached (9 consecutive correct trials for 3 halos in the given context with error performance  $< 2$  m). Mean memory performance over participants is shown as a black line. (b) Differences in the mean error between the first (trials before the learning criterion was met) and last retrieval block. Lines indicate data from individual participants. \*  $p < 0.05$ . (c-d) Top-down view of an example participants' trajectory (black line) over room positions in the Stone (c) and Wooden (d) contexts. Halo positions are superimposed in both environments.

### 5.3.2 Spatial codes in the human MTL

Previous studies have identified that population-level (e.g. theta bandpower, fMRI BOLD response) MTL neural activity is modulated in a hexadirectional manner, dependent on a participant's virtual movement direction (Doeller et al., 2010b; Chen et al., 2018; Maidenbaum et al., 2018; Stangl, 2018). This population-level hexadirectional modulation is thought to reflect the coordinated firing patterns of populations of grid cells. Specifically, the coordinated firing fields of grid cells (Fig. 5-4a, left) are thought to

result in increases in population-level neural activity when a subject is moving in a direction that is aligned with one of the six-fold directional axes (green slices in Fig. 5-4a, right) compared instances when the subject is moving in directions that are misaligned (gray slices in Fig. 5-4a, right). This can be seen in a schematic illustrated in Fig. 5-4a (bottom), where theoretical oscillatory power is plotted in red and is modulated by movement direction in a hexadirectional manner.

Here, we examined whether the VR spatial navigation task that elicited the formation of a spatial map involving hexadirectional modulation of theta bandpower in the ambulatory format. We examined theta bandpower (6-8 Hz) in the ambulatory participants as they navigated through the real-world while completing the same VR spatial navigation task on a head-mounted display. To quantify the hexadirectional modulation of theta bandpower, we split all samples into a testing and training datasets and fit a GLM to determine the putative grid axis in the training data sample and then fit a second GLM to the testing data sample to determine the strength of the hexadirectional modulation with respect to the mean grid orientation previously determined (for details, see *Methods* and Maidenbaum et al., 2018; Stangl et al., 2019). An example channel illustrating hexadirectional modulation can be seen in Fig. 5-4b. Overall, we found that 13/19 (68.4%) MTL channels exhibited hexadirectional modulation that was significant relative to a surrogate distribution. The proportion of channels that exhibited hexadirectional modulation is shown across MTL regions in Fig. 5-4c.

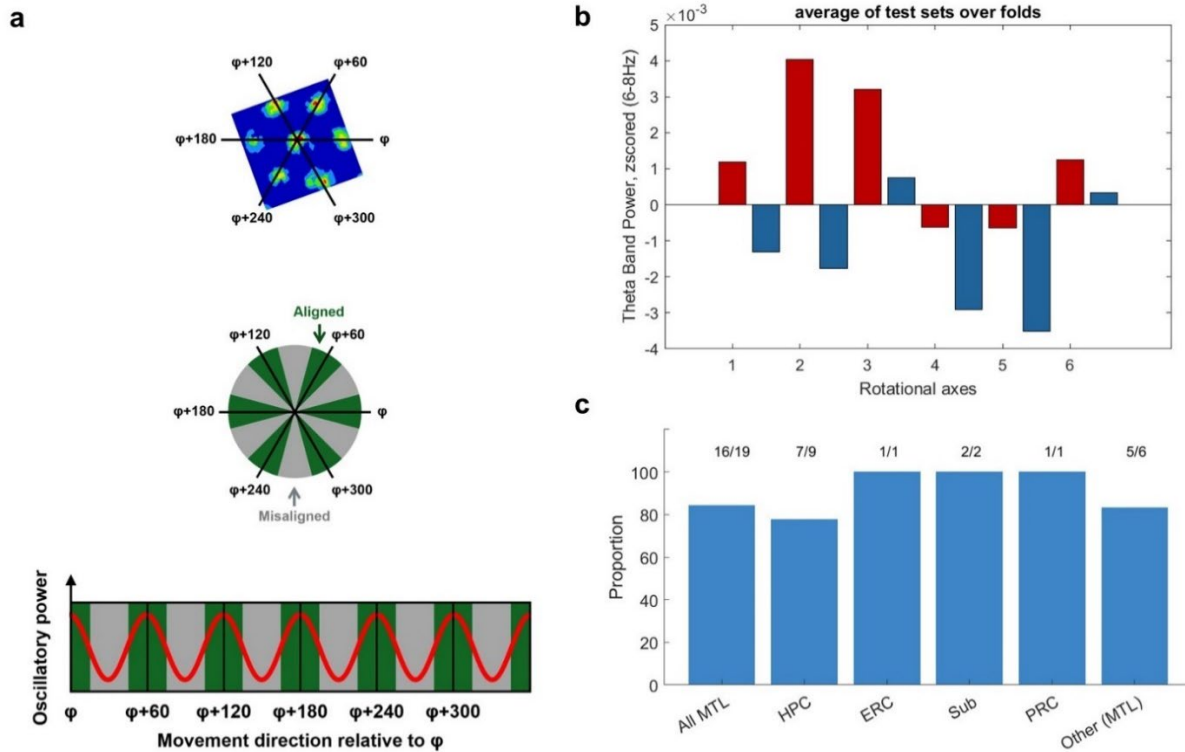


**Figure 5-4. MTL channels exhibit hexadirectional modulation.** (a) Top, firing rate map schematic of a theoretical grid cell in a square environment shown in a square environment. The firing patterns show particular orientations  $\varphi$  relative to a separate grid axis (overlaid in black). Middle, movement directions in one of twelve directions fall into angles that are aligned with the grid axis corresponding to grid cell firing fields. Movement directions categorized as aligned are shown in green and misaligned in gray, adapted from (Stangl et al., 2019). Bottom, the red line reflects the expected hexadirectional modulation of oscillatory power in alignment with the six-fold peaks from the grid axis shown in (a), adapted from (Stangl et al., 2019). (b) Example MTL channel illustrating hexadirectional modulation of theta bandpower. (c) Proportion of MTL channels exhibiting hexadirectional modulation (defined as  $p < 0.05$  relative to surrogate distribution when computed across the entire task or when computing hexadirectional modulation in a context-specific manner). HPC, hippocampus; ERC, entorhinal cortex; Sub, subiculum; PRC, perirhinal cortex; Other (MTL) refers to bipolar channels with contexts across two different regions (e.g., channel with contacts in HPC and ERC).

Hexadirectional modulation of theta bandpower in the MTL is theorized to reflect coordinated activity of grid cell populations. To investigate this hypothesis, we examined

whether the same VR spatial memory task elicited single-unit spatial codes. Across 13 participants, we isolated 342 single neurons (putative neurons) over 13 independent recording sessions. We computed the firing rate for each unit over a map of 38 x 39 bins spanning the virtual environment.

We classified a unit as a grid cell if the unit exhibited the classic peaks in firing rate along triangular lattice structure tiling the environment using the gridness score based on 30° rotations of the autocorrelation of the firing rate map, used in rodents and humans previously (Hafting et al., 2005; Barry et al., 2007; Langston et al., 2010; Jacobs et al., 2013). If a unit's gridness score exceeded the 95<sup>th</sup> percentile of the gridness scores of a surrogate distribution created by time-shuffling a unit's spike train, then it was classified as a putative grid cell. The proportions of grid cells in different regions can be seen in Fig. 5-5a. Overall, 69/342 total units were classified as grid cells (20.2%) and 28/159 MTL units were classified as grid cells (17.6%). An example firing rate map and autocorrelation of a grid cell can be seen in Fig 5-5d. The distribution of grid cell orientations over all grid cells can be seen in Fig. 5-5g. The mean grid orientation was 58.9° ( $\pm 3.3$  standard error of the mean [s.e.m.]). Given the presence of halos in the interior of the environment, we wanted to evaluate whether the position of halos located in the environment could potentially drive the firing of putative grid cells. We simulated a firing rate map in which the simulated unit exclusively fired at halo positions. The gridness score of the simulated unit did not exceed the 95<sup>th</sup> percentile of the surrogate distribution generated from the simulated unit (gridness score -0.0012, 95<sup>th</sup> percentile of surrogate distribution = 0.0163), suggesting that it is unlikely that grid cells identified in this dataset reflected an artifact of halo positions in the environment.

Next, we observed many single neurons that exhibited stripe like peaks in their firing rate maps, consistent with prior reports of spatially periodic band cells (Krupic et

al., 2012). Based on previously used methods, we classified units as spatially periodic band cells (Krupic et al., 2012) as those units that had a maximum power of the 2D Fourier transform of the firing rate map that exceeded the 95<sup>th</sup> percentile of the maximum power of the shuffled distribution. Using this method, a classified stripe cell could have multiple Fourier components that exceeded the 95<sup>th</sup> percentile threshold defined by the surrogate distribution. The distribution of the number of components can be seen in Fig. 5-5b. Overall, 103/342 units were classified as stripe cells (30.1%) and 44/159 MTL units were classified as stripe cells (27.7%). The peak number of components in stripe cells was 1 component (mean = 1.3 components, Fig. 5-5h). The mean orientation of the stripe components was 61.8 ° ( $\pm$  3.6 s.e.m., Fig. 5-5i), similar to the mean orientation observed in the grid cell population.

The population of place cells observed was quite low and was based on those units which had a significantly higher sparsity or informational content relative to a surrogate shuffled distribution. Overall, 24/342 units were classified as place cells (7%) and 9/159 MTL units were classified as place cells (5.7%), with the distribution shown in Fig. 5-5c. An example firing rate map and waveform of a place cell can be seen in Fig. 5-5f.

The spatial properties of a unit were computed first by dividing the recording session into time spent in either context (thus a unit could exhibit grid cell behavior in one context and different grid cell behavior in another context) and also by collapsing all data across both contexts, since the landmarks, geometry, and sampling of the environment were matched across the two environments, by design. Interestingly, spatial cells were present in significant proportions both inside and outside of the MTL (Fig. 5-5a-c, dark blue represents MTL and light blue represents outside of MTL). Grid cells and stripe cells had a similar mean orientation and comparable overall proportions, although a larger proportion of units exhibited stripe cell behavior relative to grid cell behavior.

In line with prior research, we found grid and stripe cell populations were present in MTL regions in expected proportions. Interestingly, we also observed spatially-modulated cell populations in some but not all regions outside of the MTL. These findings are consistent with growing reports of spatial modulation effects in regions outside of the MTL and require future follow-up studies to further characterize the potential existence of spatially-modulated neuron populations outside of the MTL.

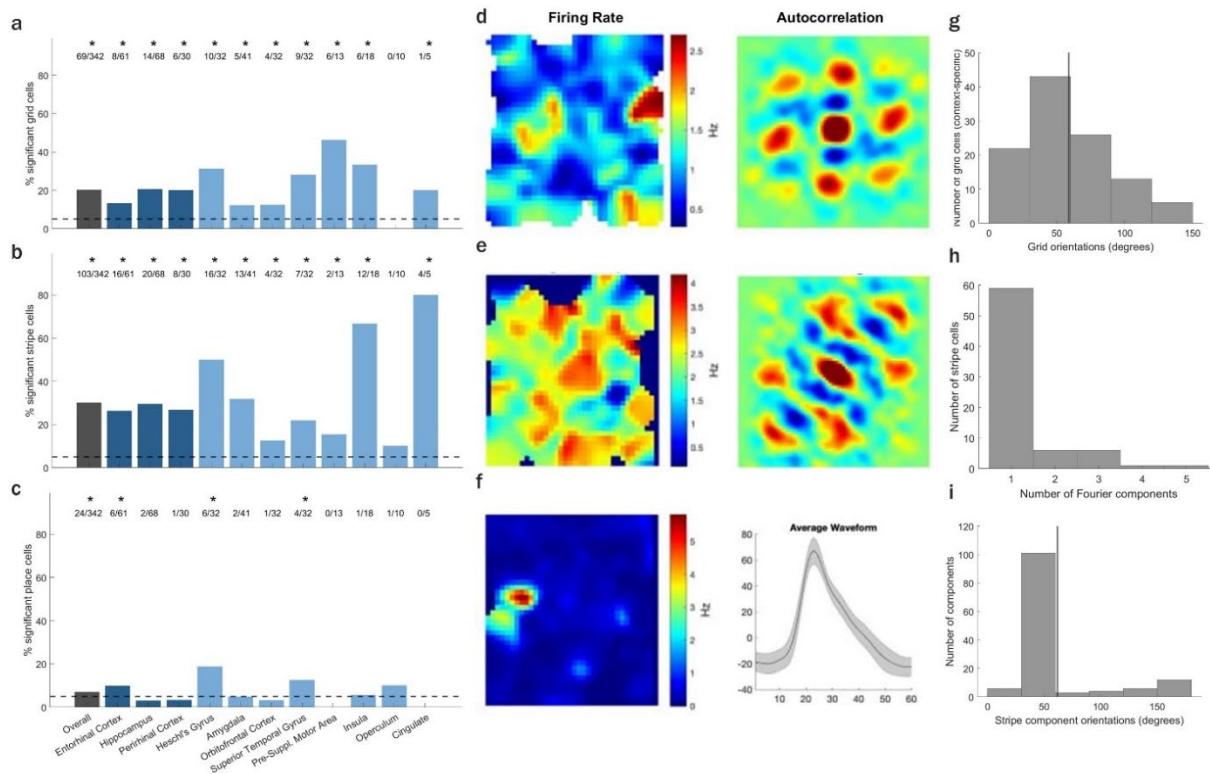


**Figure 5-5. Spatially-modulated single neurons.** (a-c) Proportion of single neurons, by regions, that classify as grid cells (a), stripe cells (b), or place cells (c). Gray bar depicts percentage overall, across regions. Dark blue depicts (spatial) MTL regions and light blue depicts regions outside of the (spatial) MTL (e.g., includes amygdala). Total number of spatial cells (including units that displayed spatial properties in one/both contexts or collapsed across contexts) out of total number of units per region are listed above each bar graph. \* Indicates a significant ( $p < 0.05$ ) proportion based on a binomial test comparing to the type I error of 5% (dashed line). (d-f) Left, firing rate map for an example spatially modulated unit in Hz and right, autocorrelation of the firing rate map for an example (d) grid cell, (e) stripe cell, and (f) place cell, left, place cell waveform with ms along x axis and  $\mu\text{V}$  along y axis. (g) Distribution of grid orientations (degrees)

for grid cells shown in (a) Horizontal line indicates mean. (h) Distribution of the number of Fourier components for the stripe cells shown in (b). (i) Distribution of orientations of the Fourier components for the components shown in (h) and stripe cells shown in (c). Horizontal line indicates mean.

### 5.3.3 Spatial representations are context-specific

Early studies of grid cell activity in rodents suggested that grid cell firing fields relational structure remain preserved across different contexts but that the orientation of the firing fields may shift (Hafting et al., 2005). More recent studies have provided evidence that grid cell firing patterns orientations can re-orient based on the geometry or dimensions of an environment (Nadasdy et al., 2017) or in relation to landmark or goal/reward locations (Butler et al., 2019; Sosa and Giocomo, 2021; Wang and Wang, 2021). We hypothesized that the repeated context changes in our task would elicit changes in both hexadirectional modulation of theta bandpower in the ambulatory participants and grid cell orientation changes in the stationary participants.

To assess the change in hexadirectional modulation orientation between different contexts we designed a comparison to account for the natural drift of hexadirectional modulation representations over time. Specifically, we divided each block in the task into a first and second half and pooled data for each participant into four categories: First Half of Context A, Second Half of Context A, First Half of Context B, and Second Half of Context B. Collapsing data across blocks for each category, we computed the hexadirectional modulation of theta bandpower for each category. For channels that exhibited hexadirectional modulation in both contexts, we computed the channel-wise difference in estimated grid orientation “within” contexts (by finding the difference in grid orientation between First Half and Second Half categories for the same context) and “across” contexts (by finding the difference in grid orientation between Context A and B for the First Half categories, and then the Second Half categories). Since each channel had two comparisons for each of “within” and “across” conditions, we took an average (e.g., the



average of: (1) First Half Context A – First Half Context B and (2) Second Half Context A – Second Half Context B) for each channel (see Fig. 5-6a for schematic). The mean change in grid orientation across channels was a difference of  $26.1^\circ$  while the mean change in grid orientation within channels was a difference of  $4.9^\circ$  ( $n_{\text{channels}} = 7$ , pairwise permutation test  $p < 0.0001$ , Fig. 5-6b). It is worth noting that by pooling data for each of the four categories across different blocks, data samples in each category had comparable time delays in the within and across conditions given that each block was divided in half and contexts alternated each block, as can be observed in the schematic in Fig. 5-6a.

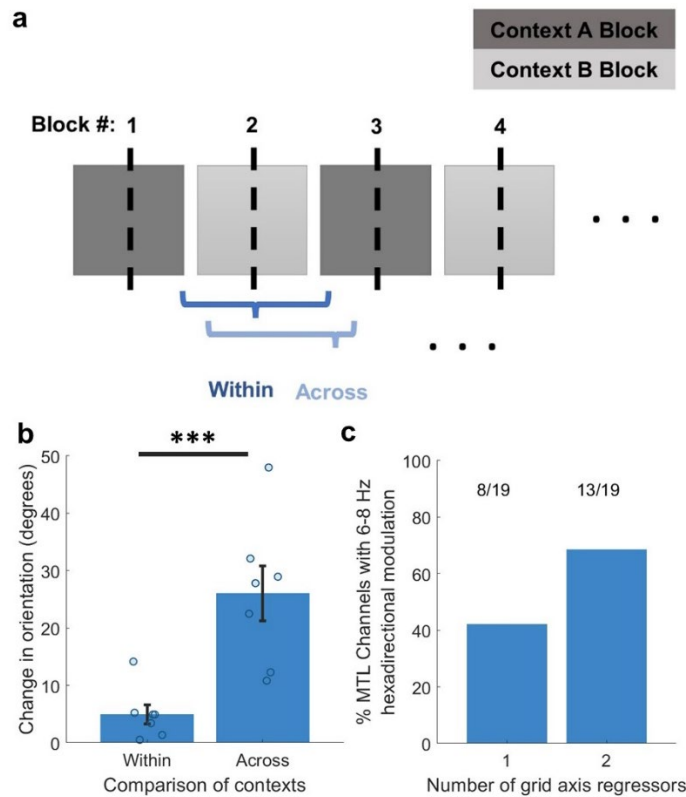


**Figure 5-6. Context-specific hexadirectional modulation.** (a) Schematic illustrating how dataset was divided to assess the change in grid orientation between contexts. All blocks were divided in half. Data was grouped into four categories: First Half of block in Context A, Second Half of block in Context A, First Half of block in Context B, Second Half of block in Context B. Hexadirectional modulation and surrogate distributions were computed in each of the four categories on every channel. In channels that demonstrated significant hexadirectional modulation, the difference in grid orientation between Context A and Context B categories

("Across") was computed and compared to the difference in orientation between First Half and Second Half categories ("Within"). By collapsing across blocks (which alternate between contexts), the time delays between blocks were comparable across the four categories, since alternating blocks were collapsed in each of the four categories. (b) Mean change in grid orientation between First Half and Second Half of a Context for "Within" and between Context A and Context B for "Across". Data points reflect channels that exhibited significant hexadirectional modulation in both contexts ( $n_{\text{channels}} = 7$ ).  $***p < 0.0001$ . (c) Proportion of MTL channels exhibiting hexadirectional modulation of 6-8 Hz theta when analysis is done with 1-regressor relative to 2 context-specific regressors.

Further, we hypothesized that if hexadirectional modulation axes varied in a context-specific manner, computing the hexadirectional modulation strength and significance in a context-specific approach would yield a higher proportion of channels exhibiting this behavior relative to estimating the hexadirectional modulation on a channel with the assumption of a single axis across the entire task, and thus collapsed over both contexts (e.g. a context-agnostic approach). To do this, we first computed hexadirectional modulation in all MTL channels by assigning an independent regressor term to each context, allowing the grid axis to vary in each context. Next, we computed hexadirectional modulation in all MTL channels with a single regressor across both contexts, thus constraining the grid axis to remain unchanged across both contexts. There was a significantly higher proportion of MTL channels that had hexadirectional modulation in either one or both contexts when hexadirectional modulation was computed using context-specific regressors compared to a context-agnostic (all channels with significant hexadirectional modulation:  $p < 0.001$ ; 8/19 channels when computed with 1 regressor; 13/19 channels when computed with 2 regressors; chi-squared test  $X^2 = 2.661$ ,  $p = 0.05$ ;  $n_{\text{channels}} = 19$ , Fig. 5-6c). Of the MTL channels that exhibited any hexadirectional modulation, 36% only had hexadirectional modulation in one channel, 57% had hexadirectional modulation in both contexts, and 7% had hexadirectional only when collapsing across both contexts using 1 regressor ( $n_{\text{channels}}$  with hexadirectional



contexts. (d-e) This unit's firing rate over binned positions in the (d) Stone and (e) Wooden contexts is shown. (f-g) Autocorrelation maps of the firing rate are shown in the (f) Stone and (g) Wooden contexts with the grid orientation in each context listed in the top right corner.

Importantly, prior work has indicated that landmarks and environmental geometries are two factors that may contribute to warped and rotated grid cell axes (Nadasdy et al., 2017). To control for this, the VR spatial memory task used in this study was designed to have identical environmental geometries, locations of landmarks, and identity of landmarks across the two environments, (Fig. 4-1g-h) thus it is unlikely that landmark positions or environmental geometries contribute to the grid reorientation observed in hexadirectional modulation and individual grid cells.

#### 5.3.4 The relationship between context-specific spatial representations and memory

Previous work has suggested that MTL spatial machinery (e.g. place cells, grid cells) are involved in supporting memory retrieval (Moser et al., 2015a; Qasim et al., 2019) and that the strength of hexadirectional modulation of population-level activity is also related to memory performance (Doeller et al., 2010b; Chen et al., 2018). To begin to explore this relationship, we investigated whether the strength of context-specific spatial representations predicted memory performance on a participant level. The linear regressions of mean trial error in a context-specific (Fig. 5-8a-f) and context-agnostic (Fig. 5-8g-i) manner on mean spatial score (gridness score, Fig. 5-8a,d,g; stripeness score, Fig 5-8b,e,h; hexadirectional modulation strength, Fig. 5-8c,f,i). Two interesting relationships emerged suggesting that this relationship between memory and strength or spatial representations warrants follow up. Mean hexadirectional modulation strength in the Wooden context was a significant predictor of trial error with a beta coefficient of -7.62 suggesting that a 1 point increase in HM strength (reflecting the beta coefficient estimate describing how well the test data is fit by hexadirectional modulation using the estimated

grid axis) as associated with a 7.6 meter distance decrease in error (coefficient estimate = -7.62,  $p = 0.049$ ,  $n_{\text{participants}} = 6$ , Fig. 5-8f). Given that the range of hexadirectional modulation strengths was 0.006 – 0.087, this relationship can be better interpreted as a 0.1 point increase in hexadirectional modulation strength is associated with a 0.76 m improvement in trial performance (reduced error). Although not significant, the linear relationship between gridness score and mean trial performance in the Stone context was approaching significance (coefficient estimate = -1.5m,  $p = 0.059$ ,  $n_{\text{participants}} = 10$ , Fig. 5-8a). One limitation of this approach is that each data point reflects a summative score across spatial representations in each participant. As such, greater numbers of units per patient, and patients overall will provide the power to make conclusions about the relationship between memory and summative strength of spatial representations. However, these preliminary results may motivate future investigations of the relationship between the strength of spatial representations and continuous memory performance.

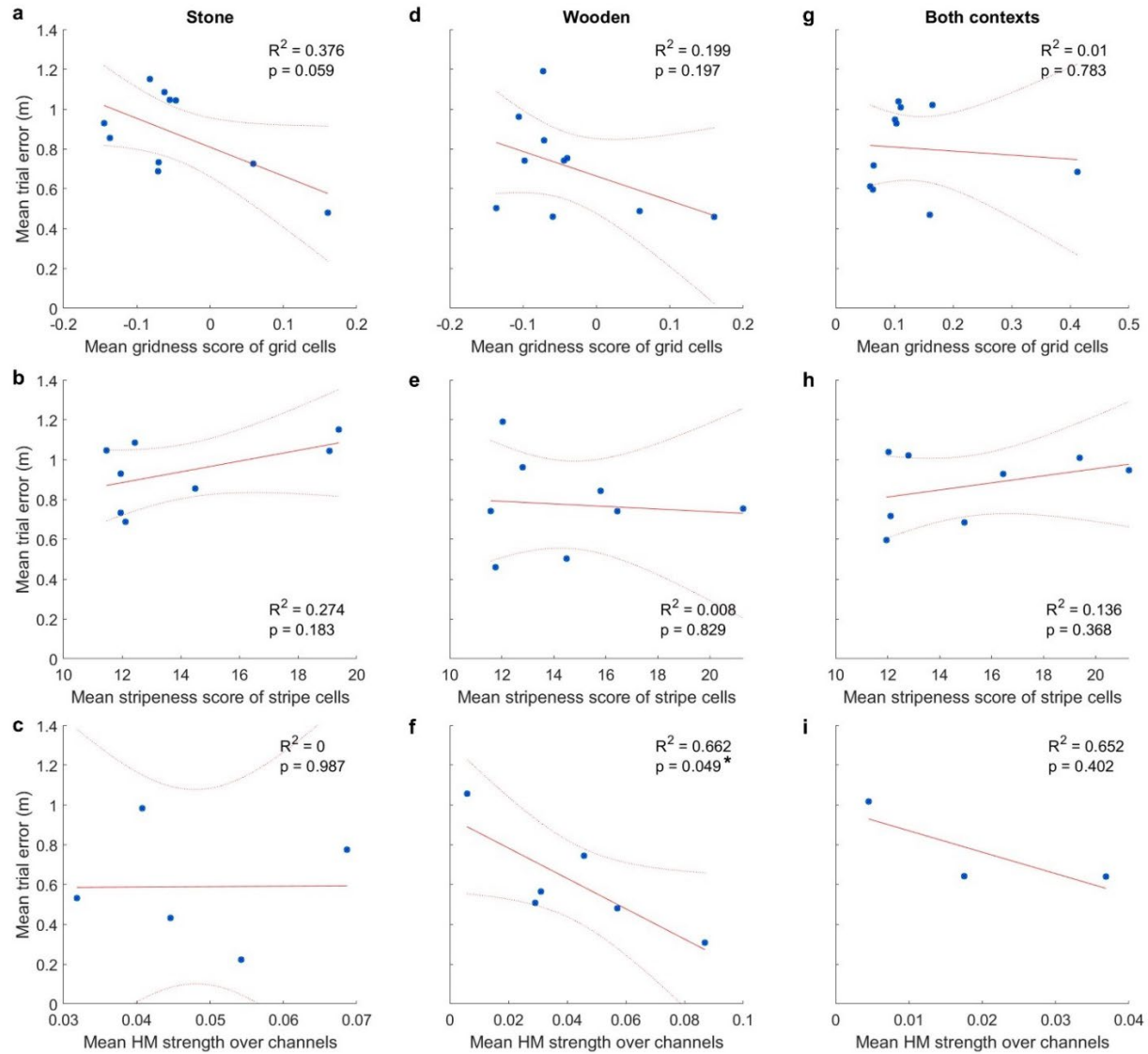


**Figure 5-8. Relationship between memory performance and spatial coding metrics.** Mean error over trials was computed for each participant ( $n_{\text{stationary}} = 13$ ,  $n_{\text{ambulatory}} = 6$ ) in a context-specific (Stone: a-c; Wooden: d-f) or context-agnostic (Both contexts: g-i) manner. Mean single neuron spatial modulation scores (gridness score: a,d,g; stripeness score: b,e,h) or mean hexadirectional modulation strength (HM; c,f,i) were computed on a per-patient basis and used to predict memory performance using a linear regression model. Blue points reflect mean spatial metrics per participant where available (e.g. all participants that have at least one grid cell in each context in a,d,g). Red line shows line of best fit with red dotted lines illustrating the 95% confidence intervals. Correlation coefficient and significance of spatial coding metric predictor are listed. \*  $p < 0.05$

Given results from mobile iEEG illustrating that theta bandpower is elevated during correct relative to incorrect trials in the time window preceding memory recall, we examined whether there were any changes in firing rate in relation to memory recall in single neuron spatial populations. Preliminary analysis of stripe cell firing rate changes preceding halo recall demonstrated that stripe cells had elevated firing rates during correct trials relative to incorrect trials in the 250 ms prior to recall (Fig 5-9a) and that mean firing rate in this 250 ms time window was significantly greater during successful recall (correct vs. incorrect,  $p = 0.0084$ , permutation test,  $n_{\text{correcttrials}} = 2937$ ,  $n_{\text{incorrecttrials}} = 2211$ , Fig 5-9b).

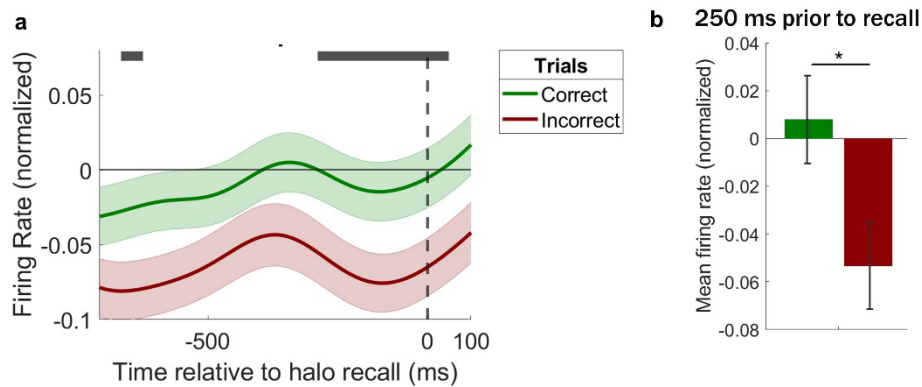


**Figure 5-9. Stripe cells increase their firing rate in relation to successful memory retrieval.** (a) Mean firing rate over trials, normalized to all retrieval periods in a single neuron, divided into correct trials and incorrect trials. Horizontal gray bar indicates 50 ms time bins with a significant difference between correct and incorrect trials ( $p < 0.05$ , FDR corrected). (b) Mean normalized firing rate between correct and incorrect trials in the 250 ms window prior to recall. \*  $p < 0.05$ .

## 5.4 Discussion

We have demonstrated that the same VR spatial memory task elicits spatial coding representations at both single-unit and iEEG levels in stationary and ambulatory participants through mechanisms neural substrates including grid cells, stripe cells, and hexadirectionally-modulated theta bandpower. Importantly, this investigation provides

insight into multi-scale (including single-unit) neural mechanisms of grid-cell encoding in humans, both freely-moving and stationary. We capitalized on immersive VR to advance the ecological validity and link stationary human single-unit recordings with findings from mobile iEEG recordings. Previous work have identified hexadirectional modulation in humans (Constantinescu et al., 2016; Bellmund et al., 2018; Chen et al., 2018; Maidenbaum et al., 2018; Stangl et al., 2018; Staudigl et al., 2018; Chen et al., 2021) and others have documented grid cell activity (Jacobs et al., 2013; Nadasdy et al., 2017), however although the two phenomenon are theorized to be related, however this is the first study to bridge these two mechanisms by investigating both in the same behavioral paradigm.

First, we characterized populations of grid cells and stripe cells concurrently in humans. Notably, we find the proportion of entorhinal cortex grid cells to be 13% which similar to previously reported a previously reported proportion of grid cells in humans from Jacobs et al as 14% and also corresponds to proportions reported from studies in rodents (Hafting et al., 2005; Doeller et al., 2010b; Killian et al., 2012; Jacobs et al., 2013). Similar to prior work in rodents demonstrating that 44% of units in the entorhinal cortex and pre-/para-subiculum were stripe cells (Krupic et al., 2012), we observed a higher proportion of stripe cells (30%) relative to grid cells (20%) overall, and although not as high in rodents, we found that 28% of entorhinal cortex and hippocampal units exhibited stripe behavior. Stripe cells have been theorized to drive the self-organization of grid cells through the co-activation of multiple  $60^\circ$  separated bands (Grossberg and Pilly, 2012; Krupic et al., 2012; Pilly and Grossberg, 2014) and may organize the activity of grid cells in this VR spatial navigation task. Interestingly, we found that the mean and most common orientation of putative grid and stripe cells were  $58.9^\circ$  and  $61.8^\circ$ , respectively, in this task. The close correspondence of these orientations of these two populations



suggests that there may be a commonality in mechanisms and interwoven relationship between the two populations.

Another interesting observation meriting further study was the presence of stripe and grid cell populations in non-MTL regions of the human brain. These included regions such as the auditory cortices, amygdala, orbitofrontal cortex, pre-supplementary motor area, insula, and cingulate. Importantly, not all regions with units contained significant spatial cells. Although this novel finding is consistent with growing reports that document spatial representations in humans in broader regions beyond the MTL, future studies will be necessary to follow-up and characterize the presence of meaningful and functional spatially-modulated neurons in regions outside of the MTL. It is relevant to note a growing body of literature that has documented hexadirectional modulation in regions globally including the prefrontal cortex, cingulate cortex, orbitofrontal cortex, among other non-MTL regions (Chen et al., 2021; Park et al., 2021; Raithel and Gottfried, 2021). Open and important questions that remain to be explored are characterization and validation of these spatial populations outside of the MTL and evaluation of the extent to which these non-MTL regions support spatial encoding, how these populations interact with MTL spatial cell populations, and whether non-MTL spatially modulated cell populations perform a unique function in spatial cognition.

A key finding of this study was that iEEG hexadirectional modulation of theta bandpower exhibited re-orientation of putative grid axes in relation to context changes. Importantly, these findings were observed in highly controlled context changes with constrained environmental geometries and landmark positions, enabled through the use of immersive VR. Prior work has suggested that grid cells may reorient in new contexts, originally in rodents through changes between circular and square environments (Fyhn et al., 2007) and more recently in humans with grid cells reorienting in relation to change environmental size and geometries (e.g. square to rectangular; Nadasdy et al., 2017b).

Further, a recent study in fMRI demonstrated that spatial representations flicker between deliberation of retrieved context (Julian and Doeller, 2021). Our finding builds on this prior work by demonstrating that the change in orientation of hexadirectional modulation is greater between contexts (semantically different in association with unique object, halo, positions in this study) compared to within contexts, offering an internal control. Moreover, we found significant changes in grid orientation across contexts in grid cell populations from single-unit recordings, suggesting a potential single-unit mechanism that could support the change in grid orientation observed in hexadirectional modulation of iEEG. Interestingly, the single-unit grid cells exhibited a similar mean change in grid axis reorientation as in hexadirectional modulation of iEEG signal. These preliminary findings merit future investigations to characterize the stimuli driving grid reorientation and to further delineate the single-unit mechanisms that may be involved in orientation changes at the population level.

Finally, we investigated whether the strength of these spatial representations relates to episodic spatial memory performance. A prior study has suggested that reactivation of a spatial context in iEEG theta bandpower relates to memory retrieval (Herweg et al., 2020a). Here, we build on this finding by examining the relationship between memory performance and context-specific spatial representations. Notably, we find preliminary results suggesting that context-specific hexadirectional modulation strength is significantly related to memory performance and that stripe cell firing rates may increase during correct relative to incorrect trials. Although these findings are preliminary, future studies will investigate how context-specific spatial representations drive memory retrieval.

## REFERENCES

- Aghajian ZM, Acharya L, Moore JJ, Cushman JD, Vuong C, Mehta MR (2015) Impaired spatial selectivity and intact phase precession in two-dimensional virtual reality. *Nat Neurosci* 18:121–128.
- Aghajian ZM, Schuette P, Fields TA, Tran ME, Siddiqui SM, Hasulak NR, Tcheng TK, Eliashiv D, Mankin EA, Stern J, Fried I, Suthana N (2017) Theta Oscillations in the Human Medial Temporal Lobe during Real-World Ambulatory Movement. *Curr Biol*.
- Aghajian ZM, Villaroman D, Hiller S, Wishard TJ, Topalovic U, Christov-Moore L, Shaterian N, Hasulak NR, Knowlton B, Eliashiv D, Rao V, Fried I, Suthana N (2019) Modulation of human intracranial theta oscillations during freely moving spatial navigation and memory. *bioRxiv*.
- Akkol S, Kucyi A, Hu W, Zhao B, Zhang C, Sava-Segal C, Liu S, Razavi B, Zhang J, Zhang K, Parvizi J (2021) Intracranial Electroencephalography Reveals Selective Responses to Cognitive Stimuli in the Periventricular Heterotopias. *J Neurosci* 41:3870–3878.
- Alexander GM, Farris S, Pirone JR, Zheng C, Colgin LL, Dudek SM (2016) Social and novel contexts modify hippocampal CA2 representations of space. *Nat Commun* 7.
- Barry C, Hayman R, Burgess N, Jeffery KJ (2007) Experience-dependent rescaling of entorhinal grids. *Nat Neurosci* 2007 106 10:682–684.
- Bellmund JLS, Gärdenfors P, Moser EI, Doeller CF (2018) Navigating cognition: Spatial codes for human thinking. *Science*.
- Benjamini Y, Hochberg Y (1995) Controlling the False Discovery Rate: A Practical and Powerful Approach to Multiple Testing. *J R Stat Soc Ser B* 57:289–300.
- Benjamini Y, Yekutieli D (2001) The control of the false discovery rate in multiple testing under dependency. <https://doi.org/10.1214/aos/1013699998> 29:1165–1188.

- Bierbrauer A et al. (2020) Unmasking selective path integration deficits in Alzheimer's disease risk carriers. *Sci Adv* 6.
- Bland BH (1986) The physiology and pharmacology of hippocampal formation theta rhythms. *Prog Neurobiol* 26:1–54.
- Bohbot VD, Copara MS, Gotman J, Ekstrom AD (2017) Low-frequency theta oscillations in the human hippocampus during real-world and virtual navigation. *Nat Commun* 8.
- Bush D, Bisby JA, Bird CM, Gollwitzer S, Rodionov R, Diehl B, McEvoy AW, Walker MC, Burgess N (2017) Human hippocampal theta power indicates movement onset and distance travelled. *Proc Natl Acad Sci U S A* 114:12297–12302.
- Butler WN, Hardcastle K, Giocomo L (2019) Remembered reward locations restructure entorhinal spatial maps. *1452:1447–1452*.
- Buzsáki G, Lai-Wo S. L, Vanderwolf CH (1983) Cellular bases of hippocampal EEG in the behaving rat. *Brain Res Rev* 6:139–171.
- Buzsáki G, Moser EI (2013) Memory, navigation and theta rhythm in the hippocampal-entorhinal system. *Nat Neurosci* 2013 162 16:130–138.
- Caplan JB, Madsen JR, Schulze-Bonhage A, Aschenbrenner-Scheibe R, Newman EL, Kahana MJ (2003) Human  $\theta$  Oscillations Related to Sensorimotor Integration and Spatial Learning. *J Neurosci* 23:4726–4736.
- Caspi A, Barry MP, Patel UK, Salas MA, Dorn JD, Roy A, Niketeghad S, Greenberg RJ, Pouratian N (2021) Eye movements and the perceived location of phosphenes generated by intracranial primary visual cortex stimulation in the blind. *Brain Stimul* 14:851–860.
- Chari A, Thornton RC, Tisdall MM, Scott RC (2020) Microelectrode recordings in human epilepsy: a case for clinical translation. *Brain Commun* 2.
- Chen D, Kunz L, Lv P, Zhang H, Zhou W, Liang S, Axmacher N, Wang L (2021) Theta

- oscillations coordinate grid-like representations between ventromedial prefrontal and entorhinal cortex. *Sci Adv* 7:200–227.
- Chen D, Kunz L, Wang W, Zhang H, Wang WX, Schulze-Bonhage A, Reinacher PC, Zhou W, Liang S, Axmacher N, Wang L (2018) Hexadirectional Modulation of Theta Power in Human Entorhinal Cortex during Spatial Navigation. *Curr Biol* 28:3310-3315.e4.
- Colgin LL (2020) Five decades of hippocampal place cells and EEG rhythms in behaving rats. *J Neurosci* 40:54–60.
- Colgin LL, Moser EI, Moser MB (2008) Understanding memory through hippocampal remapping. *Trends Neurosci* 31:469–477.
- Constantinescu AO, O'Reilly JX, Behrens TEJ (2016) Organizing conceptual knowledge in humans with a gridlike code. *Science* (80- ).
- Courellis HS, Nummela SU, Metke M, Diehl GW, Bussell R, Cauwenberghs G, Miller CT (2019) Spatial encoding in primate hippocampus during free navigation.
- Dayan P (2005) Neural Encoding I: Firing Rates and Spike Statistics BT - Theoretical Neuroscience. *Theor Neurosci*:460.
- Do TTN, Lin CT, Gramann K (2021) Human brain dynamics in active spatial navigation. *Sci Rep* 11.
- Doeller CF, Barry C, Burgess N (2010a) Evidence for grid cells in a human memory network. *Nature*.
- Doeller CF, Barry C, Burgess N (2010b) Evidence for grid cells in a human memory network. *Nature*.
- Ekstrom AD, Caplan JB, Ho E, Shattuck K, Fried I, Kahana MJ (2005) Human hippocampal theta activity during virtual navigation. *Hippocampus* 15:881–889.
- Ekstrom AD, Kahana MJ, Caplan JB, Fields TA, Isham EA, Newman EL, Fried I (2003) Cellular networks underlying human spatial navigation. *Nature* 425:184–187.

- Foo S, Bohbot VD (2020) Theta rhythm across the species: Bridging inconsistencies with a multiple memory systems approach. *Behav Neurosci* 134:475–490.
- Fried I, Rutishauser U, Cerf M, Krieman G eds. (2014) *Single Neuron Studies of the Human Brain: Probing Cognition*. USA: MIT Press.
- Fried I, Wilson CL, Maidment NT, Engel J, Behnke E, Fields TA, Macdonald KA, Morrow JW, Ackerson L (1999) Cerebral microdialysis combined with single-neuron and electroencephalographic recording in neurosurgical patients. Technical note. *J Neurosurg* 91:697–705.
- Fyhn M, Hafting T, Treves A, Moser MB, Moser EI (2007) Hippocampal remapping and grid realignment in entorhinal cortex. *Nature*.
- Gelbard-Sagiv H, Mukamel R, Harel M, Malach R, Fried I (2008) Internally generated reactivation of single neurons in human hippocampus during free recall. *Science* (80- ) 322:96–101.
- Gelinas JN, Khodagholy D, Thesen T, Devinsky O, Buzsáki G (2016) Interictal epileptiform discharges induce hippocampal-cortical coupling in temporal lobe epilepsy. *Nat Med* 22:641–648.
- Gilron R et al. (2021) Long-term wireless streaming of neural recordings for circuit discovery and adaptive stimulation in individuals with Parkinson's disease. *Nat Biotechnol* 2021 399 39:1078–1085.
- Goyal A, Goetz S, Stanslaski S, Oh Y, Rusheen AE, Klassen B, Miller K, Blaha CD, Bennet KE, Lee K (2021) The development of an implantable deep brain stimulation device with simultaneous chronic electrophysiological recording and stimulation in humans. *Biosens Bioelectron* 176:112888.
- Griffiths BJ, Martín-Buro MC, Staresina BP, Hanslmayr S, Staudigl T (2021) Alpha/beta power decreases during episodic memory formation predict the magnitude of

- alpha/beta power decreases during subsequent retrieval. *Neuropsychologia* 153:107755.
- Grossberg S, Pilly PK (2012) How Entorhinal Grid Cells May Learn Multiple Spatial Scales from a Dorsoventral Gradient of Cell Response Rates in a Self-organizing Map. *PLoS Comput Biol* 8:e1002648.
- Guderian S, Düzel E (2005) Induced theta oscillations mediate large-scale synchrony with mediotemporal areas during recollection in humans. *Hippocampus* 15:901–912.
- Hafting T, Fyhn M, Molden S, Moser MB, Moser EI (2005) Microstructure of a spatial map in the entorhinal cortex. *Nature* 436:801–806.
- Hanslmayr S, Staresina BP, Bowman H (2016) Oscillations and Episodic Memory: Addressing the Synchronization/Desynchronization Conundrum. *Trends Neurosci* 39:16–25.
- Hasselmo ME (2005) What is the function of hippocampal theta rhythm? - Linking behavioral data to phasic properties of field potential and unit recording data. *Hippocampus* 15:936–949.
- Henin S, Shankar A, Hasulak N, Friedman D, Dugan P, Melloni L, Flinker A, Sarac C, Fang M, Doyle W, Tcheng T, Devinsky O, Davachi L, Liu A (2019) Hippocampal gamma predicts associative memory performance as measured by acute and chronic intracranial EEG. *Sci Rep* 9.
- Herweg NA, Apitz T, Leicht G, Mulert C, Fuentemilla L, Bunzeck N (2016) Theta-Alpha Oscillations Bind the Hippocampus, Prefrontal Cortex, and Striatum during Recollection: Evidence from Simultaneous EEG–fMRI. *J Neurosci* 36:3579–3587.
- Herweg NA, Sharan AD, Sperling MR, Brandt A, Schulze-Bonhage A, Kahana MJ (2020a) Reactivated spatial context guides episodic recall. *J Neurosci* 40:2119–2128.
- Herweg NA, Solomon EA, Kahana MJ (2020b) Theta Oscillations in Human Memory.

Trends Cogn Sci 24:208–227.

- J. Gordon Betts, Kelly A. Young, James A. Wise, Eddie Johnson, Brandon Poe, Dean H. Kruse, Oksana Korol, Jody E. Johnson, Mark Womble PD (2013) The Action Potential. In: Anatomy and Physiology. Houston, Texas: OpenStax.
- Jacobs J (2014) Hippocampal theta oscillations are slower in humans than in rodents: implications for models of spatial navigation and memory. *Philos Trans R Soc B Biol Sci* 369.
- Jacobs J, Kahana MJ, Ekstrom AD, Mollison M V, Fried I (2010) A sense of direction in human entorhinal cortex. *PNAS*.
- Jacobs J, Weidemann CT, Miller JF, Solway A, Burke JF, Wei X-X, Suthana N, Sperling MR, Sharan AD, Fried I, Kahana MJ (2013) Direct recordings of grid-like neuronal activity in human spatial navigation. *Nat Neurosci* 2013 169 16:1188–1190.
- Julian JB, Doeller CF (2021) Remapping and realignment in the human hippocampal formation predict context-dependent spatial behavior. *Nat Neurosci* 2021 246 24:863–872.
- Jutras MJ, Fries P, Buffalo EA (2013) Oscillatory activity in the monkey hippocampus during visual exploration and memory formation. *Proc Natl Acad Sci U S A* 110:13144–13149.
- Kahana MJ, Sekuler R, Caplan JB, Kirschen M, Madsen JR (1999) Human theta oscillations exhibit task dependence during virtual maze navigation. *Nature* 399:781–784.
- Kaplan R, Doeller CF, Barnes GR, Litvak V, Düzel E, Bandettini PA, Burgess N (2012) Movement-Related Theta Rhythm in Humans: Coordinating Self-Directed Hippocampal Learning. *PLOS Biol* 10:e1001267.
- Killian NJ, Jutras MJ, Buffalo EA (2012) A map of visual space in the primate entorhinal cortex. *Nature* 491:761–764.



- Kota S, Rugg MD, Lega BC (2020) Hippocampal Theta Oscillations Support Successful Associative Memory Formation. *J Neurosci* 40:9507–9518.
- Krupic J, Burgess N, O’Keefe J (2012) Neural representations of location composed of spatially periodic bands. *Science* (80- ) 337:853–857.
- Kubie JL, Levy ERJ, Fenton AA (2019) Is hippocampal remapping the physiological basis for context? *Hippocampus*:hipo.23160.
- Kunz L, Brandt A, Reinacher PC, Staesina BP, Reifenstein ET, Weidemann CT, Herweg NA, Patel A, Tsitsiklis M, Kempter R, Kahana MJ, Schulze-Bonhage A, Jacobs J (2021) A neural code for egocentric spatial maps in the human medial temporal lobe. *Neuron* 109:2781-2796.e10.
- Kunz L, Schröder TN, Lee H, Montag C, Lachmann B, Sariyska R, Reuter M, Stirnberg R, Stöcker T, Messing-Floeter PC, Fell J, Doeller CF, Axmacher N (2015) Reduced grid-cell-like representations in adults at genetic risk for Alzheimer’s disease. *Science* (80- ) 350:430–433.
- Ladouce S, Donaldson DI, Dudchenko PA, Ietswaart M (2019) Mobile EEG identifies the re-allocation of attention during real-world activity. *Sci Reports* 2019 9:1–10.
- Langston RF, Ainge JA, Couey JJ, Canto CB, Bjerknes TL, Witter MP, Moser EI, Moser MB (2010) Development of the spatial representation system in the rat. *Science* 328:1576–1580.
- Latuske P, Kornienko O, Kohler L, Allen K (2018) Hippocampal Remapping and Its Entorhinal Origin. *Front Behav Neurosci* 11.
- Lee Y-E, Shin G-H, Lee M, Lee S-W (2021) Mobile BCI dataset of scalp- and ear-EEGs with ERP and SSVEP paradigms while standing, walking, and running. *Sci Data* 2021 8:1–12.
- Lefebvre B, Yger P, Marre O (2016) Recent progress in multi-electrode spike sorting

- methods. *J Physiol Paris* 110:327–335.
- Lin JJ, Rugg MD, Das S, Stein J, Rizzuto DS, Kahana MJ, Lega BC (2017) Theta band power increases in the posterior hippocampus predict successful episodic memory encoding in humans. *Hippocampus* 27:1040–1053.
- Liu S, Parvizi J (2019) Cognitive refractory state caused by spontaneous epileptic high-frequency oscillations in the human brain. *Sci Transl Med* 11.
- Long NM, Sperling MR, Worrell GA, Davis KA, Gross RE, Lega BC, Jobst BC, Sheth SA, Zaghoul K, Stein JM, Kahana MJ (2017) Contextually Mediated Spontaneous Retrieval Is Specific to the Hippocampus. *Curr Biol* 27:1074–1079.
- Maidenbaum S, Miller J, Stein JM, Jacobs J (2018) Grid-like hexadirectional modulation of human entorhinal theta oscillations. 115.
- Mamalek A (2014) Ethical and Practical Considerations for Human Microelectrode Recording Studies. In: *Single Neuron Studies of the Human Brain* (Fried I, Rutishauser U, Cerf M, Kreiman G, eds). MIT Press.
- Mankin EA, Aghajan ZM, Schuette P, Tran ME, Tchemodanov N, Titiz A, Kalender G, Eliashiv D, Stern J, Weiss SA, Kirsch D, Knowlton B, Fried I, Suthana N (2021) Stimulation of the right entorhinal white matter enhances visual memory encoding in humans. *Brain Stimul* 14:131–140.
- Mao D, Avila E, Caziot B, Laurens J, Dickman JD, Angelaki DE (2021) Spatial modulation of hippocampal activity in freely moving macaques. *Neuron* 109:3521-3534.e6.
- McHugh TJ, Blum KI, Tsien JZ, Tonegawa S, Wilson MA (1996) Impaired hippocampal representation of space in CA1-specific NMDAR1 knockout mice. *Cell* 87:1339–1349.
- Meisenhelter S, Testorf ME, Gorenstein MA, Hasulak NR, Tcheng TK, Aronson JP, Jobst BC (2019) Cognitive tasks and human ambulatory electrocorticography using the RNS System. *J Neurosci Methods* 311:408–417.

- Mhatre H, Gorchetchnikov A, Grossberg S (2012) Grid cell hexagonal patterns formed by fast self-organized learning within entorhinal cortex. *Hippocampus* 22:320–334.
- Miller J et al. (2018) Lateralized hippocampal oscillations underlie distinct aspects of human spatial memory and navigation. *Nat Commun* 2018 9:1–12.
- Miller JF, Neufang M, Solway A, Brandt A, Trippel M, Mader I, Hefft S, Merkow M, Polyn SM, Jacobs J, Kahana MJ, Schulze-Bonhage A (2013) Neural activity in human hippocampal formation reveals the spatial context of retrieved memories. *Science* (80- ) 342:1111–1114.
- Mobbs D, Wise T, Suthana N, Guzmán N, Kriegeskorte N, Leibo JZ (2021) Promises and challenges of human computational ethology. *Neuron* 109:2224–2238.
- Molina R, Okun MS, Shute JB, Opri E, Rossi PJ, Martinez-Ramirez D, Foote KD, Gunduz A (2018) Report of a patient undergoing chronic responsive deep brain stimulation for Tourette syndrome: proof of concept. *J Neurosurg* 129:308–314.
- Moser M-B, Rowland DC, Moser EI (2015a) Moser, M.-B., Rowland, D.C., and Moser, E.I. (2015). Place cells, grid cells, and memory. *Cold Spring Harb. Perspect. Biol.* 7, a021808. Place cells, grid cells, and memory. *Cold Spring Harb Perspect Biol* 7:a021808.
- Moser MB, Rowland DC, Moser EI (2015b) Place cells, grid cells, and memory. *Cold Spring Harb Perspect Biol* 7.
- Nadasdy Z, Nguyen TP, Török CE, Shen JY, Briggs DE, Modur PN, Buchanan RJ (2017) Context-dependent spatially periodic activity in the human entorhinal cortex. *Proc Natl Acad Sci U S A* 114:E3516–E3525.
- O’Keefe J, Dostrovsky J (1971) The hippocampus as a spatial map. Preliminary evidence from unit activity in the freely-moving rat. *Brain Res* 34:171–175.
- O’Keefe J, Recce ML (1993) Phase relationship between hippocampal place units and the

- EEG theta rhythm. *Hippocampus* 3:317–330.
- Opitz B (2014) Memory function and the hippocampus. *Front Neurol Neurosci* 34:51–59.
- Park SA, Miller DS, Boorman ED (2021) Inferences on a multidimensional social hierarchy use a grid-like code. *Nat Neurosci* 2021 249 24:1292–1301.
- Parvizi J, Kastner S (2018) Promises and limitations of human intracranial electroencephalography. *Nat Neurosci* 2018 214 21:474–483.
- Pilly PK, Grossberg S (2014) How does the modular organization of entorhinal grid cells develop? *Front Hum Neurosci* 8:337.
- Plitt MH, Giocomo LM (2019) Experience dependent contextual codes in the hippocampus. [bioRxiv:864090](https://doi.org/10.1101/386409).
- Qasim SE, Miller J, Inman CS, Gross RE, Willie JT, Lega B, Lin JJ, Sharan A, Wu C, Sperling MR, Sheth SA, McKhann GM, Smith EH, Schevon C, Stein JM, Jacobs J (2019) Memory retrieval modulates spatial tuning of single neurons in the human entorhinal cortex. *Nat Neurosci* 22:2078–2086.
- Quirk CR, Zutshi I, Srikanth S, Fu ML, Devico Marciano N, Wright MK, Parsey DF, Liu S, Siretskiy RE, Huynh TL, Leutgeb JK, Leutgeb S (2021) Precisely Timed Theta Oscillations are Selectively Required During the Encoding Phase of Memory. *Nat Neurosci* 24:1614.
- Quiroga RQ (2012) Spike sorting. *Curr Biol* 22:R45–R46.
- Quiroga RQ, Nadasdy Z, Ben-Shaul Y (2004) Unsupervised spike detection and sorting with wavelets and superparamagnetic clustering. *Neural Comput* 16:1661–1687.
- Raithel CU, Gottfried JA (2021) What Are Grid-Like Responses Doing in the Orbitofrontal Cortex? *Behav Neurosci* 135:218.
- Ramirez S, Liu X, Lin PA, Suh J, Pignatelli M, Redondo RL, Ryan TJ, Tonegawa S (2013) Creating a false memory in the hippocampus. *Science* (80- ) 341:387–391.

- Rao VR, Leonard MK, Kleen JK, Lucas BA, Mirro EA, Chang EF (2017) Chronic ambulatory electrocorticography from human speech cortex. *Neuroimage* 153:273–282.
- Ravassard P, Kees A, Willers B, Ho D, Aharoni D, Cushman J, Aghajan ZM, Mehta MR (2013) Multisensory control of hippocampal spatiotemporal selectivity. *Science* (80- ) 340:1342–1346.
- Reiser JE, Wascher E, Arnau S (2019) Recording mobile EEG in an outdoor environment reveals cognitive-motor interference dependent on movement complexity. *Sci Reports* 2019 9:1–14.
- Richardson DP, Foxe JJ, Mazurek KA, Abraham N, Freedman EG (2021) Neural Markers of Proactive and Reactive Cognitive Control Are Altered During Walking: A Mobile Brain-Body Imaging (MoBI) study. *Neuroimage*:118853.
- Sargolini F, Fyhn M, Hafting T, McNaughton BL, Witter MP, Moser MB, Moser EI (2006) Conjunctive representation of position, direction, and velocity in entorhinal cortex. *Science* (80- ) 312:758–762.
- Scangos KW, Khambhati AN, Daly PM, Makhoul GS, Sugrue LP, Zamanian H, Liu TX, Rao VR, Sellers KK, Dawes HE, Starr PA, Krystal AD, Chang EF (2021a) Closed-loop neuromodulation in an individual with treatment-resistant depression. *Nat Med* 27:1696–1700.
- Scangos KW, Makhoul GS, Sugrue LP, Chang EF, Krystal AD (2021b) State-dependent responses to intracranial brain stimulation in a patient with depression. *Nat Med* 27:229–231.
- Scoville WB, Milner B (1957) Loss of Recent Memory After Bilateral Hippocampal Lesions.
- Seager MA, Johnson LD, Chabot ES, Asaka Y, Berry SD (2002) Oscillatory brain states and learning: Impact of hippocampal theta-contingent training. *Proc Natl Acad Sci U*

S A 99:1616–1620.

- Sellers KK, Gilron R, Anso J, Louie KH, Shirvalkar PR, Chang EF, Little SJ, Starr PA (2021) Analysis-rcs-data: Open-Source Toolbox for the Ingestion, Time-Alignment, and Visualization of Sense and Stimulation Data From the Medtronic Summit RC+S System. *Front Hum Neurosci* 15:398.
- Shirvalkar P, Sellers KK, Schmitgen A, Prosky J, Joseph I, Starr PA, Chang EF (2020) A Deep Brain Stimulation Trial Period for Treating Chronic Pain. *J Clin Med* 2020, Vol 9, Page 3155 9:3155.
- Solomon EA, Lega BC, Sperling MR, Kahana MJ (2019a) Hippocampal theta codes for distances in semantic and temporal spaces. *Proc Natl Acad Sci* 116:24343–24352.
- Solomon EA, Stein JM, Das S, Gorniak R, Sperling MR, Worrell G, Inman CS, Tan RJ, Jobst BC, Rizzuto DS, Kahana MJ (2019b) Dynamic Theta Networks in the Human Medial Temporal Lobe Support Episodic Memory. *Curr Biol* 29:1100-1111.e4.
- Sosa M, Giacomo LM (2021) Navigating for reward. *Nat Rev Neurosci* 22:472–487.
- Squire LR (1992) Memory and the Hippocampus: A Synthesis From Findings With Rats, Monkeys, and Humans. *Psychol Rev* 99:195–231.
- Squire LR, Stark CEL, Clark RE (2004) The Medial Temporal Lobe. *Annu Rev Neurosci* 27:279–306.
- Staba R (2014) Subchronic In Vivo Human Microelectrode Recording. In: *Single Neuron Studies of the Human Brain* (Fried I, Rutishauser U, Cerf M, Kreiman G, eds), pp 43–58. The MIT Press.
- Stangl M (2018) Investigating human grid-cell-like representations and path integration in the context of cognitive aging.
- Stangl M, Achtzehn J, Huber K, Dietrich C, Tempelmann C, Wolbers T (2018) Compromised Grid-Cell-like Representations in Old Age as a Key Mechanism to Explain Age-Related Navigational Deficits. *Curr Biol* 28:1108-1115.e6.

- Stangl M, Topalovic U, Inman CS, Hiller S, Villaroman D, Aghajan ZM, Christov-Moore L, Hasulak NR, Rao VR, Halpern CH, Eliashiv D, Fried I, Suthana N (2021) Boundary-anchored neural mechanisms of location-encoding for self and others. *Nature* 589:420–425.
- Stangl M, Wolbers T, Shine JP (2019) Population-Level Analysis of Human Grid Cell Activation. In: *Neuromethods*. Springer Science and Business Media LLC.
- Stark SM, Reagh ZM, Yassa MA, Stark CEL (2018) What’s in a context? Cautions, limitations, and potential paths forward. *Neurosci Lett* 680:77–87.
- Staudigl T, Leszczynski M, Jacobs J, Sheth SA, Schroeder CE, Jensen O, Doeller CF (2018) Hexadirectional Modulation of High-Frequency Electrophysiological Activity in the Human Anterior Medial Temporal Lobe Maps Visual Space. *Curr Biol* 28:3325-3329.e4.
- Suthana N, Aghajan ZM, Mankin EA, Lin A (2018) Reporting Guidelines and Issues to Consider for Using Intracranial Brain Stimulation in Studies of Human Declarative Memory. *Front Neurosci* 12.
- Suthana N, Haneef Z, Stern J, Mukamel R, Behnke E, Knowlton B, Fried I (2012) Memory Enhancement and Deep-Brain Stimulation of the Entorhinal Area. *N Engl J Med* 366:502–510.
- ter Wal M, Linde-Domingo J, Lifanov J, Roux F, Kolibius LD, Gollwitzer S, Lang J, Hamer H, Rollings D, Sawlani V, Chelvarajah R, Staresina B, Hanslmayr S, Wimber M (2021) Theta rhythmicity governs human behavior and hippocampal signals during memory-dependent tasks. *Nat Commun* 2021 121 12:1–15.
- Tolman EC (1948) Cognitive maps in rats and men. *Psychol Rev* 55:189–208.
- Topalovic U et al. (2023) A wearable platform for closed-loop stimulation and recording of single-neuron and local field potential activity in freely moving humans. *Nat Neurosci* 2023 8:1–11.

- Topalovic U, Aghajan Z, Villaroman D, Hiller S, Christov-Moore L, Wishard T, Stangl M, Hasulak N, Inman C, Fields T, Eliashiv D, Fried I, Suthana N (2020) Wireless Programmable Recording and Stimulation of Deep Brain Activity in Freely Moving Humans.
- Tort ABL, Komorowski R, Eichenbaum H, Kopell N (2010) Measuring phase-amplitude coupling between neuronal oscillations of different frequencies. *J Neurophysiol* 104:1195–1210.
- Tort ABL, Komorowski RW, Manns JR, Kopell NJ, Eichenbaum H (2009) Theta-gamma coupling increases during the learning of item-context associations. *Proc Natl Acad Sci U S A* 106:20942–20947.
- Tsao A, Moser MB, Moser EI (2013) Traces of experience in the lateral entorhinal cortex. *Curr Biol* 23:399–405.
- Tsitsiklis M, Miller J, Qasim SE, Inman CS, Gross RE, Willie JT, Smith EH, Sheth SA, Schevon CA, Sperling MR, Sharan A, Stein JM, Jacobs J (2020) Single-Neuron Representations of Spatial Targets in Humans. *Curr Biol* 30:245-253.e4.
- Tulving E (1983) Ecphoric processes in episodic memory.
- Ulmer S, Jansen O (2013) fMRI: Basics and clinical applications. *fMRI Basics Clin Appl* 9783642343:1–325.
- Vanderwolf CH (1969) Hippocampal electrical activity and voluntary movement in the rat. *Electroencephalogr Clin Neurophysiol* 26:407–418.
- Vivekananda U, Bush D, Bisby JA, Baxendale S, Rodionov R, Diehl B, Chowdhury FA, McEvoy AW, Miserocchi A, Walker MC, Burgess N (2021) Theta power and theta-gamma coupling support long-term spatial memory retrieval. *Hippocampus* 31:213–220.
- Wang W, Wang W (2021) Effect of reward on electrophysiological signatures of grid cell population activity in human spatial navigation. *Sci Rep* 11:1–9.



- Wang Y, Romani S, Lustig B, Leonardo A, Pastalkova E (2014) Theta sequences are essential for hippocampal place fields. *Nat Neurosci*.
- Watrous AJ, Ekstrom AD (2014) The spectro-contextual encoding and retrieval theory of episodic memory. *Front Hum Neurosci* 8.
- Watrous AJ, Lee DJ, Izadi A, Gurkoff GG, Shahlaie K, Ekstrom AD (2013) A comparative study of human and rat hippocampal low-frequency oscillations during spatial navigation. *Hippocampus* 23:656–661.
- Whishaw IQ, Vanderwolf CH (1973) Hippocampal EEG and behavior: Change in amplitude and frequency of RSA (Theta rhythm) associated with spontaneous and learned movement patterns in rats and cats. *Behav Biol* 8:461–484.
- Whitten TA, Hughes AM, Dickson CT, Caplan JB (2011) A better oscillation detection method robustly extracts EEG rhythms across brain state changes: the human alpha rhythm as a test case. *Neuroimage* 54:860–874.
- Whittington JCR, Muller TH, Mark S, Chen G, Barry C, Burgess N, Behrens TEJ (2020) The Tolman-Eichenbaum Machine: Unifying Space and Relational Memory through Generalization in the Hippocampal Formation. *Cell* 183:1249-1263.e23.
- Winson J (1978) Loss of Hippocampal Theta Rhythm Results in Spatial Memory Deficit in the Rat. *Science* (80- ) 201:160–163.
- Winter SS, Mehlman ML, Clark BJ, Taube JS (2015) Passive Transport Disrupts Grid Signals in the Parahippocampal Cortex. *Curr Biol* 25:2493–2502.
- Wu H et al. (2020) Brain-Responsive Neurostimulation for Loss of Control Eating: Early Feasibility Study. *Neurosurgery* 87:1277–1288.
- Zutshi I, Brandon MP, Fu ML, Donegan ML, Leutgeb JK, Leutgeb S (2018) Hippocampal Neural Circuits Respond to Optogenetic Pacing of Theta Frequencies by Generating Accelerated Oscillation Frequencies. *Curr Biol* 28:1179-1188.e3.